

Synthesis and application of manganese dioxide coated magnetite for removal of metal ions from aqueous solutions

Zur Erlangung des akademischen Grades eines
DOKTORS DER INGENIEURWISSENSCHFTEN (Dr.-Ing)

der Fakultät für Chemieingenieurwesen und Verfahrenstechnik des
Karlsruher Institut für Technologie (KIT)

genehmigte
DISSERTATION
von
Dipl.-Chem. Carla Calderón Rosas
aus Chile

Referent: Prof. Dr. Matthias Franzreb

Korreferent: Prof. Dr. Hermann Nirschl

Tag der mündlichen Prüfung: 8. Juli 2010

Acknowledgements

I wish to express my warm and sincere thanks to Prof. Dr. Wolfgang Höll, for giving me the opportunity to be part of his research group, for his motivation and immense knowledge and for his continuous support throughout this work even during the hardest moments.

I would like to express my deep and sincere gratitude to Prof. Dr. Matthias Franzreb for taking over the supervision of this PhD Thesis, for his detailed and constructive comments and for the immense support to finish this work.

My sincere thank to Prof. Dr. Hermann Nirschl for taking over the coreference of this work.

At the same time I would like to thank to Prof. Dr. Carlos Basualto for the friendly discussion about this work.

I am grateful to Brigitte Kiehling and Sibylle Heidt for the analytical and practical support.

I would like also thank all my colleagues and staff of the Institute of Functional Interfaces (IFG) for providing the supportive working environment. Especially, I would like to thank to Jessica Varela for her constant support and friendship throughout this work, Martin Silvestre for the helpful discussion, Jens Bolle, for the good advices and for helping with the German translations and in particular Marcel Riegel, my office colleague, for his infinite assistance.

Finally, I owe my loving thanks to my husband Marcelo González, without his encouragement and understanding it would have been impossible for me to finish this work.

The financial support of Graduiertenkolleg 366 and CONICYT grants are gratefully acknowledged.

Abstract

A microsorbent with magnetic properties has been successfully synthesized by means of the deposition of manganese dioxide onto magnetite particles.

For the physicochemical characterization of the synthesized magnetic microsorbent different measurements were carried out. Magnetic properties were determined by means of an alternating gradient magnetometer (AGM). The specific surface area was determined based on BET theory. Further information about composition and morphology was gathered by the use of an environmental scanning electron microscopy with energy-dispersive X-ray spectroscopy analysis (ESEM/EDAX). By means of microelectrophoresis measurements of the zeta potential of the particle surface were carried out.

The results showed, that the resulting microsorbents have a particle size between 0.5 and 18 μm . Magnetization of the material is between 41 and 75 Am^2/kg , in the order of magnitude of that of magnetite. Therefore efficient solid-liquid separation by means of the application of a moderate magnetic field is possible. Due to the properties of MnO_2 the point of zero charge of the surface was found to be close to 3. Therefore, the adsorbent is almost exclusively a cation exchanger although sorption of oxyanions is also possible.

Sorption experiments were carried out and evaluated by means of the Langmuir and Freundlich relationships. The influence of pH, competitive sorption, and complexing ligands was studied. Results of the equilibrium experiments carried out with Cd^{2+} , Ni^{2+} , and Pb^{2+} ions, showed that the sorption process was highly dependent on the pH of the solution and the uptake of heavy metal ions is preferred against the sorption of other cations. Sorption of alkaline earth ions such as Ca^{2+} affects the uptake only at high concentrations. Other ions such as chloride ions affect also the uptake due to changes in the metal ion speciations.

Kinetic experiments were carried out in batch systems. The sorption kinetics was evaluated by means of four models; film diffusion, Lagergren or pseudo-first-order, pseudo-second-order, and the Elovich model. It was found, that the film diffusion model can successfully describe the sorption kinetics and in conjunction with the equilibrium parameters, the sorption at determined conditions can be modeled well.

Because of the small size of the particles and the respective large specific surface, sorption is fast. It was observed that within the first 10 minutes around 90% of the final uptake takes place and sorption equilibrium was reached within one hour.

Besides the experiments with heavy metal cations, kinetic and equilibrium sorption experiments with the oxyanion MoO_4^{2-} were carried out. It was found that the sorption of oxyanions onto the magnetic micro-sorbent was possible too. As well as for the metal ions the sorption process was fast and highly dependent on the pH of the solution.

On the basis of the results the order of sorption capacity was found to be: $\text{Pb}^{2+} > \text{Ni}^{2+} \geq \text{Cd}^{2+} \gg \text{MoO}_4^{2-}$.

Finally, results of consecutive sorption-desorption cycles demonstrated that the magnetic micro-sorbent can be recycled, although the sorption capacity drops considerably within the first few cycles. Nevertheless, the high selectivity for bivalent heavy metal ions makes the synthesized micro-sorbents an interesting alternative to conventional ion exchangers. Therefore, in the outlook a possible set-up to apply the magnetic micro-sorbents in industrial scale is suggested.

Zusammenfassung

Ein Mikrosorbens mit magnetischen Eigenschaften wurde durch Anlagerung von Mangandioxid auf Magnetitpartikel erfolgreich hergestellt.

Für die physikalisch-chemische Charakterisierung dieses magnetischen Mikrosorbens wurden verschiedene Messtechniken angewendet. Die magnetischen Eigenschaften wurden mittels eines alternierenden Gradientenmagnetometers (AGM) und die spezifische Oberfläche mittels der BET-Theorie bestimmt. Weitere Informationen über die Zusammensetzung und die Morphologie der resultierenden Partikel brachte die Vermessungen in einem Elektronenmikroskop unter Wasseratmosphäre (ESEM) und angeschlossener disperser Röntgenspektroskopie (EDAX). Das Zeta-Potential der Partikeloberflächen ergaben Messungen mittels Mikro-Elektrophorese.

Die Ergebnisse zeigten, dass die hergestellten Mikrosorbentien Durchmesser von 0.5 μm bis 18 μm aufweisen. Da die Magnetisierung mit 41 Am^2/kg bis 75 Am^2/kg im Bereich von reinem Magnetit liegt, ist eine effektive Abtrennung des suspendierten Mikrosorbens mittels eines moderaten Magnetfeldes möglich. Der isoelektrische Punkt liegt bei pH 3 und entspricht dabei den Werten von reinen MnO_2 . Dadurch verhält sich das Sorbens fast ausschließlich als Kationenaustauscher, wobei aber auch die Sorption von Oxyanionen möglich ist.

Sorptionsexperimente wurden durchgeführt und mittels Langmuir- und Freundlich-Isothermen ausgewertet. Dabei wurde der Einfluss des pH-Wertes, von kompetitiver Sorption und von Komplexbildnern bestimmt. Gleichgewichtsversuche mit Cd^{2+} , Ni^{2+} und Pb^{2+} -Ionen zeigten, dass die Sorption stark vom pH der Lösung abhängt. Die unerwünschte Sorption von alkalischen Ionen, wie Ca^{2+} , findet nur bei sehr hohen Konzentrationen statt. Andere Ionen, z.B. Chlorid, beeinflussen ebenfalls den Austausch, da dadurch Änderungen in der Metallionenspezifikation auftreten.

Die Versuche zur Sorptionskinetik wurden über vier kinetische Modelle ausgewertet: Film-Diffusion, Lagergren bzw. Reaktion pseudo-erster Ordnung, Reaktion pseudo-zweiter Ordnung und das Kinetikmodell nach Elovich. Die tatsächlich stattfindende Sorptionskinetik lässt sich hierbei am besten durch die Theorie der Film-Diffusion beschreiben. Mit Hilfe dieses Modells und unter Verwendung der bestimmten Gleichgewichtsparameter wurde eine gute theoretische Beschreibung des Verlaufs der Sorption bei allen untersuchten Bedingungen erreicht.

Aufgrund der kleinen Partikeldurchmesser und der dadurch bedingten großen spezifischen Oberfläche verläuft die Sorption sehr schnell. Es konnte beobachtet werden, dass in den ersten 10 Minuten eines Sorptionsexperiment etwa 90% der Gesamtadsorption stattfinden und das Gleichgewicht nach etwa einer Stunde erreicht wird.

Zusätzlich zu den Versuchen mit Schwermetallkationen wurden auch Sorptionsexperimente zur Kinetik und zum Gleichgewicht mit MoO_4^{2-} -Oxyanionen durchgeführt. Dabei wurde herausgefunden, dass auch für diese eine effektive Sorption möglich ist und dieser Prozess ebenfalls sehr schnell und stark pH-abhängig abläuft.

Mittels der durchgeführten Experimente und deren Ergebnissen konnte die Reihenfolge der Sorptionskapazität wie folgt bestimmt werden: $\text{Pb}^{2+} > \text{Ni}^{2+} \geq \text{Cd}^{2+} \gg \text{MoO}_4^{2-}$.

Abschließend zeigten aufeinanderfolgende Sorptions-Desorptions-Zyklen, dass die hergestellten magnetischen Mikrosorbentien regeneriert und wiederverwendet werden können. Allerdings nimmt die Sorptionskapazität während der ersten Zyklen deutlich ab. Gleichwohl macht die hohe Selektivität des hergestellten Mikrosorbens für zweiwertige Schwermetallionen diesen zu einer interessanten Alternative gegenüber klassischen Ionenaustauschern. Im Ausblick der vorliegenden Arbeit wird daher ein Prozessschema vorgeschlagen, das sich für eine Anwendungen der magnetischen Mikrosorbentien im industriellen Maßstab eignet.

Table of Contents

Acknowledgements	i
Abstract	iii
Zusammenfassung	v
1 Introduction	1
2 General Aspects	4
2.1 Manganese Oxides and Hydrous Oxides.....	4
2.1.1 Sorption evidence	7
2.1.2 Application in technical processes	10
2.2 Metal Ions and Oxyanions.....	12
2.2.1 Speciation of Metal Ions.....	12
2.2.1.1 Cadmium speciation	13
2.2.1.2 Nickel speciation	15
2.2.1.3 Lead speciation.....	17
2.2.2 Speciation of Oxyanions.....	19
2.2.2.1 Molybdenum speciation	19
2.3 Sorption of Cations and Anions	21
2.3.1 Factors affecting the adsorption	22
2.3.1.1 Effect of pH	22
2.3.1.2 Effect of complexing ligands.....	25
2.3.1.3 Effect of competitive adsorption	25
2.4 Particles Coating.....	25
2.4.1 Synthesis of magnetic microparticles	26
2.4.1.1 Synthesis of MnO ₂	27
2.4.1.2 Coating of magnetic particles used as core	27
3 Evaluation of Sorption	29
3.1 Sorption Equilibrium	29

3.1.1	Experimental determination of sorption isotherms.....	29
3.1.1.1	Langmuir isotherm.....	30
3.1.1.2	Freundlich isotherm.....	33
3.2	Sorption Kinetics.....	33
3.2.1	Film diffusion.....	34
3.2.1.1	Mathematical approaches for describing the film diffusion.....	35
3.2.1.2	Mass transfer correlations.....	37
3.2.2	Alternative models for describing sorption kinetics.....	40
3.2.2.1	Pseudo first order approach.....	40
3.2.2.2	Pseudo-second order approach.....	41
3.2.2.3	Elovich equation.....	42
4	Experimental Part.....	43
4.1	Synthesis of magnetic micro sorbent (MMS).....	43
4.1.1	Reproducibility.....	44
4.2	Elemental analyses.....	45
4.3	Characterization measurements.....	45
4.3.1	ESEM and EDX analysis.....	45
4.3.2	Specific surface area measurements by means of BET adsorption method....	45
4.3.3	Density measurements.....	45
4.3.4	Particle size and distribution measurements.....	46
4.3.5	Magnetic susceptibility measurements.....	46
4.4	Magnetic solid-liquid separation.....	46
4.5	Chemical stability.....	47
4.6	Zeta potential measurements.....	47
4.7	Equilibrium studies.....	48
4.7.1	Influence of different paramateres on sorption equilibrium.....	49
4.7.1.1	Effect of pH.....	49

4.7.1.2	Effect of complexing ligands.....	49
4.7.1.3	Effect of competitive adsorption	49
4.8	Kinetic studies	50
4.8.1.1	Effect of initial concentration.....	50
4.8.1.2	Effect of mass of adsorbent	51
4.8.1.3	Effect of competitive adsorption	52
4.9	Desorption and reusability studies.....	52
5	Results and Discussion	54
5.1	Synthesis of magnetic microsorbent (MMS).....	54
5.1.1	Physicochemical analyses	54
5.1.1.1	Reproducibility of the synthesis	55
5.1.2	ESEM images	56
5.1.3	Particle size and distribution.	58
5.1.4	Density.....	58
5.1.5	Chemical stability.....	59
5.1.6	Magnetic characterization.....	60
5.1.7	Magnetic solid-liquid separation.....	62
5.1.8	Zeta potential	66
5.2	Equilibrium studies.....	69
5.2.1	Effect of pH	69
5.2.2	Effect of competitive ions	79
5.2.3	Effect of complexing ions	84
5.3	Kinetic studies	89
5.3.1	Cadmium sorption kinetics.....	89
5.3.2	Nickel sorption kinetics.....	91
5.3.3	Lead sorption kinetics.....	92
5.3.4	Molybdenum sorption kinetics.....	94

5.3.5	Numerical evaluation of the sorption kinetics	95
5.3.5.1	Film diffusion model.....	96
5.3.5.2	Lagergren model (pseudo-first-order model).....	100
5.3.5.3	Pseudo-second-order	102
5.3.6	Sorption kinetic modelling.....	105
5.4	Consecutive cycles of adsorption – desorption.....	107
6	Conclusions.....	110
7	Bibliography	115
8	Appendix.....	123
8.1	List of symbols.....	123
8.2	Analytical methods, Chemicals and Apparatus	125
8.2.1	Analytical methods	125
8.2.2	Used chemicals	125
8.2.3	Apparatus	125
8.3	Others.....	126
8.4	Curriculum vitae	127

List of Tables

Table 2.1: Manganese oxide minerals.	5
Table 2.2: Comparison of the $pH_{(PZC)}$ values for various metal oxides.....	8
Table 2.3: Equilibrium constants of hydroxyl complexes of cadmium metal ions at 25°C.	13
Table 2.4: Formation constants of complexes and solids from cadmium metal ions and Cl^- as ligand.....	15
Table 2.5: Equilibrium constants of hydroxyl complexes of nickel metal ions at 25°C.	17
Table 2.6: Equilibrium constants of complexes for lead metal ions.	18
Table 2.7: Formation constants of complexes from molybdenum anions and H^+ as ligand, at 25°C.	20
Table 2.8: Molybdate species in aqueous solutions.	21
Table 3.1 : Ionic mobility values for Cd^{2+} , Ni^{2+} , and Pb^{2+}	38
Table 3.2 : Hydrated ionic radius values for Cd, Ni, and Pb	39
Table 4.1 : Digestion program for the decomposition procedure of the micro-sorbent material.	45
Table 4.2 : Initial concentration range of Cd(II), Ni(II), Pb(II), and Mo(VI) used for the equilibrium studies.	48
Table 4.3 : Variables used for the kinetic experiments based on the variation of bulk solution concentration with time.....	50
Table 4.4 : Variables used for the kinetic experiments based on the variation of bulk solution concentration with time.....	51
Table 4.5 : Variables used for the steps involved in the desorption and reusability studies.	53
Table 5.1 : Elemental analyses of magnetic micro-sorbents.....	54
Table 5.2 : Specific surface area values obtained for different Fe_3O_4 : MnO_2 ratios.	54
Table 5.3 : Disolution of MMS at various pH values.....	59
Table 5.4 : Saturation magnetization of Fe_3O_4 : MnO_2 materials.	61
Table 5.5 : Equilibrium parameters for sorption of Cd^{2+} , Ni^{2+} , and Pb^{2+} onto MMS at different pH values deduced by means of Langmuir and Freundlich relationships. T = 25°C.	73
Table 5.6 : Equilibrium parameters for sorption of molybdate species onto MMS deduced by means of Langmuir and Freundlich relationships.....	76
Table 5.7 : Equilibrium parameters for the sorption of Cd^{2+} , Ni^{2+} , and Pb^{2+} onto MMS at different concentrations of Ca^{2+} deduced by means of Langmuir and Freundlich relationships. T = 25°C.....	82

Table 5.8 : Equilibrium parameters for sorption of Cd^{2+} , Ni^{2+} , and Pb^{2+} onto MMS at different electrolyte solutions deduced by means of Langmuir and Freundlich relationships. $T = 25^\circ\text{C}$	87
Table 5.9 : Mass transfer coefficients experimentally obtained by means of the Film diffusion model for sorption of Cd^{2+} , Ni^{2+} , Pb^{2+} , and MoO_4^{2-} onto MMS at different initial concentrations and sorbent dosage. $T = 25^\circ\text{C}$	97
Table 5.10 : Diffusion coefficients of cations in water at 25°C	98
Table 5.11 : Schmidt numbers for the metal ions Cd^{2+} , Ni^{2+} , Pb^{2+} , and MoO_4^{2-} at 25°C	99
Table 5.12 : Theoretic mass transfer coefficients for the metal ions Cd^{2+} , Ni^{2+} , Pb^{2+} , and MoO_4^{2-}	99
Table 5.13 : Kinetic parameters obtained by means of the Largegren model for sorption of Cd^{2+} , Ni^{2+} , Pb^{2+} , and MoO_4^{2-} onto MMS at different initial concentrations and amounts of sorbent. $T = 25^\circ\text{C}$	101
Table 5.14 : Kinetic parameters obtained by means of the pseudo-second-order model for sorption of Cd^{2+} , Ni^{2+} , Pb^{2+} , and MoO_4^{2-} onto MMS at different initial concentrations and amounts of sorbent. $T = 25^\circ\text{C}$	103
Table 5.15 : Kinetic parameters obtained by means of the pseudo-second-order model for sorption of Cd^{2+} , Ni^{2+} , Pb^{2+} , and MoO_4^{2-} onto MMS at various initial concentrations and amount of adsorbent.	104
Table 5.16 : Langmuir parameteres for Cd(II), Ni(II), Pb(II), and Mo(VI) used for sorption kinetic modelling.	105
Table 8.1 : Physicochemical characteristics of magnetite (Bayoxide E 8710), Bayer.	126

List of Figures

Figure 2.1: Polyhedral representations of the crystal structures of (A) pyrolusite, (B) ramsdellite, (C) hollandite, (D) romanechite, and (E) todorokite, looking approximately parallel to the Mn octahedral chains (Post 1999).....	6
Figure 2.2: Polyhedral representation of (A) lithiophorite showing alternately stacked layers of MnO ₆ (blue) and (Al, Li)(OH) ₆ (red) octahedra, (B) chalcophanite with Zn cations (green octahedra) occupying positions above and below vacancies in the Mn octahedral layers, and (C) Na-rich birnessite-like phase showing disordered H ₂ O/Na sites (yellow) sandwiched between the Mn octahedral sheets (Post 1999).	7
Figure 2.3: Distribution diagram for cadmium hydroxy complexes in an aqueous solution of Cd(II). $c_{Cd} = 10^{-6}$ mol/L, T= 25 °C (MINEQL+ [©]).....	14
Figure 2.4: Distribution diagram for nickel hydroxy complexes in an aqueous solution of Ni(II). $c_{Ni} = 10^{-6}$ mol/L, T= 25°C (MINEQL+ [©]).....	16
Figure 2.5: Distribution diagram for lead hydroxy complexes in an aqueous solution of Pb(II). $c_{Pb} = 10^{-6}$ mol/L, T= 25°C (MINEQL+ [©]).....	18
Figure 2.6: Distribution diagram of molybdenum species in an aqueous solution of Mo(VI). $c_{Mo} = 10^{-6}$ mol/L, T= 25°C (MINEQL+ [©]).....	20
Figure 2.7: Schematic of the preparation of coated particles by the precipitation from solution onto dispersed particles.	26
Figure 3.1: Langmuir isotherm and its limiting cases, at constant V_L/m_s and varying c_i	32
Figure 3.2: Development of concentrations during film diffusion.....	35
Figure 4.1: Schematic design of the batch system on a laboratory scale. A: Preparation of the initial suspension; B: Formation of the MnO ₂ coating.....	44
Figure 5.1: Reproducibility of material synthesis tested by means of sorption experiments with a solution of Cd(II) onto 8 magnetic microsorbents with a Fe ₃ O ₄ : MnO ₂ ratio of 1:1. $c_{Cd} = 8.9 \times 10^{-3}$ mmol/L, pH = 7, T = 25°C.	55
Figure 5.2: ESEM image of MMS synthesized by the precipitation of MnO ₂ in the presence of magnetite particles.	56
Figure 5.3: ESEM image of MMS. Magnification of Figure 5.2.	57
Figure 5.4: EDX analysis of the surface of the MMS particles shown in Figure 6.3.....	57
Figure 5.5: Particle size distribution (q_0) of the synthesized MMS.	58
Figure 5.6: Dissolution process at an oxide surface site proton-promoted.	59

Figure 5.7: Magnetization curves of micro magnetic adsorbents for different Fe_3O_4 : MnO_2 ratios.	60
Figure 5.8: Magnetization curves of Fe_3O_4 and MMS.	61
Figure 5.9: Relative turbidity of MMS suspension at various settling times and pH ranging from 3 to 9. No external magnetic field applied.	62
Figure 5.10: Relative turbidity of MMS suspension under a magnetic field at various settling times and pH ranging from 3 to 9.	63
Figure 5.11: Relative turbidity of MMS suspension at various settling times in water as well as in 0.001 and 0.01 mol/L NaNO_3 solutions. No influence of an external magnetic field.	64
Figure 5.12: Relative turbidity of supernatants of MMS suspension at various settling times under a magnetic field for water and 0.001 and 0.01 mol/L NaNO_3 solutions.	65
Figure 5.13: Zeta potential versus pH for the material MMS measured by means of the microelectrophoresis technique (MET). 0.01 mol/L NaNO_3 . $T = 25^\circ\text{C}$	66
Figure 5.14: Zeta potential versus pH for pure MnO_2 measured by means of the microelectrophoresis technique (MET). 0.01 mol/L NaNO_3 . $T = 25^\circ\text{C}$	67
Figure 5.15: Experimental curve corresponding to the immersion technique (IT) for the determination of the $\text{pH}_{(\text{PZC})}$ of MMS. 0.01 mol/L NaNO_3 , $T = 25^\circ\text{C}$	68
Figure 5.16: Sorption isotherms of Cd^{2+} ions at different initial pH values. $c_{\text{NaNO}_3} = 0.01$ mol/L, $m_s = 5$ mg, $T = 25^\circ\text{C}$. Evaluation by means of the Langmuir relationship.	69
Figure 5.17: Sorption isotherms of Cd^{2+} ions at different initial pH values. $c_{\text{NaNO}_3} = 0.01$ mol/L, $m_s = 5$ mg, $T = 25^\circ\text{C}$. Evaluation by means of the Freundlich relationship.	70
Figure 5.18: Sorption isotherms of Ni^{2+} ions at different pH values. $c_{\text{NaNO}_3} = 0.01$ mol/L, $m_s = 5$ mg, $T = 25^\circ\text{C}$. Evaluation by means of the Langmuir relationship.	71
Figure 5.19: Sorption isotherms of Pb^{2+} ions at different pH values. $c_{\text{NaNO}_3} = 0.01$ mol/L, $m_s = 1.25$ mg, $T = 25^\circ\text{C}$. Evaluation by means of the Langmuir relationship.	72
Figure 5.20: Sorption isotherms of molybdate species at various pH values. $m_s = 40$ mg. Evaluation by means of the Freundlich relationship. $T = 25^\circ\text{C}$	75
Figure 5.21: Schematic figure of the charge acquisition onto manganese dioxide surface.	77
Figure 5.22: Sorption isotherms of Cd^{2+} ions at different concentrations of Ca^{2+} . $\text{pH} = 7$, $m_s = 5$ mg, $T = 25^\circ\text{C}$. Evaluation by means of the Langmuir relationship.	79
Figure 5.23: Sorption isotherms of Ni^{2+} ions at different concentrations of Ca^{2+} . $\text{pH} = 7$, $m_s = 5$ mg, $T = 25^\circ\text{C}$. Evaluation by means of the Langmuir relationship.	80

Figure 5.24: Isotherms of the sorption of Pb^{2+} ions at different concentrations of Ca^{2+} . pH = 6, $m_s = 1.25$ mg/L, $T = 25^\circ C$. Evaluation by means of the Langmuir relationship....	80
Figure 5.25: Isotherms of the sorption of Cd^{2+} ions with different electrolyte solutions. pH 7, $m_s = 5$ mg, $T = 25^\circ C$. Evaluation by means of the Langmuir relationship.	84
Figure 5.26: Sorption isotherms of Ni^{2+} ions with different electrolyte solutions. pH = 7, $m_s = 5$ mg, $T = 25^\circ C$. Evaluation by means of the Langmuir relationship.....	85
Figure 5.27: Sorption isotherms of Pb^{2+} ions with different electrolyte solutions. pH = 6, $m_s = 1.25$ mg, $T = 25^\circ C$. Evaluation by means of the Langmuir relationship.....	86
Figure 5.28: Plot of the relative concentration versus time for the sorption of Cd^{2+} onto MMS at different initial concentrations. pH = 7, $m_s = 10$ mg, $T = 25^\circ C$	89
Figure 5.29: Plot of the relative concentration versus time for the adsorption of Cd^{2+} onto MMS at various sorbent dosage. pH = 7, $c_{Cd} = 8.5 \times 10^{-3}$ mmol/L, $T = 25^\circ C$	90
Figure 5.30: Plot of the relative concentration versus time for the adsorption of Ni^{2+} onto MMS at different initial concentrations. pH = 7, $m_s = 10$ mg, $T = 25^\circ C$	91
Figure 5.31: Plot of the relative concentration versus time for the adsorption of Ni^{2+} onto MMS at different amounts of adsorbent. pH = 7, $c_{Ni} = 1.6 \times 10^{-2}$ mmol/L, $T = 25^\circ C$	92
Figure 5.32: Plot of the relative concentration versus time for the adsorption of Pb^{2+} onto MMS at different initial concentrations. pH = 6, $m_s = 10$ mg, $T = 25^\circ C$	93
Figure 5.33: Plot of the relative concentration versus time for the adsorption of Pb^{2+} onto MMS at different amounts of adsorbent. pH = 6, $c_{Pb} = 10 \times 10^{-3}$ mmol/L, $T = 25^\circ C$	93
Figure 5.34: Plot of the relative concentration versus time for the adsorption of MoO_4^{2-} at different initial concentrations. pH = 4, $m_s = 20$ mg, $T = 25^\circ C$	94
Figure 5.35: Plot of the relative concentration versus time for the adsorption of MoO_4^{2-} at different amounts of MMS. pH = 4, $c_{Mo} = 1.0 \times 10^{-2}$ mmol/L, $T = 25^\circ C$	95
Figure 5.36: Sorption of Pb onto MMS for five consecutive cycles. $c_{Pb} = 3.6 \times 10^{-3}$ mmol/L, pH = 6, $V_{L,s} = 1$ L, $m = 3.4$ mg, $T = 25^\circ C$	107
Figure 5.37: Desorption of Pb^{2+} from MMS for five consecutive cycles. $V_L = 0.01$ L, pH = 3.5, $T = 25^\circ C$	108
Figure 6.1: Illustration of a heavy metal treatment process using magnetic microsorbents and different solid-liquid separations applying magnet technology. A: Sorption process, B: Desorption and washing processes.....	113

1 Introduction

Pollution of ground and surface water with heavy metals is a major concern with respect to human health due to their extreme toxicity and to the fact of not being chemically or biologically degradable. Some of these metal ions are dangerous even at very low concentrations. Heavy metals may have natural origins such as leaching of underground minerals or they are introduced into the water streams as a result of anthropogenic and industrial activities. Metal processing facilities, mining operations, battery manufacturing, production of paints and pigments, glass production, etc. are responsible for emissions of metal ions among other contaminants. Inputs of heavy metals into bodies of water lead to a deterioration of water quality and cause an obvious necessity of purification and elimination of a variety of contaminating species (Economopoulos 1996; Aksu, Açıkel et al. 2002) .

Toxicity levels depend on the type of metal, its biological role, and the type of organisms that are exposed. Heavy metals linked most frequently to human health problems are lead, mercury, arsenic and cadmium. Other heavy metals, including copper, zinc, and chromium, are essential trace components required by the body in small amounts, but can be toxic in larger doses (Wood 1975; Nies 1999).

Various treatment techniques have been applied to remove metal ions from contaminated waters such as chemical precipitation (Christensen and Delwiche 1982), adsorption and ionic exchange, membrane technology (Tripathy, Sarangi et al. 2002) and solvent extraction (Stenström 1987). Over the last few decades, sorption has gained importance as an effective purification technique used in wastewater treatment, and the removal of heavy metals is considered an important application of adsorption processes using a suitable adsorbent. A number of adsorbents such as polymeric materials, zeolites (Peric, Trgo et al. 2004), activated carbon (Leyva-Ramos, Rangel-Mendez et al. 1997), clay minerals (Puls and Bohn 1988) and biosorbents (Volesky 2001; Aksu, Açıkel et al. 2002) have been used in the adsorption process.

In recent years, many researchers have applied metal oxides for the adsorption of heavy metals from water systems (Davranche 2000; Kanungo, Tripathy et al. 2004; Kanungo, Tripathy et al. 2004; Dong, Liu et al. 2007). Hydrous manganese oxide belongs to those metal oxides thought as natural scavengers of heavy metals in water systems. In the natural environment, trace metals, such as Cu^{2+} , Pb^{2+} , Ni^{2+} and Zn^{2+} , can be strongly associated with manganese oxides. Because of its large surface area, microporous structure, and OH

functional groups capable of reacting with metals and other specifically sorbing ions; hydrous manganese oxides provide an efficient capture pathway for heavy metals (Al-Sewailem, Khaled et al. 1999). Hydrous manganese oxide is one kind of surface acidic oxides, whose pH_{PZC} (point of zero charge) value is about 1.5 – 4.5 and the charge of the hydrous oxide depends on the pH of the medium. Commonly, the surface charge of manganese oxide is negative, and it can be used as an adsorbent to remove heavy metals from wastewater (Mc Kenzie 1989). However, pure hydrous manganese oxide as a filter media is not completely favorable. The fine particle size makes it very difficult to separate from the water phase or to infiltrate through. Nevertheless, coating manganese oxide to a media surface which can improve the solid-liquid separation may provide a promising adsorbent for heavy metals from wastewater.

Regarding these difficulties many researchers have combined metal oxides with other materials because of their potential as effective sorbents. Respective examples are the combination of hydrous oxides with materials such as activated carbon (Fan and Anderson 2005), zeolite (Han, Zou et al. 2006) and sand (Han, Zou et al. 2006) for metal ions removal.

Another kind of adsorbent materials possessing high adsorption capacity comprises metal oxide adsorbents with magnetic properties. The application of polymeric and inorganic magnetic micro-sorbents technology to solve environmental problems is a method that has received considerable attention in recent years (Zhang, Vigneswaran et al. 2006; Mergen, Jefferson et al. 2008; Zhang, Ma et al. 2008). Magnetic inorganic micro-sorbents can be used to adsorb contaminants from either aqueous or gaseous effluents and once the adsorption is carried out, the “loaded adsorbent” can be separated from the medium by a simple magnetic process. Clay materials and zeolites (Oliveira, Rios et al. 2003; Oliveira, Petkowicz et al. 2004), activated carbon (Safarik, Nymburská et al. 1997), carbon nanotubes (Peng, Luan et al. 2005) have been combined with iron oxide, such as maghemite or magnetite, to produce a magnetic adsorbent.

Magnetic micro-sorbents prepared from hydrous manganese oxide can be produced by means of the oxidation of manganese ions due to the action of an oxidizing agent in presence of magnetic particles such as magnetite. The advantage of such sorbent material is its very large specific surface and, therefore, the fast adjustment of sorption equilibria. The magnetic property allows the material to be easily recovered by means of magnetic separation methods after adsorption or regeneration, which overcomes the disadvantage of separation difficulties with common adsorbents.

Therefore, the objective of the studies described here was to investigate the synthesis of manganese oxide-coated magnetite and its application as magnetic micro-sorbent (MMS) for removing metal species from aqueous solutions. The respective work was to have several subtopics: i) the reproducible production of stable materials, ii) their physical and chemical characterization, iii) investigations about sorption equilibria and kinetics, and iv) the theoretical description by means of physicochemical and engineering approaches.

2 General Aspects

2.1 Manganese Oxides and Hydrrous Oxides

The most extensive deposition of manganese oxides today occurs in the ocean as nodules, microconcretions, coatings and crusts (Crerar and Barnes 1974) and associated to these nodules other minerals such as clay minerals, quartz, calcite, apatite, biotite and feldspars are also found (Riley and Sinhaseni 1958). Ocean nodules were first discovered in 1873 during the expedition of the H.M.S. Challenger (Office 1979) and since then they have been found at almost all depths and latitudes in all of the oceans and seas of the world (Crerar and Barnes 1974); it has been estimated that they cover about 10-30% of the deep Pacific floor (Menard and Shipek 1958) nodules are heterogeneous mixtures of very fine grained iron and manganese oxides, detrital mineral grains, and biogenic components deposited in semiconcentric layers around a central nucleus of variable composition (Margolis and Burns 1976). Several studies of the bulk chemistry of manganese nodules in different regions confirm that marine nodules are enriched in many metals including Mn, Fe, Co, Ni, Cu, Zn, Pb, Mo, and Ti (Glasby and Lawrence 1974).

Research on the complex mineralogy of the iron and manganese oxides in ocean manganese nodules has been hampered by the fact that the minerals typically occur as thin layers of fine-grained, poorly crystalline mixtures. Nevertheless, it has been concluded that the predominant minerals are manganese (IV) related to the terrestrial minerals todorokite, birnessite and nsutite. Disordered phases showing only short range crystallographic order include δ -MnO₂ and hydrated ferric oxyhydroxide polymer (incipient goethite) (Burns and Burns 1978). The mineralogy of manganese oxides is more varied than other oxides such as aluminum or iron oxides, because besides Mn⁴⁺ they may contain Mn³⁺ and Mn²⁺ and for the charge balancing foreign ions as Li, Na, K, Ca, Ba, Al and Fe are easily accommodated in the structure. Thus, manganese oxides are frequently non-stoichiometric compounds (Scheffer and Schachtschabel 1989).

Many naturally occurring and synthetic oxide phases of manganese relevant to our understanding are listed in Table 2.1 (Burns and Burns 1978).

Table 2.1: Manganese oxide minerals.

Group	Mineral or compound	Composition
β -MnO ₂	Pyrolusite	MnO ₂
	Ramsdellite	MnO ₂
γ -MnO ₂	Nsutite	Mn ⁴⁺ _(1-x) Mn ²⁺ _x O _(2-2x) (OH) _{2x}
Hollandite	Synthetic α - MnO ₂	MnO ₂ ·nH ₂ O
Hollandite	Hollandite	Ba _x (Mn ⁴⁺ , Mn ³⁺) ₈ O ₁₆
Hollandite	Cryptomelane	K _x (Mn ⁴⁺ , Mn ³⁺) ₈ O ₁₆
Hollandite	Coronadite	Pb _x (Mn ⁴⁺ , Mn ³⁺) ₈ O ₁₆
Psilomelane	Romanèchite	Ba _{.66} (Mn ⁴⁺ ,
Birnessite	Synthetic sodium manganese (II,III) manganate (IV)	Na ₄ Mn ₁₄ O ₂₇ ·9H ₂ O
	7-Å manganite	(4MnO ₂ ·Mn(OH) ₂ ·2H ₂ O)
	Synthetic δ -MnO ₂	
	Birnessite	(Na, Ca)(Mn ²⁺ Mn ⁴⁺)O ₁₄ ·3H ₂ O
Chalcophanite	Chalcophanite	ZnMn ₃ O ₇ ·3H ₂ O
Buserite	Buserite or synthetic sodium (manganese(II, III) manganite(IV) hydrate)	
	10-Å manganite	(Na,Mn)Mn ₃ O ₇ ·nH ₂ O
Todorokite	Todorokite	(Na, Ca, K, Ba, Mn ²⁺) ₂ Mn ₅ O ₁₂ ·3H ₂ O
Lithiophorite Oxide	Lithiophorite	(Al, Li)MnO ₂ (OH) ₂
Hydroxides		
α - MnOOH	Groutite	MnOOH
β -MnOOH	Feitknechtite	MnOOH
γ -MnOOH	Manganite	MnOOH

Despite the fact that manganese oxides have been extensively studied for the past several decades, the details of many of these are poorly understood. Nevertheless, a convenient general description of manganese oxides may be discussed as follows:

The basic building block for most of the manganese oxide atomic structures is the MnO₆ octahedron. These octahedra can be assembled by sharing edges and/or corners into a large variety of different structural arrangements, most of which are part of one of two major groups: i) chain, or tunnel structures and ii) layered structures. The tunnel Mn oxides are constructed of single, double or triple chains of edge-sharing MnO₆ octahedra, and the chains

share corners with each other to produce frameworks that have tunnels with square or rectangular cross sections. Tunnel structures are shown in Figure 2.1.

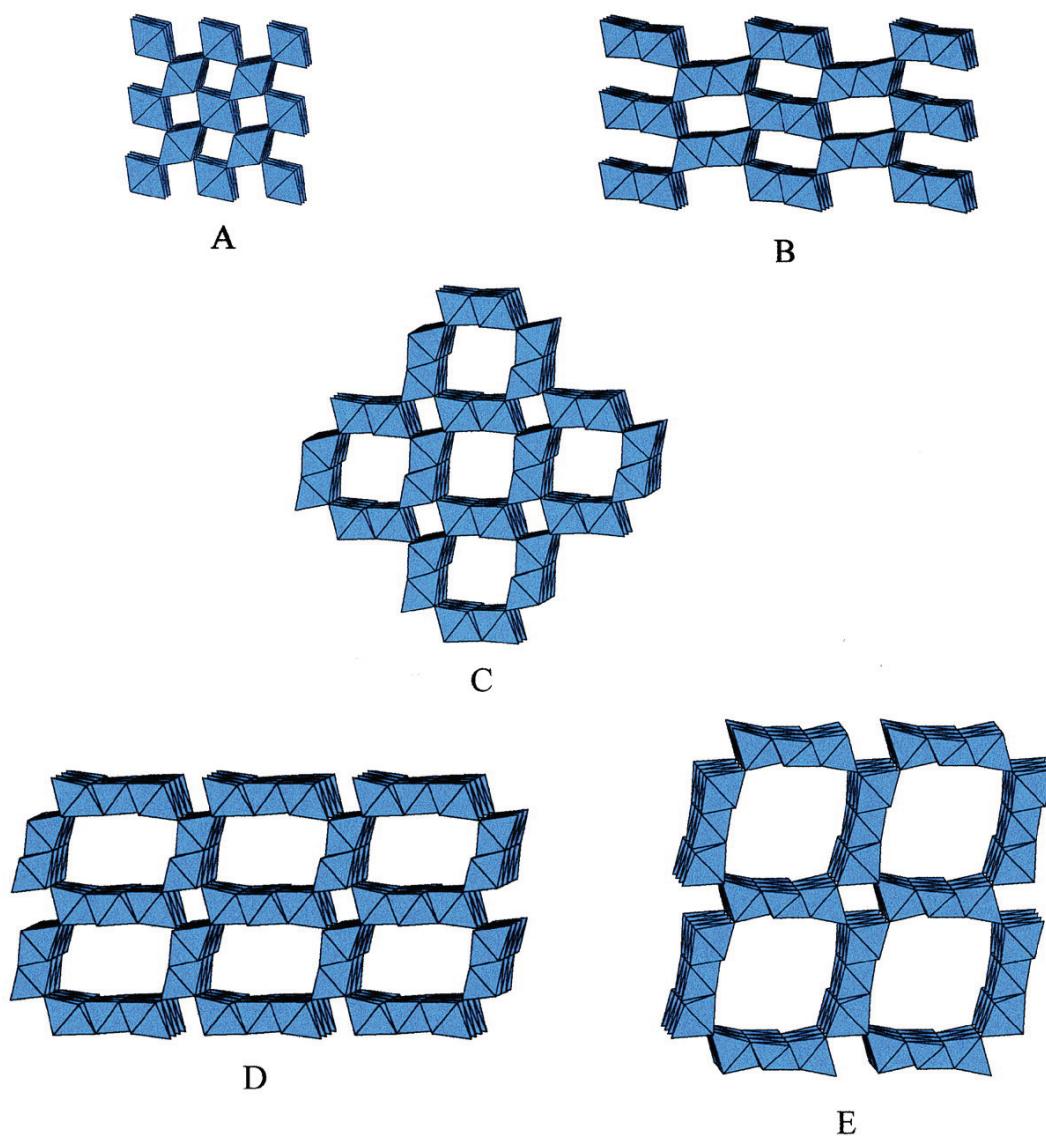


Figure 2.1: Polyhedral representations of the crystal structures of (A) pyrolusite, (B) ramsdellite, (C) hollandite, (D) romanèchite, and (E) todorokite, looking approximately parallel to the Mn octahedral chains (Post 1999).

The layer Mn oxides consist of stacks sheets, or layers, of edge-sharing MnO₆ octahedra where the interlayer regions can host water molecules and a wide range of cations (Post 1999). In the group of tunnel structures pyrolusite, ramsdellite, nsutite, hollandite, cryptomelane and coronadite besides romanèchite and todorokite are included, while in the group of layered structures birnessite, vernadite, chalcophanite, busserite and lithiophorite are found (Mc Kenzie 1989). Layered structures are shown in Figure 2.2.

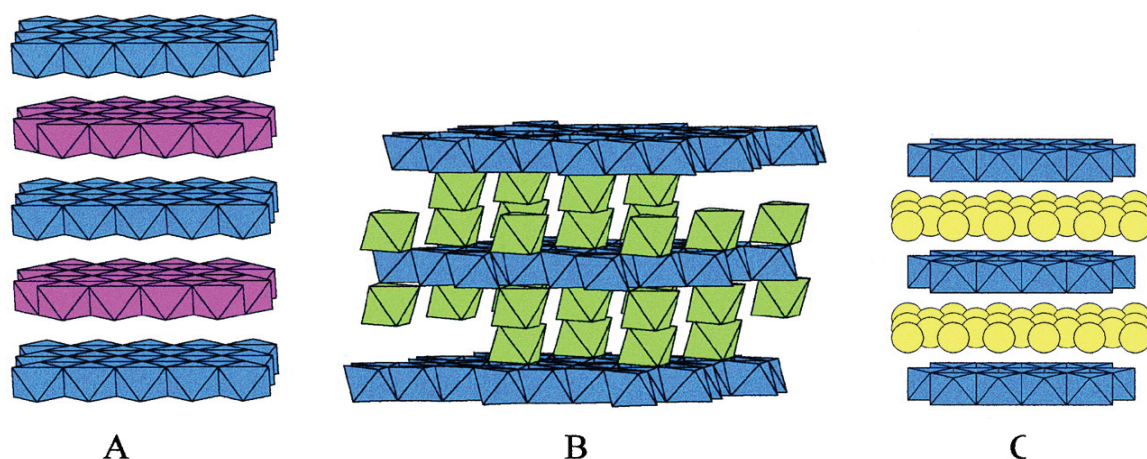


Figure 2.2: Polyhedral representation of (A) lithiophorite showing alternately stacked layers of MnO_6 (blue) and $(\text{Al}, \text{Li})(\text{OH})_6$ (red) octahedra, (B) chalcophanite with Zn cations (green octahedra) occupying positions above and below vacancies in the Mn octahedral layers, and (C) Na-rich birnessite-like phase showing disordered $\text{H}_2\text{O}/\text{Na}$ sites (yellow) sandwiched between the Mn octahedral sheets (Post 1999).

2.1.1 Sorption evidence

It has been proposed that hydrous oxides of manganese and iron widely control and determine the concentrations of certain transition metals in soils and natural waters. The occurrence of the hydrous oxides in soils and sediments as partial coatings on certain minerals rather than as discrete, well-crystallized minerals, allows the oxides to exert chemical influences far out of proportion to their concentration (Jenne 1968).

Manganese oxides are particularly surface-active with large amounts of pH-dependent surface charges, rather low $\text{pH}_{(\text{PZC})}$ (point of zero charge), large surface areas and high oxidizing capacities. In natural systems such as soils, sediments and water such as the hydrous oxides of iron, aluminium, manganese and silicon which have the potential to form surface complexes with the various cationic and anionic dissolved species (Ure and Davidson 2002).

In general hydrous manganese oxides suspended in waters and present in sedimentary and soil concretions are frequently amorphous, characterized by high specific surface areas; areas up to $300\text{m}^2\text{g}^{-1}$ have been reported (Stumm and Morgan 1966). They possess surface charges which vary with the pH of the medium, called pH-dependent surface. The potential determining ions are principally H^+ and OH^- determining the point of zero charge, $\text{pH}_{(\text{PZC})}$, a useful quantity for predicting how the charge depends on pH. $\text{pH}_{(\text{PZC})}$ values of types of

manganese dioxides occurring in soils range from 1.5 for birnessite to 4.5 for the hollandite group (Healy, Herring et al. 1966). In the case of hydrous manganese oxide, the $\text{pH}_{(\text{PZC})}$, has been determined to be about 2.2 (Murray 1974). Thus, for pH values greater than 2.2 the surface of hydrous manganese oxide has a negative charge. $\text{pH}_{(\text{PZC})}$ values of some metal oxides are summarized in Table 2.2. Because of the low $\text{pH}_{(\text{PZC})}$, large negative charge, and large surface area of the manganese oxides, specific adsorption of cations is, therefore, strongly expressed (Mc Kenzie 1989).

Correlations among certain elements such as Co^{2+} , Ni^{2+} , Cu^{2+} and Mn^{2+} in manganese nodules, in sediments and in suspended matter have suggested that the adsorption onto manganese surface is one of the mechanisms which explain these relationships (Goldberg 1954; Jenne 1968; Crerar and Barnes 1974).

Table 2.2: Comparison of the $\text{pH}_{(\text{PZC})}$ values for various metal oxides.

Oxide	$\text{pH}_{(\text{PZC})}$
Hydrous manganese dioxide	2.2
δ - MnO_2	1.5
α - MnO_2	4.5
γ - MnO_2	5.5
β - MnO_2	7.3
SiO_2 (amorphous)	1.8-2.0
TiO_2	6.0
γ - Al_2O_3	8.5
α - Fe_2O_3	8.5
ZnO	8.9
MgO	12.5

To understand the mechanism of adsorption through which the enrichment of manganese nodules with metals occurs, different studies on the surface chemistry of hydrous manganese dioxide have been carried out (Morgan and Stumm 1964; Murray, Healy et al. 1968; Posselt, Anderson et al. 1968). A comprehensive study of the surface chemistry of hydrous manganese dioxide was obtained from experiments performed using a synthetically prepared hydrous manganese dioxide with similar structure and oxidation grade to manganese phases found in nature. It is referred as hydrous manganese dioxide (Murray 1974; Murray 1975). Experiments have shown that the adsorption capacity of freshly precipitated hydrous manganese oxides is extremely high for a variety of metal cations.

Experimental results have indicated that the alkali metal ions show no specific adsorption to manganese oxides; thus they only react electrostatically with the surface (Murray 1975). Na^+ and K^+ are not adsorbed onto hydrous manganese dioxide below the $\text{pH}_{(\text{PZC})}$. The transition metal ions react more strongly with hydrous manganese dioxide than do the alkaline earth species. Among the alkaline earths, Ba^{2+} interacts more strongly than Mg^{2+} , and among the transition metals, Co^{2+} interacts more strongly than Ni^{2+} . The selectivity sequence for all of these metal studies is:



The ions that are most strongly adsorbed by increasing the pH are the most difficult to be desorbed by decreasing the pH.

Results of laboratory experiments for the adsorption of cobalt by hydrous manganese dioxide (Murray 1975) and data for the adsorption of cobalt ions by both hydrous ferric oxide (Kurbatov, Wood et al. 1951) and illite (Chester 1965) have determined that cobalt species are much better removed (by more than one order magnitude) by hydrous manganese dioxide than by clay minerals. They proved that the adsorption onto manganese dioxide is an important mechanism for controlling trace metal concentrations in sea water.

Further information about the adsorption of metal ions such as Co^{2+} , Ni^{2+} , Cd^{2+} , Cu^{2+} and Zn^{2+} onto synthetic hydrous manganese dioxide has been published during the last years. These studies have been focused on the adsorption behavior of trace metals by the hydrous manganese oxide and by admixtures with hydrous iron oxides. Interfacial properties of manganese dioxide in simple and complex electrolyte solutions have been investigated. The results have indicated that the adsorption of metal ions onto hydrous manganese dioxide is highly influenced by pH and take place on the highly heterogeneous oxide surface with different binding energies (Kanungo and Parida 1984). The studies carried out with complex electrolyte solutions have shown that the formation of certain chlorocomplexes of metal ions may change the type of sorption (Kanungo, Tripathy et al. 2004; Tripathy and Kanungo 2005; Tripathy 2006).

As a general result, it can be stated that adsorption or desorption of heavy metals occurs in response to the following factors: (1) aqueous concentration of the metal in question; (2) aqueous concentration of other metal ions; (3) pH; and (4) amount and strength of organic chelating agents and inorganic complex ion forming species present in solution (Jenne 1968).

Other studies regarding the adsorption capacity of hydrous manganese oxide have involved sorption experiments of other species such as selenium in the anionic forms of both selenate (SeO_4^{2-}) and selenite (SeO_3^{2-}). Studies have shown that by decreasing the pH of the solution the adsorption of selenium increases and that selenite shows a higher affinity for hydrous manganese oxide (Balistrieri and Chao 1990).

Additionally, it has been reported that manganese dioxide can act as important adsorbent of phosphate in natural waters as well as in surface sediments (Yao and Millero 1996).

2.1.2 Application in technical processes

The unusually high adsorption capacities and scavenging capabilities of manganese oxide/hydroxide minerals gave rise to investigations for applying these materials as adsorbent in technical processes. However, an important disadvantage of hydrous oxides for being used as adsorbents is the required solid-liquid separation after the adsorption. The difficulty is principally due to the fine particle size which does not allow a use as conventional filter media. Regarding these difficulties many researchers have combined metal oxides with other materials because of their potential as effective sorbents.

Among the materials with which manganese dioxide has been combined for metal ions removal, e.g. activated carbon, zeolite, and sand can be used; for which the solid-liquid separation is not a problem.

In the case of activated carbon, it has been found that the adsorption capacity for metal ions in a column process, is significantly improved by the presence of manganese oxide as a coating (Fan and Anderson 2005). Column experiments for the adsorption of Cu^{2+} and Pb^{2+} by using manganese oxide coated zeolite, have demonstrated an efficient removal of both metal ions from aqueous solutions. The removal followed the descending order: $\text{Pb(II)} > \text{Cu(II)}$ (Han, Zou et al. 2006). On the other hand batch experiments have shown that manganese oxide coated zeolite present much higher adsorption capacity for removing Cu^{2+} and Pb^{2+} ions than the pure zeolite (Zou 2006). Comparable results for the same metal species have been found for manganese oxide coated sand, where the competitive adsorption showed that the uptake of each metal was considerably reduced with an increasing concentration of the other, the adsorption of Cu^{2+} being more strongly influenced by Pb^{2+} than vice versa due to the higher affinity of the adsorbent for the latter (Han, Zou et al. 2006).

Application in other fields of water treatment have also been reported, e.g. manganese dioxide coated sand was effective for removal of arsenic from ground water in column experiments (Bajpai and Chaudhur 1999) .

The application of cellulose acetate impregnated with manganese oxides for the removal of metal ions has shown a high removal efficiency for Cu^{2+} , Pb^{2+} , and Zn^{2+} from aqueous solutions (Brandao and Galembeck 1990). It has also been reported that diatomite and manganese oxide modified diatomite are effective adsorbents for removing Pb^{2+} , Cu^{2+} , and Cd^{2+} ions. The sorption capacity of Mn-diatomite was considerably higher compared to the original material for removing the studied metals (Al-Degs, Tutunju et al. 2000; Al-Degs, Khraisheh et al. 2001).

From the above citations it can be stated that the application of metal oxides, particularly manganese oxides, has improved the metal adsorption capacity of materials which can easily be separated from aqueous solutions.

Another way to improve the solid-liquid separation is the application of magnetic technology. The application of polymeric and inorganic magnetic microsorbents to solve environmental problems is a method that has received considerable attention in recent years. Both, polymeric and inorganic magnetic microsorbents have been developed to enable adsorption of target contaminants; once they are loaded they can easily be separated from the aqueous solution by magnetic separation methods (Zhang, Vigneswaran et al. 2006; Mergen, Jefferson et al. 2008). Inorganic magnetic microsorbents have been obtained by using materials such as activated carbon, carbon nanotubes, clay materials and zeolites.

Adsorption features of activated carbon and the magnetic properties of iron oxides have been combined in a composite material to produce magnetic adsorbents. These magnetic particles can be used as adsorbent for a wide range of organic contaminants in water and can subsequently be removed from the medium by a simple magnetic procedure (Safarik, Nymburská et al. 1997; Oliveira, Rios et al. 2002).

The synthesis of carbon nanotubes iron oxide magnetic composites for the removal of Pb^{2+} and Cu^{2+} has been successfully carried out. By a simple magnetic process a recovery rate of 98% has been achieved (Peng, Luan et al. 2005). Clay iron oxide magnetic composites have been applied for the adsorption of metal ions such as Ni^{2+} , Cu^{2+} , Cd^{2+} and Zn^{2+} and it has been found that besides the magnetic properties, the presence of iron oxides has improved the adsorption capacity for such metal ions (Oliveira, Rios et al. 2003). Zeolite magnetic composites have also been successfully generated, but in this case the presence of iron oxides

has neither improved nor diminished the adsorption capacity for Cr^{3+} , Cu^{2+} and Zn^{2+} (Oliveira, Petkowicz et al. 2004).

In all the cases materials have been combined with iron oxides, such as maghemite or magnetite, to produce a magnetic adsorbent. The synthesis of all of these inorganic magnetic microsorbents has been obtained by means of the precipitation of iron oxides.

However, the use of magnetic technology can also be applied to allow the use of manganese oxide as an adsorbent. Thus, manganese oxide coated magnetite can be applied for the removal of metal ions such as Pb^{2+} and other species such as Ba, Ra and Po (Towler, Smith et al. 1996). Another example is a magnetic powdered $\text{MnO-Fe}_3\text{O}_4$ composite, which is obtained by co-precipitation method. This composite possesses good magnetic properties and shows excellent adsorption towards organic compounds under acidic conditions (Wu, Qu et al. 2005). More recently the synthesis of magnetic nanosized $\text{Fe}_3\text{O}_4/\text{MnO}_2$ has been reported, composite particles which exhibit super-paramagnetic properties. Experiments using methyl orange have demonstrated a good ability for chemical adsorption (Shu and Wang 2009).

2.2 Metal Ions and Oxyanions

In the frame of this investigation four species were selected for the sorption studies. These species were Cd(II), Ni(II), Pb(II), and Mo(VI). Cadmium, nickel and lead are toxic metal ions, and especially cadmium and lead have been appointed as particularly harmful metals (WHO 2007).

2.2.1 Speciation of Metal Ions

The chemical speciation of an element is relevant because it mostly determines its adsorption and transport properties (Kiss and Odani 2007). In all liquid systems the bare metal ions are in continuous search of partners. All metal cations in water are hydrated; which means that they form aquo complexes. The coordination reactions in which metal cations participate in aqueous solutions are exchange reactions with the coordinated water molecules exchanged for some preferred ligands (Stumm and Morgan 1996).

Metal ion speciation in natural waters is influenced by many variables. Some variable may influence the distribution of metal species available for uptake. The size distribution of metal ion complexes may be strongly influenced by pH; the H^+ ion competes with metals for ligands such as OH^- , Cl^- , CO_3^{2-} , HCO_3^- , HS^- , S^{2-} , sulphate and phosphate, and metal complexation

will change adsorption abilities. In most cases, pH is the most important variable influencing metal speciation (Stumm and Morgan 1996).

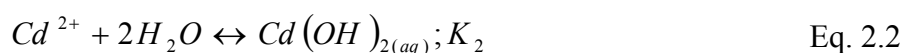
The distribution of inorganic metal species in natural waters with known composition of major anions is predictable by means of the knowledge of the formation constants of particular species.

2.2.1.1 Cadmium speciation

Cadmium may exist in water as the hydrated ion, as inorganic complexes such as carbonates, hydroxides, chlorides or sulphates, or as organic complexes with humic acids (OECD 1994).

The predominant cadmium species in aquatic systems are: Cd^{2+} , $CdCl^+$, $CdCl_2$, $CdCl_3^-$, $CdOH^+$, CdS , $Cd(HS)_2$, $Cd(HS)_3^-$, $Cd(HS)_4^{2-}$, $Cd_{(s)}$, $CdCO_{3(s)}$, and $Cd(OH)_{2(s)}$ (Morel 1983).

Regarding to the hydroxides, the equilibria pertaining to the hydroxyl complexes or hydrolysis products of cadmium can be represented in terms of the following equilibrium constants:



Values for the equilibrium constants for cadmium in water at 25°C obtained by means of MINEQL+[©] software are given in Table 2.3.

Table 2.3: Equilibrium constants of hydroxyl complexes of cadmium metal ions at 25°C.

Equilibrium constants Log K		
K ₁	K ₂	K ₃
-10.1	-20.3	-32.5

The distribution diagram for cadmium hydroxy complexes reveals that Cd^{2+} is the predominant species below pH 8, and the species, CdOH^+ , and $\text{Cd}(\text{OH})_{2(\text{aq})}$ contribute increasingly to the solubility of cadmium in the range pH 8-12 (see Figure 2.3).

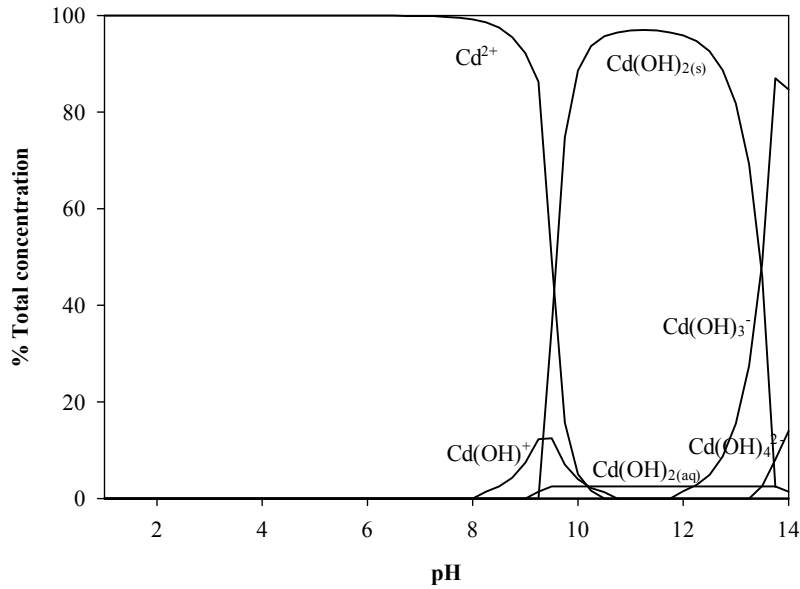


Figure 2.3: Distribution diagram for cadmium hydroxy complexes in an aqueous solution of Cd(II). $c_{\text{Cd}} = 10^{-6}$ mol/L, $T = 25$ °C (MINEQL+[®]).

As has been mentioned cadmium may form very stable soluble complexes with Cl^- ligands. CdCl^+ , CdCl_2 , and CdCl_3^- exist as significant species in solution. The reactions that describe the formation of these species are given below:



In Table 2.4 the stepwise formation constants of cadmium chloride complexes are given (Jenkins 2004).

Table 2.4: Formation constants of complexes and solids from cadmium metal ions and Cl⁻ as ligand.

Equilibrium constants Log K			
K ₁	K ₂	K ₃	K ₄
1.32	0.90	0.09	-0.45

Aqueous cadmium solubility at any pH and the possible formation of Cd(CO₃)₂ can be calculated from the corresponding solubility product equations (Speight 2003):



with: K_{sp} = solubility product constant in mol/L at 25°C

$$K_{sp,Cd(OH)_2} = (Cd^{2+})(OH^{-})^2 = 2.5 \times 10^{-14} \quad \text{Eq. 2.10}$$

$$K_{sp,CdCO_3} = (Cd^{2+})(CO_3^{2-}) = 5.2 \times 10^{-12} \quad \text{Eq. 2.11}$$

2.2.1.2 Nickel speciation

In the case of nickel, the hydrated Ni²⁺ cation is regarded as the most bioavailable nickel species because it is able to be transported through or interact with external membranes of a biological organism. Among the physicochemical parameters that control Ni²⁺ ions in the environment pH, redox potential, temperature, ionic strength, Ca²⁺ content can be mentioned as the most important ones (Schaumlöffel 2005).

In Figure 2.4 a distribution of nickel hydroxyl complexes in aqueous solution as function of pH is given. In this distribution diagram it is seen that from acidic pH levels to about pH 9, Ni²⁺ is the dominant form, NiOH⁺ begins to form at just below pH 8, peaks at about 9.5 never exceeds 20% of the total hydroxylated species of Ni. At pH levels between 9.5 and 11, Ni(OH)₂ is the predominant form, and above pH 11, Ni(OH)₃⁻ dominate, as is shown in Figure 2.4 (Babich 1983). Complexes with ligands, such as OH⁻, SO₄²⁻, HCO₃⁻, Cl⁻, and NH₃, are formed to a minor degree in this pH range (WHO 2005).

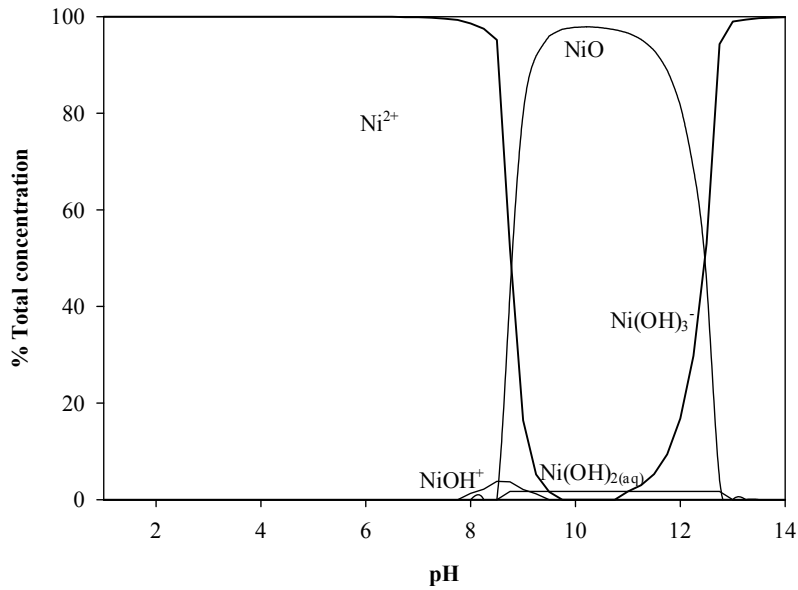
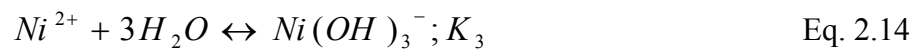
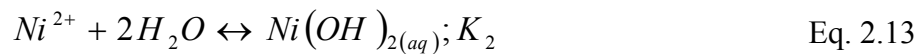


Figure 2.4: Distribution diagram for nickel hydroxy complexes in an aqueous solution of Ni(II). $c_{\text{Ni}} = 10^{-6}$ mol/L, $T = 25^\circ\text{C}$ (MINEQL+[©]).

The hydroxyl complexes or hydrolysis products of nickel can be represented in terms of the following equilibrium constants:

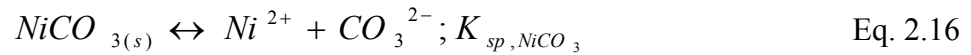


Values for the equilibrium constants for nickel complexes in water at 25°C obtained by means of MINEQL+[©] software are given in Table 2.5:

Table 2.5: Equilibrium constants of hydroxyl complexes of nickel metal ions at 25°C.

Equilibrium constants Log K		
K ₁	K ₂	K ₃
-9.89	-19.0	-29.9

The aqueous nickel solubility at any pH and the possible formation of NiCO_{3(s)} can be calculated from the corresponding solubility product equations (Speight 2003):



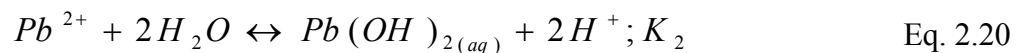
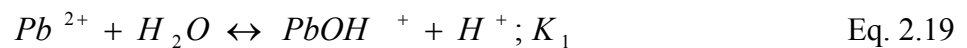
with: K_{sp} = solubility product constant in mol/L at 25°C

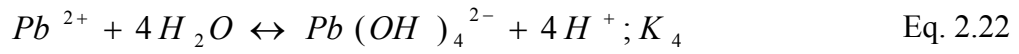
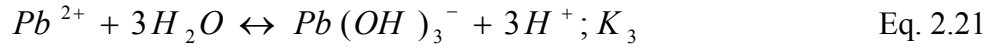
$$K_{sp, Ni(OH)_2} = (Ni^{2+})(OH^{-})^2 = 6.0 \times 10^{-16} \quad \text{Eq. 2.17}$$

$$K_{sp, Ni(CO_3)_2} = (Ni^{2+})(CO_3^{2-}) = 1.3 \times 10^{-7} \quad \text{Eq. 2.18}$$

2.2.1.3 Lead speciation

Inorganic lead bearing species existing in water include Pb(OH)₂, Pb(OH)₃⁻, as well as dimeric or tetrameric lead ions such as Pb₂(OH)₃⁺ and Pb₄(OH)₄⁴⁺ (Hill 2005). At pH lower than 6, Pb²⁺ is the main specie that contains lead. Low solubility compounds are formed by complexation with inorganic ligands such as Cl⁻, CO₃²⁻, SO₄²⁻, and PO₄³⁻ (Evanko 2000).





Numerical values for some equilibrium constants for lead complexes in water at 25°C, obtained by means of MINEQL+[©] software are given in Table 2.6.

Table 2.6: Equilibrium constants of complexes for lead metal ions.

Equilibrium constants Log K			
K ₁	K ₂	K ₃	K ₄
-7.59	-17.1	-28.1	-39.7

The distribution of lead species as function of pH is shown in Figure 2.5.

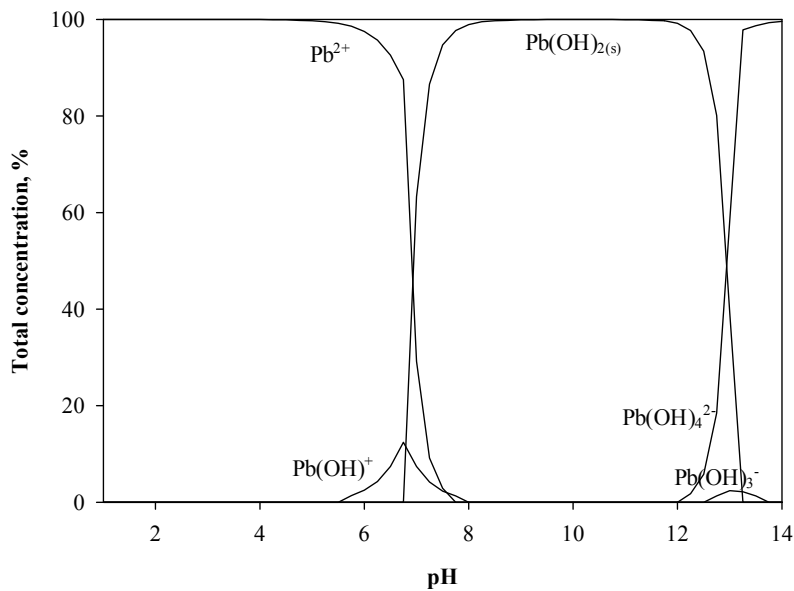


Figure 2.5: Distribution diagram for lead hydroxy complexes in an aqueous solution of Pb(II). $c_{Pb} = 10^{-6}$ mol/L, $T = 25^\circ\text{C}$ (MINEQL+[©]).

Like the aqueous solubility constants of cadmium and nickel, the aqueous lead solubility at any pH and the possible formation of $Pb(CO_3)_{2(s)}$ can be calculated from the corresponding solubility product equations (Speight 2003).

$$K_{sp, Pb(OH)_2} = (Pb^{2+})(OH^-)^2 = 1.2 \times 10^{-5} \quad \text{Eq. 2.23}$$

$$K_{sp, Pb(CO_3)_2} = (Pb^{2+})(CO_3^{2-})^2 = 7.4 \times 10^{-14} \quad \text{Eq. 2.24}$$

with: K_{sp} = solubility product constant in mol/L at 25°C.

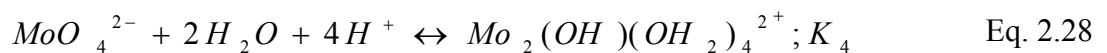
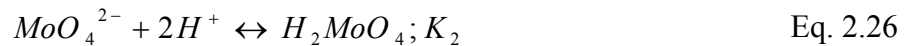
2.2.2 Speciation of Oxyanions

2.2.2.1 Molybdenum speciation

Molybdenum generally forms dissolved anionic species in aqueous solution. The predominant aqueous species of molybdenum in most natural systems is the molybdate anion MoO_4^{2-} . In the pH range between 2.5 and 6.5, polymerization occurs with the formation of polyanions (Gupta 1992).

Molybdenum does not form strong aqueous complexes with major ions such as Na^+ , K^+ , Mg^{2+} , or Ca^{2+} (Reddy, Munn et al. 1997) and the concentrations of molybdenum in water are generally lower under acidic conditions than under approximately neutral or alkaline conditions.

At the relatively low concentrations typical of most natural aqueous systems, different sets of reactions occur (Stiefel 2002).



The formation constants values for the molybdenum complexes described above are summarized in Table 2.7 (Gupta 1997).

Table 2.7: Formation constants of complexes from molybdenum anions and H^+ as ligand, at 25°C.

Log of stability constants			
K_1	K_2	K_3	K_4
4.23	8.23	8.17	8.64

At concentrations in the range of 10^{-5} mol/L, in alkaline and neutral solutions, molybdate is present as the monomeric $[MoO_4]^{2-}$ ion. As the pH is lowered the anion becomes protonated. At pH 6 the species $HMoO_4^-$ occur, reaching a maximum in concentration at pH 4 slightly greater than 40% (see Figure 2.6).

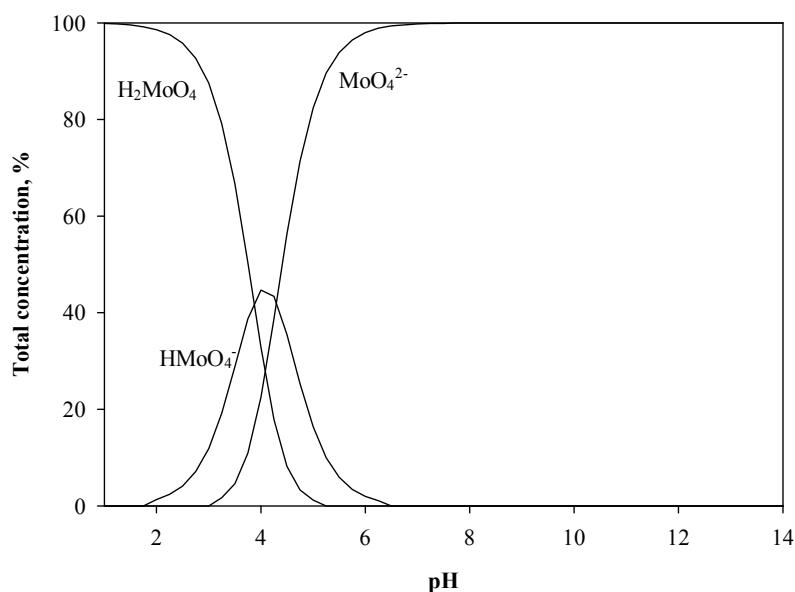


Figure 2.6: Distribution diagram of molybdenum species in an aqueous solution of Mo(VI). $c_{Mo} = 10^{-6}$ mol/L, $T = 25^\circ C$ (MINEQL+[©]).

An overview of molybdenum species in aqueous solutions at different pH values and concentrations is shown in Table 2.8.

Table 2.8: Molybdate species in aqueous solutions.

[Mo(IV)], mol/L	pH	Main species
All	>6	$[\text{MoO}_4]^{2-}$
10^{-5}	>5	$[\text{MoO}_4]^{2-}$ (ca.100%)
10^{-5}	4	$[\text{MoO}_4]^{2-}$ (30%) $[\text{HMoO}_4]^-$ or $[\text{MoO}(\text{OH})_5]^-$ (10%) H_2MoO_4 or $\text{Mo}(\text{OH})_6$ (60%)
10^{-5}	2- 3	H_2MoO_4 or $\text{Mo}(\text{OH})_6$ (ca 100%)
10^{-5}	1	H_2MoO_4 or $\text{Mo}(\text{OH})_6$ (80%) $[\text{H}_3\text{MoO}_4]^+$ or $[\text{Mo}(\text{OH})_5(\text{H}_2\text{O})]^+$
$< 10^{-3}$	> 1	Monomeric species only
$> 10^{-3}$	5- 6	$[\text{Mo}_7\text{O}_{24}]^{6-}$, $[\text{HMo}_7\text{O}_{24}]^{5-}$,
$> 10^{-3}$	4- 5	$[\text{Mo}_8\text{O}_{26}]^{4-}$

Polymerisation occurs at higher Mo concentrations. At Mo concentrations above 10^{-3} mol/L and pH 5 – 6 the heptamolybdate ion forms and at pH 3 – 5 octamolybdate. At pH 0.9 MoO_3 precipitates (Mitchell 1990).

2.3 Sorption of Cations and Anions

Hydrous oxides and aluminium silicate surfaces, as well as organically coated and organic surfaces, contain functional surface groups ($=\text{MOH}$, $=\text{ROH}$, $=\text{R-COOH}$) that are able to act as coordinating sites. The functional groups at the surface undergo acid-base and other coordinative interactions; thus their coordination properties are similar to those of their counterparts in soluble compounds (Stumm and Morgan 1996).

The two basic mechanisms, by which a metal ion is adsorbed, are sometimes referred to as specific adsorption, where more selective and less reversible adsorption reactions occur involving chemisorbed inner-sphere complexes and ion exchange involving rather weak and less selective outer-sphere complex formation (Schindler and Stumm 1987; Dzombak and Morel 1990; McBride 1994; Apak 2006).

Metal cations that form strong complexes with OH^- in water also bind strongly to hydrous oxides surfaces, whatever the surface nature. For anions, the affinity for the surface and the form of the surface complex, inner- or outer-sphere complex, depend on the valence of the adsorbed species (Marmier 2002).

Metal sorption by variable charge adsorbents depends on the aqueous solution parameters, due to both the extent and sign of the surface charge, as well as the metal speciation in the aqueous solution, changes in response to liquid phase parameters, above all the pH and ionic strength.

2.3.1 Factors affecting the adsorption

The most important factors that can affect the adsorption of cations by a variably charged adsorbents are the pH of the medium, presence of complexing agents, and ions competition.

2.3.1.1 Effect of pH

Studies have demonstrated the importance of pH as a factor controlling the extent of cation adsorption by hydrous metal oxides. For hydrous metal oxides, particularly those of iron, aluminium and manganese, the efficiency of removal of ions from solution has invariably been found to be strongly pH dependent. A rapid increase in uptake of the metal ion usually occurs over a narrow pH range (Kinniburgh and Jackson 1981). The adsorption of anions is similar to cationic species, showing usually the inverse dependence on solution pH. The adsorption reaction involves competition with OH⁻ ions for the surface sites, therefore, the adsorption of ligands is strong at low pH where the competition due to the presence of OH⁻ is weak (Butcher 1992).

Of course, pH influences the chemical species available in solution and plays an important part for solubility, complexation, and precipitation behavior, but moreover, a change in pH means a change of the surface characteristics of the mineral adsorbent.

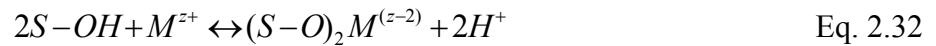
As mentioned previously, many solid surfaces contain ionisable functional groups: -OH, -COOH, -OPO₃H₂, and -SH. The surface charge of these particles becomes dependent on the degree of ionization (proton transfer) and consequently on the pH of the medium. Most oxides and hydroxides exhibit such amphoteric behavior; thus the charge is strongly pH dependent. (Stumm and Morgan 1996).

The effect of pH on the surface charge can be described as follows in Eq. 2.29 and Eq. 2.30:



Depending on the pH values the surface groups will be protonated Eq. 2.29 or deprotonated Eq. 2.30. Thus, in the case of protonation, a positive surface charge is generated, and in the case of deprotonation a negative surface charge is generated.

Related to the above and according to the Eq. 2.30 the adsorption of metal ions in general can be described by the following equations:



This adsorption can involve one or two surface hydroxyls as shown in Eq. 2.31 and Eq. 2.32 (Schindler and Stumm 1987). In the case of divalent cations, there is a coordination of the metal ions with the oxygen donor atoms and the release of protons from the surface as shown in Eq. 2.33:

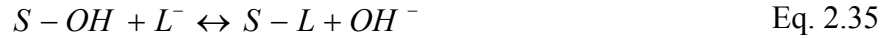


Formation of bidentate surface complexes is also a possibility:



In the case of ligands of both anions and weak acids the main adsorption mechanism is ligand exchange. The extent of adsorption, as with metal ions, is strongly dependent on pH and because the adsorption of anions is accompanied with a release of OH⁻ ions, the adsorption is favored by lower pH values.

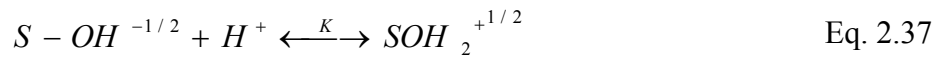
The adsorption of ligands can be expressed as follows:



Having explained the effect of the pH onto the surface charge, it is convenient at this point to introduce the term point of zero charge ($\text{pH}_{(\text{PZC})}$), which is defined as the pH value where the surface charge is equal to zero, namely, the pH at which the charge due to the positive surface groups is equal to that due to the negative ones. In systems formed by aqueous solutions and oxides, hydroxides, or oxide hydroxides, the H^+ and OH^- ions are the potential determining species; therefore the surface charge depends on the pH of the solution.

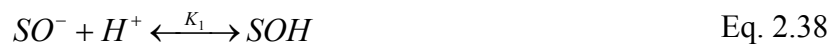
The value of the $\text{pH}_{(\text{PZC})}$ is related to the acidity constants of the surface groups. Examples of the models used for describing the acid-base behaviour of a solid surface are the 1site/1pK and the 1 site/2pK (Bourikas, Vakros et al. 2003).

The 1site/1pK model is described for the following reaction:



where the point of zero charge is expressed as $|pK| = pzc$

In the same manner the 1site/2pK model is described as follows:



with $(|pK_1| + |pK_2|) / 2 = pzc$

By determining the value of the $\text{pH}_{(\text{PZC})}$ of a given mineral surface, it is possible to establish whether the surface will be positive or negative charged depending on the solution pH, and therefore predict if either cations or anions are going to be sorbed. Thus, at solution pH values below the $\text{pH}_{(\text{PZC})}$ a positive surface charge allows the adsorption of anions, while at pH values greater than the $\text{pH}_{(\text{PZC})}$, a negative surface charge may allow the adsorption of cations.

2.3.1.2 Effect of complexing ligands

Another factor that can affect the adsorption of a charged species is the presence of complexing ligands. They may alter the adsorption behaviour of metal ions compared to a ligand free system, either by changes in solution speciation or by interaction at the adsorbing mineral surface (Hoins, Charlet et al. 1993). In some cases metal uptake is increased by the presence of adsorbed ligands at the surface. Other ligands form nonsorbing complexes in solution and compete with the surface for coordination of metal ion (Davis and Leckie 2002).

2.3.1.3 Effect of competitive adsorption

Finally a third factor that affects the adsorption of metal ions is the competitive adsorption. Natural systems usually contain a mixture of ions and generally, any additional sorbates potentially affect the adsorption of the other one. An example is the adsorption of metal ions at different ionic strengths.

On the other hand, the presence of another species representing the same class should lower the adsorption of the species of interest. There is a competition for the surface sites (the number of surface sites available for adsorption of the species of interest is lower in presence of a competitor). Moreover, related to ionic species, the presence of a competitor in the interfacial region leads to less favourable electrostatic conditions for the adsorption (Kosmulski 2001).

2.4 Particles Coating

Coated particles sometimes referred to as composite particles; consist of particles of a given solid coated with a thin or thick layer of another material. In principle, the coating can be amorphous, polycrystalline, or single crystalline. Coated particles can be prepared by several techniques, but we shall consider only the method based on precipitation from solution. The success of a particle coating process requires control of several variables to produce the interaction between a particulate suspension (A) and the material that is to be precipitated out of solution (B). At least four types of A-B interactions are possible, as follows:

- i. B can nucleate homogeneously in the solution and grow to form particles which do not interact with A, as a result a mixture of A and B is obtained.
- ii. Homogeneously nucleated particles of B grow and eventually heterocoagulate with particles A, producing deposits that are rough and nonuniform.

- iii. The homogeneously nucleated particles of B heterocoagulate with A at an early stage, and the growth of B continues on these aggregates, thus a particulate coating of B on A is produced.
- iv. B nucleates heterogeneously on the surface of A and growth produces a uniform layer of B on A.

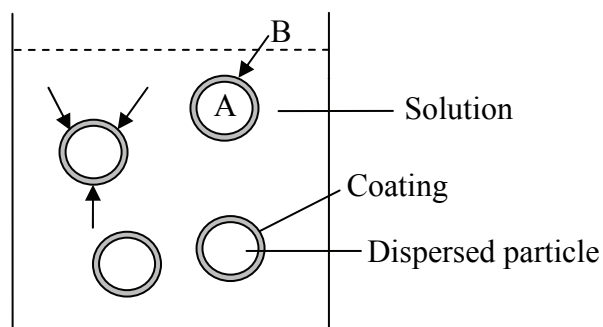


Figure 2.7: Schematic of the preparation of coated particles by the precipitation from solution onto dispersed particles.

The production of coated particles with a uniform layer requires some consideration that must be met. These are described below:

Colloidal stability of the suspension: in order to obtain well-dispersed, coated particles, the dispersion must be stable against flocculation and settling during nucleation and growth.

Surface area of core particles: The surface area of the core particles A must be sufficient to prevent the homogeneous precipitation of B, otherwise a system with coated particles and free particles of B will be obtained (Rahaman 2006).

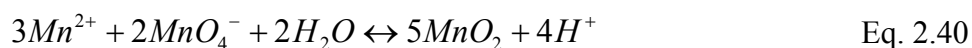
2.4.1 Synthesis of magnetic microparticles

For the synthesis of magnetic microparticles where manganese dioxide acts as sorbent, a heterogeneous precipitation method is applied. By means of this precipitation method, a suitable manganese dioxide modification can be obtained. The modification which would fulfill the requirements for being used as adsorbent is the δ -MnO₂. Because of the layered structure, the δ -MnO₂ modification has a low crystallinity and its high specific surface area also allows it to be highly reactive. At neutral pH, the surface is negatively charged; therefore the adsorption of cations is preferred. Nevertheless, due to the characteristics of the charge

acquisition, this modification is also able to adsorb anions depending on the pH at which it is contacted. Several procedures are used for the synthesis of hydrous manganese dioxide, which are discussed in the following section.

2.4.1.1 Synthesis of MnO₂

In general, MnO₂ can be produced by oxidation of Mn (II) or by reduction of permanganate. Within the first method can be mentioned: (i) the reaction involving both Mn⁷⁺ from permanganate and Mn²⁺ from a manganous salt; an example is the use of a KMnO₄ solution with an excess of NaOH and the slow addition of a MnClO₄ solution (Morgan and Stumm 1964) as well as (ii) the addition of MnCl₂ to a NaMnO₄/NaOH solution (Murray 1974). The reduction of permanganate can be carried out by the slow addition of concentrated hydrochloric acid to a boiling solution of potassium permanganate (Mc Kenzie 1971). Another method for producing MnO₂ is by means of the oxidation of manganous hydroxide or other salts, for example the oxidation of Mn (II) by introducing oxygen into a MnSO₄/KOH solution during five hours at a temperature of 5°C (Mc Kenzie 1971). The reaction by oxidizing MnCl₂ with the slow addition of KMnO₄ under alkaline conditions (Balistrieri and Murray 1982) and other modifications have been frequently used, (Driehaus 1994; Tripathy, Kanungo et al. 2001; Tripathy and Kanungo 2005). The reaction equation is as follows:



2.4.1.2 Coating of magnetic particles used as core

The coating process by means of heterogeneous precipitation in an aqueous solution has been widely used for particle coating. The coating is usually controlled by adjusting the concentration of the solution complex changing the experimental parameters, e.g., concentration of coating reagent, pH, and temperature (Wu, Wang et al. 2007).

The process involves dissolving a salt precursor, usually a chloride, oxychloride, or nitrate. The corresponding metal hydrous oxides usually form and precipitate in water upon addition of a base solution such as sodium hydroxide or ammonium hydroxide solution.

Investigations have shown that magnetic particles can be coated by precipitation in an aqueous solution; an example is the deposition of titanium dioxide onto silica-coated magnetite particles to develop a novel magnetic photocatalyst (Watson, Beydoun et al. 2002).

In the framework of this thesis the deposition of manganese onto magnetic particles has been applied for obtaining manganese dioxide/magnetite particles. The deposition is carried out by the reaction of MnCl_2 and KMnO_4 in solution (Towler, Smith et al. 1996). The particles to be used as core correspond to a synthetic commercial magnetite which has been previously used in other investigations of this research group to give magnetic properties e.g. to alumina oxide to remove fluoride ions from water.

3 Evaluation of Sorption

3.1 Sorption Equilibrium

The sorption process involves a solid phase (sorbent) and a liquid phase containing a dissolved species to be sorbed (sorbate e.g. metal ions). In the state of a dynamic equilibrium, after sufficiently long time, both the concentration of species in the liquid phase and the loading of the sorbent, i.e. the concentration in solid phase, are constant. The equilibrium is characterized by the equality of the electrochemical potentials of the dissolved substance in both phases. Sorption is often described in terms of isotherms, which show the relationship between the bulk aqueous phase activity (concentration) of the free sorbate and the amount sorbed at constant temperature (Stumm and Morgan 1996).

3.1.1 Experimental determination of sorption isotherms

The state of equilibrium of the sorption of a single component can be derived from experimental data by means of applying of mass balances. In batch methods the equilibrium is determined by contacting a solution of a given composition with a sorbent material of known solid-phase composition.

In the case of a binary system the mass balance of the system is (see Eq. 3.1):

$$m_s q_{i,0} + V_L c_{i,0} = m_s q_{i,e} + V_L c_{i,eq} \quad \text{Eq. 3.1}$$

If the initial loading $q_{i,0} = 0$, the Eq. 3.2 is obtained:

$$q_{i,e} = \frac{V_L}{m_s} (c_{i,0} - c_{i,eq}) \quad \text{Eq. 3.2}$$

This equation describes the so-called operation line from the initial state of the system to the state of equilibrium.

By varying either the initial concentration or, the mass of sorbent that is applied to a constant volume of solution, various points of the isotherm can be obtained.

The sorption isotherm is important from both theoretical and practical point of view. Its shape is related to the energy of the adsorption and the number of adsorption sites (Kinniburgh and Jackson 1981).

The principle governing adsorption at low solution concentrations is Henry's law, which gives a linear adsorption isotherm passing through the origin. This linearity is normally observed only at very low concentrations. At higher concentrations, the adsorbed quantity is below the one that is expected from Henry's law. This is partly due to the filling up of a significant number of the total possible adsorption sites. This results in a smaller chance of an ion from the solution to find a vacant site, and therefore being adsorbed.

For the description of the sorption equilibrium processes two main sorption equilibrium models are frequently applied, the Langmuir and Freundlich sorption isotherms.

3.1.1.1 Langmuir isotherm

The Langmuir relationship has originally been derived for the adsorption of gases onto solid surfaces. It is based on a model with the basic assumptions:

- There is only a mono-molecular layer of adsorbed molecules.
- The equilibrium is characterized by the fact that the rates of adsorption and desorption are equal.

The approach can also be applied to the description of the sorption of a single component onto an adsorbent. The rate of sorption of one kind of ions is proportional to the non-occupied sites and to the concentration of species in the liquid phase:

$$r_{sorption} = k_s (q_m - q_i) c_i \quad \text{Eq. 3.3}$$

Contrary to that the rate of desorption is proportional to the existing loading of the sorbent:

$$r_{desorption} = k_{des} q_i \quad \text{Eq. 3.4}$$

In the state of equilibrium both rates are equal which leads to the relationship:

$$q_i = q_m \frac{c_i}{\frac{k_{des}}{k_s} + c_i} \quad \text{Eq. 3.5}$$

or with $b = \frac{k_{des}}{k_s}$

$$q_i = q_m \frac{c_i}{b + c_i} \quad \text{Eq. 3.6}$$

where q_m corresponds to q_{\max} .

By means of the reverse ratio $K_L = \frac{k_s}{k_{des}}$ another usual form of the Langmuir relationship is obtained:

$$q_i = q_{\max} \frac{K_L c_i}{1 + K_L c_i} \quad \text{Eq. 3.7}$$

As obvious from Eq. 3.7, the Langmuir relationship has two quantities by which the equilibrium is described. The first one is q_{\max} , which corresponds to the maximum loading of a mono-molecular layer that can be obtained, and the second one is K_L which corresponds to the equilibrium or Langmuir constant. Both parameters can be deduced from experimental values either by means of non-linear regression calculations or by means of two different linearization methods.

A first linearization can be as follows:

$$\frac{1}{q_i} = \frac{1}{q_{\max}} + \frac{1}{q_{\max} K_L} \frac{1}{c_i} \quad \text{Eq. 3.8}$$

Another one is obtained by dividing the concentration by the adsorbent loading:

$$\frac{c_i}{q_i} = \frac{1}{q_{\max} K_L} + \frac{1}{q_{\max}} c_i \quad \text{Eq. 3.9}$$

Both relationships can be interpreted as straight lines. The first one gives $1/q_i$ as a linear function of $1/c_i$. Its extension and intersection with the ordinate axis equals $1/q_{\max}$ and hence q_{\max} can be derived and from the slope the value of K_L can be deduced.

The second equation is a linear relationship of c_i/q_i as a function of the concentration c_i . In this case the slope is equal to the reciprocal of q_{\max} and K_L is obtained from the intersection of the line with the ordinate axis.

The Langmuir relationship has two limiting cases:

For very low concentrations the denominator of Eq. 3.7 tends to the unit ($1 \gg K_L c_i$) and the equation is simplified to:

$$q_i = q_{\max} K_L c_i \quad \text{Eq. 3.10}$$

The amount adsorbed is directly proportional to its concentration in the solution.

At high concentrations the Eq. 3.7 becomes to:

$$q_i = q_{\max} \quad \text{Eq. 3.11}$$

The sorption capacity has reached a maximum. The entire surface is covered with a monomolecular layer of sorbed molecules, and a further increase in the solution concentration does not increase the amount adsorbed. An illustration of these relations is seen in Figure 3.1:

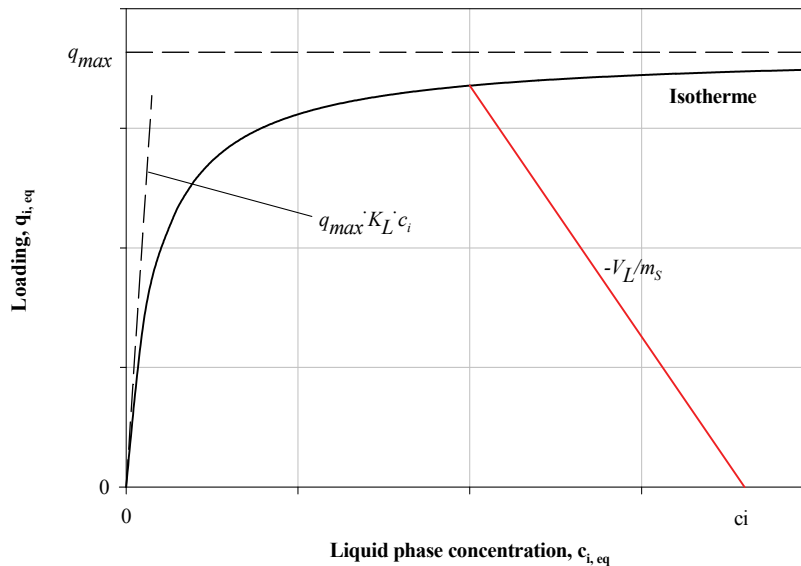


Figure 3.1: Langmuir isotherm and its limiting cases, at constant V_L/m_s and varying c_i .

3.1.1.2 Freundlich isotherm

The Freundlich relationship was originally an entirely empirical relationship of the form:

$$q_i = K_F c_i^n \quad \text{Eq. 3.12}$$

In the Freundlich isotherm equation, the coefficient K_F is an indication of adsorption capacity while n reflects affinity of the sorbent for the sorbate, i.e. the curvature of the isotherm.

This equation is very convenient for plotting adsorption data empirically in a $\log q_i$ vs $\log c_i$:

$$\log q_i = \log K_F + n \log c_i \quad \text{Eq. 3.13}$$

The Freundlich isotherm does not exhibit a maximum number of adsorption sites. However, it is more general than the Langmuir isotherm because it allows taking into account the surface heterogeneity of the sorbent. Thus, the equation applies very well to solids with heterogeneous surface properties and generally for heterogeneous solid surfaces (Stumm and Morgan 1996).

Adsorption isotherms are useful for illustrating the dependence between the concentration of a contaminant at the solid phase of a sorbent, q , and its concentration in the aqueous phase at a given pH. However, the adsorption of inorganic ions is pH-dependent and the form of the isotherm should be known over the entire pH range where is probably that a site can be found (Boulding 1996).

Both models, Langmuir and Freundlich, have been widely applied for many authors to describe the concentration dependence of cation uptake by hydrous manganese dioxide (Zasoski and Burau 1988; Kanungo, Tripathy et al. 2004; Tripathy 2006).

3.2 Sorption Kinetics

The sorption process is not an instantaneous process, the species dissolved in the liquid phase have to diffuse from the solution to the surface of the sorbent, and then to the internal surface areas. The rate of this approach to equilibrium is described by the sorption kinetics.

The rate of sorption is usually limited by mass transfer and depends on the properties of the sorbate and sorbent. Nevertheless, the hydrodynamics of the system is an important factor that influences the mass transfer.

Solid-liquid sorption processes are dominated either by the transport of solute molecules from the bulk solution across a film surrounding the adsorbent particles (film diffusion) or by the transport of the sorbate from the particle surface into interior sites by diffusion in the porous system of the adsorbent (particle diffusion) (Faust and Aly 1998). Usually both mechanisms affect the adsorption. Depending on the conditions of sorption one transport step may be much slower than the other one and, hence, exclusively control the adsorption.

Film diffusion is considered as the rate-controlling step in systems with poor mixing, small concentration of solute, small particle size and high affinity of the sorbate for the adsorbent. Internal diffusion dominates in systems with high concentration of sorbate, fast superficial overflow, large particle size of adsorbent and low affinity of the sorbate for the adsorbent (Small 1989; Vadivelan and Kumar 2005).

Due to the characteristics of the system to be studied, the small concentration of the solutes, in conjunction with the small particle size of the sorbent, film diffusion is the process expected to be the controlling step, therefore a brief discussion regarding to the film diffusion is given in the next section.

3.2.1 Film diffusion

In an agitated system of a solid and a liquid, the convection mechanism is present throughout the liquid phase. However, the convection, and hence mass transfer by convection, diminishes gradually as we approach the solid-liquid boundary.

The Nernst film is an approximation for treating the complex problem of mass transfer in a liquid which is adjacent to a phase boundary, e. g. a liquid-solid interphase. It considers a stirred liquid phase as comprising of two zones: Zone I is a bulk liquid phase up to a distance δ from the liquid-solid interface, in this zone mass transfer is by convection and is rapid. Zone II is a thin film adherent to the solid through which mass transfer takes place by diffusion and is relatively slow. This zone is the Nernst film (Nernst 1904).

The solute molecules migrating from the liquid phase to the adsorbent particle first have to diffuse from the free solution to the surface of the sorbent. In this way they have to pass the Nernst film around the particle, a stagnant, non-mixed part of the liquid phase in which the

concentration drops from the bulk concentration to a value at the surface. The schematic concentrations and the resulting flux are represented in Figure 3.2.

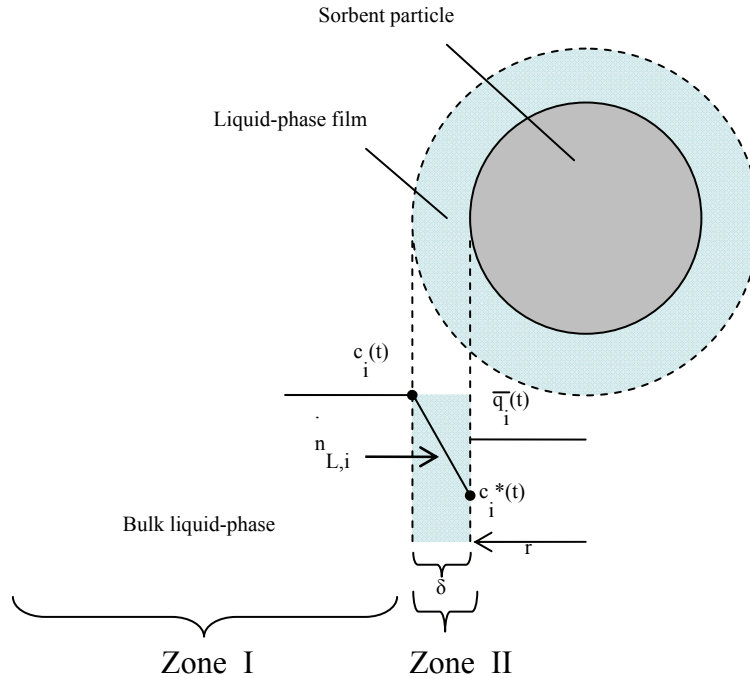


Figure 3.2: Development of concentrations during film diffusion.

3.2.1.1 Mathematical approaches for describing the film diffusion

Diffusion mainly depends upon the concentration gradient, which means that the driving force for diffusion to occur is a difference in concentrations (Begum 2005). For the diffusion in one direction (x), the specific mass flux of a component “ i ” is described as the product of the diffusion coefficient, $D_{L,i}$, and the concentration gradient dc_i/dx . Assuming quasi-stationary diffusion, Fick’s first law can be applied:

$$\frac{\dot{N}}{A} = \dot{n}_{L,i} = -D_{L,i} \frac{dc_i}{dx} \quad \text{Eq. 3.14}$$

Normally, the concentration gradient cannot be determined. Nevertheless, the species to be sorbed are present only in a trace concentration and therefore a linear slope is assumed (see Figure 3.2). Thus, the mathematical description of the diffusion through the film is as follows:

$$\dot{n}_{L,i} = -D_{L,i} \frac{c_i - c_i^*}{\delta} \quad \text{Eq. 3.15}$$

with c_i^* as the concentration at the surface of the adsorbent.

Considering that $\beta_{L,i} = \frac{D_{L,i}}{\delta}$, the following relation is obtained:

$$\dot{n}_{L,i} = -D_L \frac{c_i - c_i^*}{\delta} = -\beta_{L,i} (c_i - c_i^*) \quad \text{Eq. 3.16}$$

The resulting quotient from the diffusion coefficient D_L and the liquid film thickness δ is summarized as the mass transfer coefficient in the liquid phase β_L .

To calculate the sorption rate of a system, a certain volume of fluid in contact with a given mass of sorbent is considered. Furthermore, if the film diffusion is the only rate-limiting step the loading within the particle can be assumed homogeneous.

From Eq. 3.16, the change of concentration in a limited volume can be deduced:

$$-\frac{dc_i}{dt} = \frac{m}{V_L} a_s \beta_{L,i} (c_i - c_i^*) \quad \text{Eq. 3.17}$$

Considering that the mass balance for the system is:

$$V_L c_{0,i} = V_L c_i + m \bar{q}_i \quad \text{Eq. 3.18}$$

With the assumption that the surface concentration is in equilibrium with the surface loading (average):

$$\bar{q}_i = f(c_i^*) \quad \text{Eq. 3.19}$$

and the application of the Eq. 3.17 and Eq. 3.18 both the variation of the concentration and the loading can be calculated.

3.2.1.2 Mass transfer correlations

The mass transfer coefficient in the liquid phase, β_L , can be both experimentally determined and theoretically calculated. This coefficient depends on the geometry of the boundary layer, the hydrodynamics, and the material specific properties. In general the mass transfer coefficient can be correlated with the three dimensionless groups, the Sherwood – Reynolds – Schmidt (Sh – Re – Sc) number relationship.

$$Sh = a(Re)^b (Sc)^c \quad \text{Eq. 3.20}$$

where a, b, and c are constants.

In the frame of this investigation the mass transfer β_L is determined by means of the application of relationships for a suspension in stirred systems which are shown in the next section.

3.2.1.2.1 Mass transfer correlations for stirred systems

To estimate the mass transfer in stirred systems, the following approaches for the determination of Sherwood number can be considered:

$$Re_p < 1 \quad Sh = 2 + 0.6\sqrt{Re_p} \sqrt[3]{Sc} \quad \text{Eq. 3.21}$$

$$Re_p > 1 \quad Sh = 0.991 \sqrt[3]{(Re_p \cdot Sc)} \quad \text{Eq. 3.22}$$

$$\text{with : } Re_p = \left(\frac{v_{rel} \cdot d_p \cdot \rho_f}{\eta} \right) \quad \text{Eq. 3.23}$$

The Reynolds number depends on the term v_{rel} , which corresponds to the average of the relative velocity between the particles and the aqueous phase.

The relative velocity varies from point to point within a vessel, and the average value is difficult to estimate. Therefore, in practice, v_{rel} , is assumed to be equal to the free settling velocity, v_t (Victor A. Atiemo Obeng 2004).

The expressions for the free settling velocity, v_t , for laminar and turbulent regime are, respectively:

$$\text{Re}_p < 1 \quad v_t = \frac{gd_p^2(\rho_s - \rho_f)}{18\eta} \quad \text{Eq. 3.24}$$

$$1000 < \text{Re}_p < 3.5 \times 10^4 \quad v_t = 1.73 \left[\frac{gd_p(\rho_s - \rho_f)}{\rho_f} \right]^{1/2} \quad \text{Eq. 3.25}$$

To complete the set of equations that allows the mass transfer coefficient in the liquid phase to be determined, the Schmidt number must be included. The definition of this number is given in Eq. 3.26:

$$Sc = \frac{v}{D_L} \quad \text{Eq. 3.26}$$

This number is defined as the ratio of kinematic viscosity of the liquid phase and the molecular diffusion coefficient.

Typical values of diffusion coefficients for divalent cations are in the order of $10^{-9} \text{ m}^2/\text{s}$ (Anders Johnson 1996). This last term can be obtained by means of the Einstein relationship:

$$D_L = \frac{uRT}{zF} \quad \text{Eq. 3.27}$$

Here the diffusion coefficient is a function of the ion mobility, u . Typical values for ions are in the order of $10^{-8} \text{ (m}^2/\text{sV)}$. Values of ionic mobilities for the metal ions used in this investigation are in Table 3.1.

Table 3.1 : Ionic mobility values for Cd^{2+} , Ni^{2+} , and Pb^{2+} .

Ion	$u, \times 10^{-8} \text{ m}^2/\text{sV}$
Cd^{2+}	5.58
Ni^{2+}	5.29
Pb^{2+}	7.20

Another alternative for determining the diffusion coefficient is by means of the Stoke's – Einstein relationship which describes the molecular diffusion coefficient as a function of the radius, r , of the particle (Étienne Guyon 2001):

$$D_L = \frac{k_B T}{6\pi\eta r} \quad \text{Eq. 3.28}$$

The dependence of the diffusion coefficient on the nature of the solute is simply through its radius.

Metal ions in water exist in numerous forms and despite what the formula implies a metal ion cannot exist as a separate entity in water. The highest stability of their outer electron shell is ensured by bonding or coordinating water molecules in forms such as the hydrated metal ion $M(\text{H}_2\text{O})_x^{n+}$ might present. Thus, the hydrated radius is the most adequate value to taking into account for the calculation of the diffusion coefficient by applying the Eq. 3.28. Values for the hydrated ionic radius of Cd, Ni, and Pb are shown in Table 3.2 (Louis W. Chang 1996) .

Table 3.2 : Hydrated ionic radius values for Cd, Ni, and Pb .

Ion	$r, \text{Å}$
Cd^{2+}	4.26
Ni^{2+}	4.04
Pb^{2+}	4.01

In the case of Mo, the radius corresponding to the hydrated ion MoO_4^{2-} has a value of 4.50Å (Perk 2006).

The overall diffusion coefficient of a ion par consisting of a cation of charge z_1 and anion of charge z_2 is:

$$D_L = \frac{\frac{|z_1| + |z_2|}{|z_2|} + \frac{|z_1| + |z_2|}{|z_1|}}{D_{L,1} + D_{L,2}} \quad \text{Eq. 3.29}$$

where D_1 and D_2 are the diffusion coefficients of the cation and the anion, respectively. As seen in Eq. 3.29, the overall diffusion coefficient is determined by the slower ion. The

diffusion coefficients are weighted by the charge and therefore, the faster ion with a much smaller charge can dominate the overall diffusion coefficient (Nguyen 2008).

3.2.2 Alternative models for describing sorption kinetics

Although the film kinetics model is commonly used, there exist sorption systems in which the model does not result in a satisfying description of the experimental data. Possible reasons for this may be very slow intraparticle diffusion or the slow formation of metal complexes at the surface. In these cases alternative approaches for description of the sorption kinetics of metal ions onto different adsorbents have to be applied. Among these, two simple kinetic models most frequently are applied: the pseudo-first-order and pseudo-second-order chemical reaction (Das and Jana 2006; Han, Zou et al. 2006; Wang, Gong et al. 2007). Furthermore, the Elovich approach has been also applied (Das and Jana 2006; Han, Zou et al. 2006; Wang, Gong et al. 2007). A brief discussion will be given below.

3.2.2.1 Pseudo first order approach

The pseudo-first order equation was applied for describing the adsorption of liquid-solid systems based on solid capacity (Lagergren 1898). A relationship has been derived, similar to that of a first-order chemical reaction, with the change of loading being proportional on the difference between the equilibrium loading, q_e , and the actual loading at time t , q_t , on the solid phase as the driving force.

The pseudo-first-order approach thus considers that the rate of saturation of functional sites depends on the number of unoccupied sites the sorbent.

The pseudo-first order kinetics using the Lagergren equation is as follows (Ho and McKay 1998):

$$\frac{dq_t}{dt} = k_1(q_e - q_t) \quad \text{Eq. 3.30}$$

After integration and applying boundary conditions $t=0$ to $t=t$ and $q_t=0$ to $q_t=q_t$, the integrated form of Eq. 3.30 becomes :

$$\log(q_e - q_t) = \log(q_e) - \frac{k_1}{2.303}t \quad \text{Eq. 3.31}$$

This relationship differs from a true first order equation in two ways:

- The parameter $k_1(q_e - q_t)$ does not represent the number of available sites.
- The parameter $\log(q_e)$ is an adjustable parameter and is often found not to be equal to the intercept of a plot of $\log(q_e - q_t)$ vs t whereas in the case of a true first-order reaction $\log(q_e)$ should be equal to the intercept of a plot of $\log(q_e - q_t)$ vs t .

In order to fit the Eq. 3.31, to experimental data, the equilibrium sorption capacity, q_e , has to be known.

3.2.2.2 Pseudo-second order approach

In the pseudo-second-order approach the rate of sorption is proportional to the square of the number of unoccupied sites of the adsorbent.

The rate expression of the pseudo-second-order approach can be expressed as follows (see Eq. 3.32) (Ho and McKay 1998):

$$\frac{dq}{dt} = k_2(q_e - q_t)^2 \quad \text{Eq. 3.32}$$

Integrating Eq. 3.32 for the boundary conditions $t = 0$ to $t = t$ and $q_t = 0$ to $q_t = q_t$, gives:

$$\frac{1}{(q_e - q_t)} = \frac{1}{q_e} + k_2 t \quad \text{Eq. 3.33}$$

which is the integrated rate law for a pseudo-second order reaction.

Eq. 3.33 can be rearranged to obtain:

$$q_t = \frac{t}{\frac{1}{k_2 q_e^2} + \frac{t}{q_e}} \quad \text{Eq. 3.34}$$

which has a linear form of:

$$\frac{t}{q_t} = \frac{1}{kq_e^2} + \frac{1}{q_e}t \quad \text{Eq. 3.35}$$

If the initial sorption rate is:

$$h = k_2 q_e^2 \quad \text{Eq. 3.36}$$

then Eq. 3.34 can be written as:

$$q_t = \frac{t}{\frac{1}{h} + \frac{t}{q_e}} \quad \text{Eq. 3.37}$$

and Eq. 3.35 becomes:

$$\frac{t}{q_t} = \frac{1}{h} + \frac{1}{q_e}t \quad \text{Eq. 3.38}$$

If the pseudo-second-order approach is applicable, the plot of t/q_t vs t of Eq. 3.38 should give a linear relationship, from which q_e , k_2 , and h can be determined from the slope the intersection with the ordinate axis. There is no need to know any parameter beforehand.

3.2.2.3 Elovich equation

The Elovich equation was originally developed to describe the kinetics of heterogeneous chemisorption of gases on solid surfaces (Low 1960). Since then it has found application in other areas to describe the kinetics of sorption and desorption of various inorganic substances on solid materials. The Elovich equation is expressed as follows:

$$q_t = \left(\frac{1}{\beta} \right) \ln \alpha \beta + \frac{1}{\beta} \ln t \quad \text{Eq. 3.39}$$

where α and β are constants during any one experiment.

Thus, a plot of q_t vs $\ln(t)$ should give a linear relationship if the Elovich equation is applicable with a slope of $1/\beta$ and an intercept of $(1/\beta) \ln \alpha \beta$.

4 Experimental Part

4.1 Synthesis of magnetic micro sorbent (MMS)

The magnetic micro sorbent (MMS) was prepared by the deposition of MnO₂ onto magnetite particles.

For the synthesis synthetic magnetite (Fe₃O₄ Bayoxide E 8710) was used as core. This commercial material has a specific surface area between 3 - 6 m²/g and a saturation magnetization between 84 and 92 Am²/kg (see Table 8.1 in the Appendix). Onto the surface of this material manganese dioxide was deposited. The reaction for obtaining MnO₂ is described in Eq. 4.1:



The synthesis of manganese dioxide was carried out by the slow addition of a manganese chloride solution to an alkaline permanganate solution. The amounts of manganese chloride, potassium permanganate and potassium hydroxide mixed were in the mole ratio 3:2:4 (Driehaus 1994).

First, in a 1L batch reactor a certain amount of magnetite, between 0.5 and 10 g, was suspended in 500 mL of deionized water (18 MΩ/cm). To ensure the homogenous distribution of the magnetite particles into the solution, a constant agitation at 500 rpm by means of a mechanical stirrer was applied (IKA Labortechnik). To this suspension 14 mL of 1 mol/L KOH and 23 mL of 0.2 mol/L KMnO₄ were added. The pH of the solution was continuously measured by means of a pH-meter (SCHOTT Instruments).

Once the pH of the suspension reached a constant value of about 12.4, the addition of 7 mL of 1 mol/L MnCl₂·4H₂O was carried out within 5 min at 1.4mL/min. The suspension was continuously agitated for a period of 30 min (see Figure 4.1).

The color of the suspension immediately turned to dark brown, indicating formation and precipitation of MnO₂.

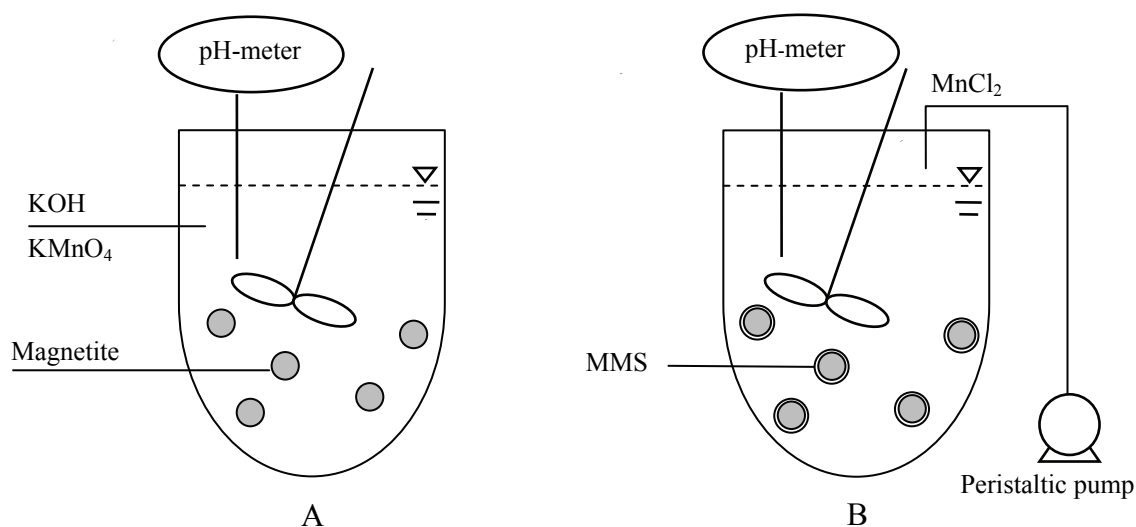


Figure 4.1: Schematic design of the batch system on a laboratory scale. A: Preparation of the initial suspension; B: Formation of the MnO₂ coating.

Finally, at the time at which the reaction was completed the entire solid phase (the magnetic micro-sorbent material) was separated from the solution by using a hand magnet. Before using the magnetic micro-sorbent material (MMS) in sorption studies, this was washed with deionized water and kept in a 0.01 mol/L NaNO₃ solution. The so prepared micro-sorbent was used in further equilibria and kinetic experiments.

4.1.1 Reproducibility

In order to assess the reproducibility of the synthesis of the material, the micro-sorbent was synthesized various times and used in sorption experiments. An amount of 5 mg of the adsorbents were contacted with 1000 mL of a Cd(II) solution at a concentration of 8.9 μmol/L at pH 7. To adjust the solutions at different pH values 0.1 mol/L HNO₃ or 0.1 mol/L NaOH solutions were added. The metal ion concentration prior contacting and at the end of the equilibrium period was determined by Atomic Absorption Spectrometry (AAS). The experiment was carried out in duplicate.

4.2 Elemental analyses

The amount of manganese present in the magnetic microsorbent material was measured by means of Atomic Absorption Spectrometry (VARIAN Spectra AA-220-FS). For the measurements, an amount of 0.1 g of freeze dried microsorbent was digested with a volume of 5 mL of HCl suprapure solution by using microwave digestion (MLS-Ethos, MLS GmbH). The digesting program is described in Table 4.1.

Table 4.1 : Digestion program for the decomposition procedure of the microsorbent material.

Run	Time, min	Power, W	T, °C
1	3	500	80
2	3	500	80
3	3	500	160
4	10	500	160
5	20	0	20

4.3 Characterization measurements

Analyses of the physical characteristics of MMS including specific surface area, density, particle size distribution and magnetization properties were measured.

4.3.1 ESEM and EDX analysis

Environmental scanning electron microscopy (ESEM) (XL30, ESEM-FEG, Philips, Netherlands), was used to obtain surface information of MMS.

4.3.2 Specific surface area measurements by means of BET adsorption method

The surface area of the resulting microsorbent was determined by using the BET N₂ adsorption method, using Autosorb 1 MP (Quantachrome). For the measurements an amount of about 0.150 g of the freeze dried adsorbent was used. Prior to the determination, the samples were degassed in a vacuum for a period of 12 hours at 95° C. The measured values were analysed with the program Autosorb (Quantachrome).

4.3.3 Density measurements

The density of the microsorbent was measured by a pycnometer (AccuPyc 1330, Micromeritics). For the measurement of the density of a freeze dried sample of the

magnetic micro-sorbent was used. In order to ensure reproducible results, the preparation of the sample included a drying step of about 24h at 60°C, after this time the sample was left to cool down in a desiccator with silica gel for a period of 3h.

4.3.4 Particle size and distribution measurements

The particle size was determined, in the range of 0.1-3600 μm , by means of a computerized system for particle size analysis with an Ankersmid Eye Tech instrument (Ankersmid Ltd., Netherlands). For the measurements cells of 1 cm /1.5 mL were used and the samples were directly taken from the suspension without any previous treatment.

4.3.5 Magnetic susceptibility measurements

Magnetic characterization of the micro-sorbent was performed by means the measurement of magnetic susceptibility. For this purpose an alternating gradient magnetometer (AGM) (Micromag 2900, Measurements, Princeton USA) was used. The magnetic susceptibility of the particles as a function of the applied field strength was measured using freeze dried samples.

4.4 Magnetic solid-liquid separation

To assess the magnetic solid-liquid separation of the micro-sorbent from solution, measurements of turbidity were carried out.

For the turbidity measurements suspensions comprising the micro-sorbent and solutions at different pH values ranging between 3 and 9 were left to settle down in presence and absence of a magnetic field. For the magnetic separation a permanent magnet was used (NdFeB permanent magnet). The dimensions of the magnet were: 4 x 2 x 0.5 cm.

The separation efficiency is given by the relative turbidities, T/T_0 , where T corresponds to the measurement of turbidity in NTU at time t , and T_0 to the measurement at time zero. Values of T/T_0 were calculated by measuring the turbidity at determined intervals of time until a period of 60 min was completed. The same experiment was carried out with deionized water, as well as, 0.01 mol/L and 0.001 mol/L NaNO_3 solutions as a media. The ratio of MMS mass to solution for each test was 50 mg/L. For the turbidity measurements a turbidimeter (HACH 2100 AN IS) was used.

4.5 Chemical stability

The chemical stability of MMS was related to the dissolution of MnO_2 . Thus, the amount of manganese released from the MnO_2 when the microsorber is contacted with solutions at different pH values was measured.

For the dissolution test, an amount of 3 mg of the microsorber in 250 mL of the solution was used. The contacting solution were prepared at pH values ranging from 2.0 to 7.0. The pH of the solutions was adjusted by adding 0.01 mol/L HNO_3 or 0.01 mol/L NaOH. The amount of manganese released from MMS to the solution was analyzed by means of Atomic Absorption Spectrometry (VARIAN Spectra AA-220-FS).

4.6 Zeta potential measurements

By means of microelectrophoresis the zeta potential of MMS as function of pH was measured. In microelectrophoresis the movement of individual colloidal particles under the influence of a known electrical field is followed directly in an ultramicroscope assembly. If the field is known in the area of observation the electrophoretic mobility and the zeta potential is easily calculated from the observed particle velocity.

The ζ potential measurements was carried out by using a Zetasizer 5000 (Malvern Instruments Ltd.) at 25° C.

Sufficiently dilute suspensions of the magnetic sorber (MMS) were prepared at constant ionic strength, 0.01 mol/L NaNO_3 . The titration was carried out by the addition of 0.1 mol/L HNO_3 or NaOH solutions.

Another technique applied for the estimation of the $\text{pH}_{(\text{PZC})}$ is the immersion technique (Bourikas, Vakros et al. 2003).

By means of this technique, the $\text{pH}_{(\text{PZC})}$ of the samples is determined by simple pH measurements. A certain amount of adsorbent is contacted with solutions at different initial pH values containing the same electrolyte. The solutions were agitated for a period of time after which the pH is measured. The change of pH (ΔpH) during equilibration is calculated and the $\text{pH}_{(\text{PZC})}$ is identified as the initial pH with minimum (ΔpH).

The procedure for the immersion technique was as follows:

To a series of 300 mL flasks containing the appropriate solutions of electrolyte a certain amount of adsorbent was added. The electrolyte media used was 0.01 mol/L NaNO_3 . To

adjust the solutions at different pH values 0.1 mol/L HNO₃ or 0.1 mol/L NaOH solutions were added. The suspensions were agitated for a period of 24 h in a shaker at 100 rpm until an equilibrium pH was reached.

4.7 Equilibrium studies

For the investigation of sorption equilibrium, constant amounts of MMS were contacted with different concentrations of metal ions solutions for a period of time at a predetermined initial pH. The metal ion concentration prior to the contacting with the MMS and at the end of the equilibration period was determined by Atomic Absorption Spectrometry (VARIAN Spectra AA-220-FS).

The metal ion solutions were prepared from standard solutions of Cd(II), Ni(II), Pb(II), and Mo(VI) in HNO₃. The initial concentration range used is shown in Table 4.2:

Table 4.2 : Initial concentration range of Cd(II), Ni(II), Pb(II), and Mo(VI) used for the equilibrium studies.

Metal solution	$c_0, \times 10^{-3} \text{ mmol/L}$
Cd(II)	0.7 - 9
Ni(II)	1.4 - 17
Pb(II)	0.4 - 5
Mo(VI)	5.5 - 20

The volume of the solutions used for the equilibrium experiments was 1000 mL and the amount of MMS added was 5 mg for cadmium and nickel ion solutions and 1.25 mg for lead ion solutions.

The pH of the metal ion solutions was adjusted by adding 0.1 mol/L HNO₃ or 0.1 mol/L NaOH solutions and 0.01 mol/L NaNO₃ solution was used in each solution as a matrix.

The solutions were placed in flasks and agitated in a shaker at 100 rpm for a period of 180 min. After this period the pH was measured and samples were taken for the corresponding analysis. Prior to the analysis, the samples were filtered (0.45µm acetate membrane) and acidified with concentrated HNO₃. For all experiments the final pH was recorded.

The evaluation of the data was carried out by applying the relationships of section 3.1. Thus, with the equilibrium concentrations and the corresponding mass balances the loadings were calculated and the sorption isotherms were determined.

4.7.1 Influence of different parameters on sorption equilibrium

The influence of pH, complexing ligands and competitive ions was studied as follows.

4.7.1.1 Effect of pH

The effect of pH on sorption capacity of MMS was investigated using solutions described in the previous section (see section 4.7). The pH range for the study was determined taking into account the aqueous speciation of the metal ions. The speciation was carried out by using the MINEQL+[©] program which was supplied with both the concentrations of metal ions and matrix solutions. For the experiments the initial pH of the solutions was adjusted to the desired pH value by adding 0.01 mol/L HNO₃ or 0.01 mol/L NaOH.

4.7.1.2 Effect of complexing ligands

The effect of complexes formation on the sorption capacity of MMS was investigated using solutions described in section 4.7 with the difference that 0.01 mol/L NaCl solution instead of 0.01 mol/L NaNO₃ solution was used as a matrix. For the experiments the initial pH of the solutions was adjusted by adding 0.01 mol/L HNO₃ or 0.01 mol/L NaOH.

4.7.1.3 Effect of competitive adsorption

Isotherms were carried out in presence of different amounts of calcium. The solutions used for the experiments are described in section 4.7 to which Ca²⁺, in a concentration of 50 mg/L and 100 mg/L, corresponding to 1.25 and 2.5 μmol/L respectively, was added. The initial pH of the solutions was adjusted to the desired pH value by adding 0.01 mol/L HNO₃ or 0.01 mol/L NaOH.

4.8 Kinetic studies

For the investigation of sorption kinetics, the effect of initial concentration and mass of adsorbent were considered. The kinetic experiments were carried out in a batch reactor.

4.8.1.1 Effect of initial concentration

Metal ions bearing solutions were prepared in different initial concentrations and contacted with an accurately measured suspension sample. The following experimental bulk solution concentrations were used (see Table 4.3):

Table 4.3 : Variables used for the kinetic experiments based on the variation of bulk solution concentration with time.

Metal solution	pH	$c_0, \times 10^{-3} \text{ mmol/L}$
Cd(II)	7	4.5
		8.9
		18
Ni(II)	7	8.5
		17
		34
Pb(II)	6	4.8
		9.7
Mo(VI)	4	5.6
		10
		20

For the experiments carried out with Cd(II), Ni(II), and Pb(II) solutions an amount of 10 mg of MMS was used, while for Mo(VI) solution the amount was 20 mg. For each experiment a volume of 1000 mL of solution was needed. Previous to the addition of the adsorbent the initial pH was adjusted to the desired pH by adding 0.01 mol/L HNO₃ or 0.01 mol/L NaOH.

The procedure for each of the preceding experiments is described as follows:

The solutions were contacted with an accurately measured MMS suspension sample of sorbent and agitated by means of a mechanical stirrer (IKA Labor Technik) at 300 rpm. Aliquots of 10 mL were taken from the reacting solution at determined time intervals and filtered (0.45 μm acetate membrane). The pH was not adjusted during the reaction period and any pH change was measured and recorded at the time the samples were taken. The duration of the experimental runs was 60 min. Prior to analysis, the samples were acidified using 50

concentrated HNO₃ and the target metal species concentrations determined by Atomic Absorption Spectrometry (VARIAN Spectra AA-220-FS). The evaluation of the data was carried out by applying the relationships of section 3.2.

4.8.1.2 Effect of mass of adsorbent

Metal ion bearing solutions were prepared at determined initial concentrations and contacted with a different amount of MMS.

Table 4.4 : Variables used for the kinetic experiments based on the variation of bulk solution concentration with time.

Metal solution	pH	m MMS, mg
Cd(II)	7	5
		10
		20
Ni(II)	7	5
		10
		20
Pb(II)	6	5
		10
		20
Mo(VI)	4	-
		20
		30

For cadmium as well as for nickel ions, a volume of 1000 mL of metal ion bearing solution with initial concentration of 8.9×10^{-3} mmol/L for Cd(II) and 17×10^{-3} mmol/L for Ni(II) and initial pH 7 were prepared. The solutions were contacted with an accurately measured MMS suspension sample corresponding to 5, 10, and 20 mg of sorbent mass and agitated by means of a mechanical stirrer at 300 rpm for a period of 60 min.

The procedure of the experiments was as follows:

Samples of 10 mL were taken at different intervals of time and filtered (0.45 μ m acetate membrane). Similar to the previous experiments the pH was not adjusted during the reaction period and any pH change was measured and recorded at the time the samples were taken. The samples were acidified by using concentrated HNO₃ and subsequently the concentrations

of Cd^{2+} and Ni^{2+} measured by Atomic Absorption Spectrometry (VARIAN Spectra AA-220-FS).

In the case of lead metal ion, a volume of 1000 mL of metal ion bearing solution with initial concentration of 9.7×10^{-3} mmol/L and initial pH 6. The solution was contacted with a measured suspension of MMS corresponding to 5, 10, and 20 mg of mass, and stirred by means of a mechanical stirrer at 300 rpm for a period of 60 min. The experimental procedure was carried out similar to sorption experiments described previously. Aliquots of 10 mL were collected at different intervals of time. Firstly the samples were filtered through a $0.45\mu\text{m}$ membrane filter and then acidified to pH 2 with HNO_3 .

Finally for molybdenum, a volume of 1000 mL of metal ion bearing solution with initial concentration of 1×10^{-5} mmol/L and initial pH 4 was contacted with 10, 20, and 30 mg of mass of adsorbent (m). The experimental procedure was the same as for the metal ions. The concentration of Mo(VI) as well as of Pb(II), Cd(II), and Ni(II) was measured by means of Atomic Absorption Spectroscopy (VARIAN Spectra AA-220-FS).

4.8.1.3 Effect of competitive adsorption

For carrying out experiments of competitive sorption between Cd^{2+} and Ni^{2+} equal quantities of both metal ions were contacted with a determined amount of adsorbent. 1000 mL of metal ion solution with an initial concentration of $5.0 \mu\text{mol/L}$ for both Cd^{2+} and Ni^{2+} was contacted with an amount of 10 mg of MMS. The suspension was stirred at 300 rpm for a period of 60 min. Samples at different intervals of time were collected and the concentration of Cd^{2+} and Ni^{2+} were measured by Atomic Absorption Spectrometry (VARIAN Spectra AA-220-FS) measured.

By means of the kinetic studies the determination of the mass transfer coefficient β_L in the liquid phase for the sorption of cadmium, nickel, lead, and molybdenum onto MMS was obtained. In addition, the data generated were evaluated by means of the simplified approaches as described also in 3.2.

4.9 Desorption and reusability studies

To examine the desorption of the metal ions from the MMS, and the reusability of the micro-sorbent, a series of batch experiments were devised. For the desorption and reusability experiments the following conditions were applied:

Table 4.5 : Variables used for the steps involved in the desorption and reusability studies.

Step	Metal	pH	V _L , L
Sorption	Pb(II)	6	1
Desorption	-	3.5	0.01
Washing	-	MQ water	0.01

The desorption and reusability procedure is divided in three steps: sorption, desorption, and washing. The description of each step is as follows:

Sorption: In a first cycle a volume of 1 L of the metal ion solution with a concentration of 4.6 $\mu\text{mol/L}$ was contacted with a certain amount of the microsorbent. The suspension was agitated in a shaker at 200 rpm for a period of 30 min. After this period the solid was separated from the solution by using a hand magnet.

Desorption: For desorption, the microsorbent, previously used in the sorption step, was contacted with a volume of 10 mL of a solution of pH 3.5. The suspension was agitated at 200 rpm for a period of 30 min. Once the time was completed the magnetic solid-liquid separation was carried out.

Washing: In order to remove remanent metal ions from the desorption step the microsorbent was contacted with a volume of 10 mL of MQ water. After magnetic separation the solid was ready for the next cycle. The procedure was repeated until 5 cycles were completed.

Samples of the solution were taken in each step, filtered through a 0.45 μm membrane filter and acidified to pH 2 with HNO_3 . Initial and final concentrations, as well as concentration for the washing step were measured by means of Atomic Absorption Spectrometry (VARIAN Spectra AA-220-FS).

5 Results and Discussion

5.1 Synthesis of magnetic microsorbent (MMS)

5.1.1 Physicochemical analyses

For the preparation of the magnetic microsorbent material, different Fe_3O_4 : MnO_2 ratios were investigated as it was explained in section 4.1.

The Table 5.1 shows the amounts of dissolved manganese from MnO_2 in the magnetic microsorbent calculated in mg/100mg of sorbent.

Table 5.1 : Elemental analyses of magnetic microsorbents.

Fe_3O_4 : MnO_2	Dissolved Mn, mg/100 mg sorbent
10 : 1	5.50
5 : 1	10.2
2.5 : 1	22.3
1 : 1	28.1

As obvious, to the extent that the ratio Fe_3O_4 : MnO_2 decreases, the concentration of manganese in the sorbent increases. Smaller proportions of Fe_3O_4 : MnO_2 were not included for two reasons: (i) it is not possible to obtain a higher degree of fixation of MnO_2 onto the magnetite particles due to the washing process, and (ii) smaller amounts of Fe_3O_4 would imply lower levels of saturation magnetization.

In Table 5.2 are summarized the values of specific surface area obtained for the magnetic microsorbents at various Fe_3O_4 : MnO_2 ratios by means of BET measurements.

Table 5.2 : Specific surface area values obtained for different Fe_3O_4 : MnO_2 ratios.

Fe_3O_4 : MnO_2	Surface area, m^2/g
10 : 1	32.4
5 : 1	57.2
2.5 : 1	97.7
1 : 1	126

It has been seen that to a greater ratio of Fe_3O_4 : MnO_2 smaller values of specific surface area are observed, and vice-versa. As mentioned in section 4.1, magnetite has a specific surface area ranging between 3 and 6 m^2/g , thus the high values of surface area can be attributed to the presence of MnO_2 in the adsorbent, which has an estimated value about 235 m^2/g .

5.1.1.1 Reproducibility of the synthesis

Depending on the method of preparation various morphologies and consequently various adsorption properties were obtained. Thus, the reproducibility of the synthesis of the magnetic microsorbent was evaluated directly by means of adsorption experiments.

The reproducibility of the synthesis of the material was tested by the adsorption of Cd^{2+} onto 8 magnetic microsorbents synthesized as explained in section 4.1 for obtaining the 1:1 ratio. Figure 5.1 shows the amount of cadmium adsorbed plotted versus the batch number of the synthesis.

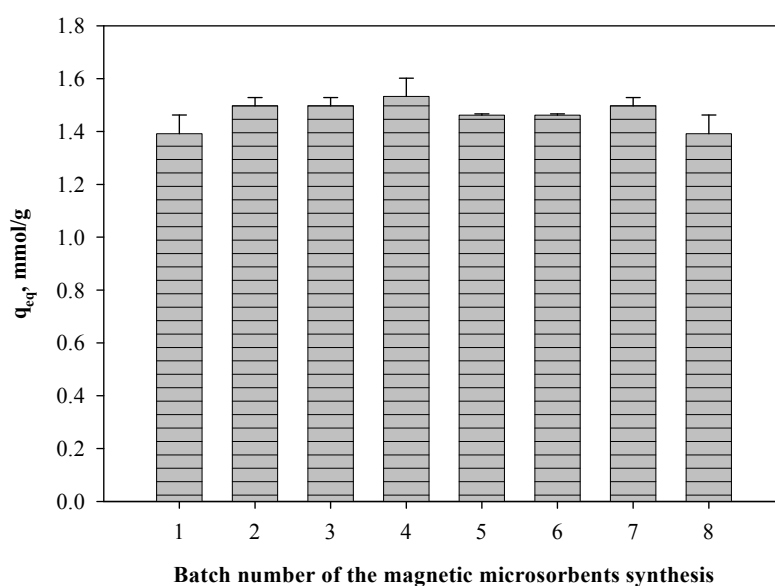


Figure 5.1: Reproducibility of material synthesis tested by means of sorption experiments with a solution of $\text{Cd}(\text{II})$ onto 8 magnetic microsorbents with a Fe_3O_4 : MnO_2 ratio of 1:1. $c_{\text{Cd}} = 8.9 \times 10^{-3}$ mmol/L, $\text{pH} = 7$, $T = 25^\circ\text{C}$.

By comparing the equilibrium sorption capacities obtained for the adsorption of cadmium onto the microsorbents, it can be seen that the values are in a range between 1.39 and 1.53 mmol/g. The average value was observed to be 1.46 mmol/g, with a deviation not greater than 5%, which can be considered a good deviation for adsorption results. On the basis of the small

deviation of the equilibrium sorption capacities, it can also be said that the reproducibility of the material synthesis method was successfully achieved.

5.1.2 ESEM images

Connected with the previous section, in order to obtain information about the morphology and size distribution of the particles of the material synthesized, combined ESEM imaging techniques with EDX analysis techniques were applied. Figure 5.2 corresponds to an imaging of the magnetic microsorbent.

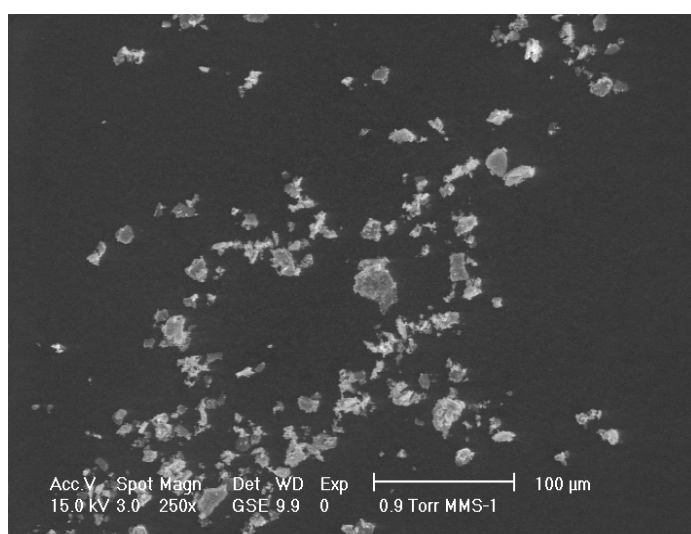


Figure 5.2: ESEM image of MMS synthesized by the precipitation of MnO_2 in the presence of magnetite particles.

In the image a nonuniform particle distribution is observed. The material is conformed by very small particles and other agglomerates of a greater size. A second image of the MMS material corresponding to a magnification of a section of the Figure 5.2 is shown in Figure 5.3.

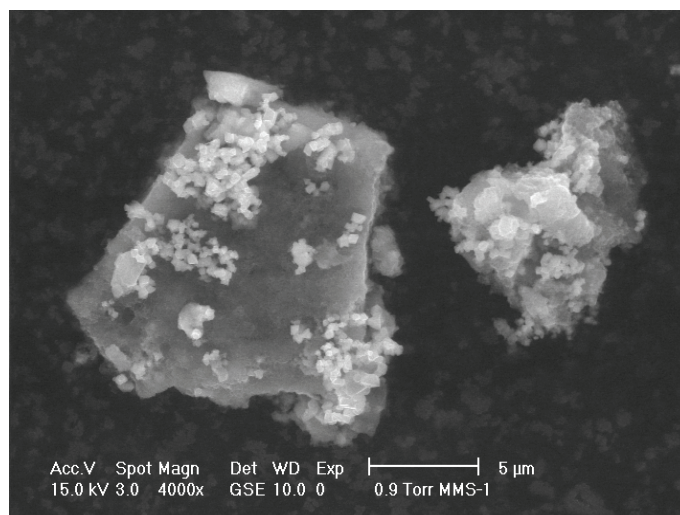


Figure 5.3: ESEM image of MMS. Magnification of Figure 5.2.

In Figure 5.3, the ESEM image reveals that the microsorbent consists in two phases, small crystals and a major form; the first ones are placed as aggregates on the second one.

In order to identify the main components of the microsorbent, Fe_3O_4 and MnO_2 , EDX analyses of the surface of the microsorbent was applied.

In Figure 5.4 a comparison of EDX analyses of two areas of the surface of the MMS is shown.

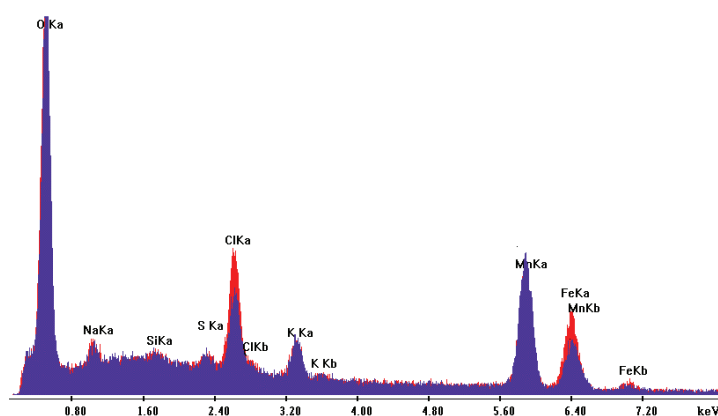


Figure 5.4: EDX analysis of the surface of the MMS particles shown in Figure 6.3.

Both EDX analyses show the presence of manganese and iron which is consistent with the composition of the microsorbent. Nevertheless, it should be appointed that for one of the EDX analysis the intensity of the peak at 6.40 keV rises. This EDX analysis was performed in the

area where the small crystals lie, thus can be determined that while the small crystals correspond to magnetite, Fe_3O_4 , the major form would correspond to manganese dioxide, MnO_2 .

5.1.3 Particle size and distribution.

Figure 5.5 shows the percentage density distribution of MMS as function of the size.

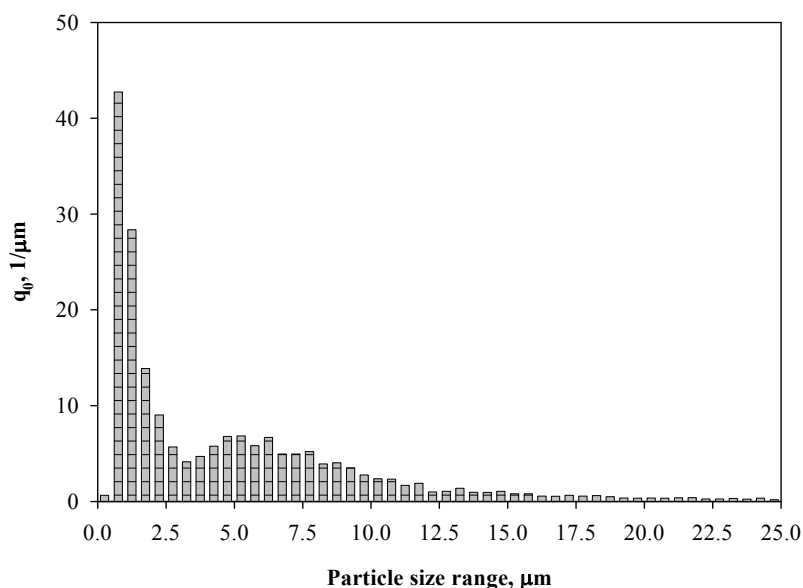


Figure 5.5: Particle size distribution (q_0) of the synthesized MMS.

In this figure a bimodal distribution can be seen with peaks at 1 and 5 μm . The particle size analyses of the MMS shows that 50% of the particles were ranged under 2.85 μm and a 90% under 12.51 μm . The particle size distribution was between 0.5 and 18 μm . This nonuniform distribution is attributed to the formation of agglomerates (see Figure 5.2).

5.1.4 Density

The density of the MMS was found to be $3.8039 \pm 0.005 \text{ g/cm}^3$. This value is in the range of that of magnetite which has a value of 4.6 g/cm^3 (see Table 8.1 in Appendix).

5.1.5 Chemical stability

Chemical stability is an additional criterion that allows establishing e.g. the pH range in which the adsorbent is applicable. The chemical stability of MMS was examined by means of its dissolving behavior in aqueous solutions at various pH values in a range between 2 and 7. Table 5.3 gives the amounts of manganese (Mn^{2+}) measured in solution at different pH values.

Table 5.3 : Disolution of MMS at various pH values.

pH _i	2	2.5	3	3.5	4	5	6	7
Mn^{2+} , mg/L	0.101	0.036	0.016	< 0.01	< 0.01	< 0.01	< 0.01	< 0.01

The results show that in a pH interval from 3.5 to 7 the micro-sorbent has a rather high stability, while in the pH interval from 2 to 3, the micro-sorbent slightly dissolved. The dissolution in the most acidic pH interval can be attributed to the interaction of manganese dioxide with the protons in the solution. To explain this interaction an scheme with consecutive reactions step of the dissolution of an oxide (M_2O_3) is shown in (Furrer 1987).

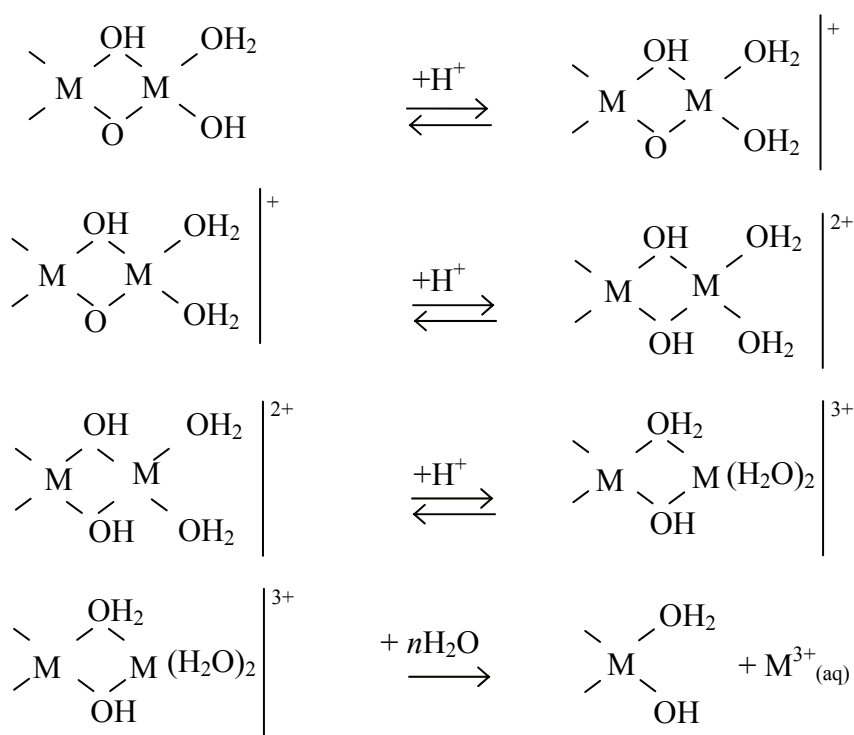


Figure 5.6: Dissolution process at an oxide surface site proton-promoted.

The protons in the solution can bind to the hydroxyl groups at the manganese oxide (or MMS surface), and promote the dissolution. On the basis of these results it can be concluded that the synthesized material can be used in solutions whose pH values are above pH 3.5.

5.1.6 Magnetic characterization

Magnetization curves of the magnetic microsorbents obtained for various resulting Fe_3O_4 : MnO_2 ratios are shown in Figure 5.7.

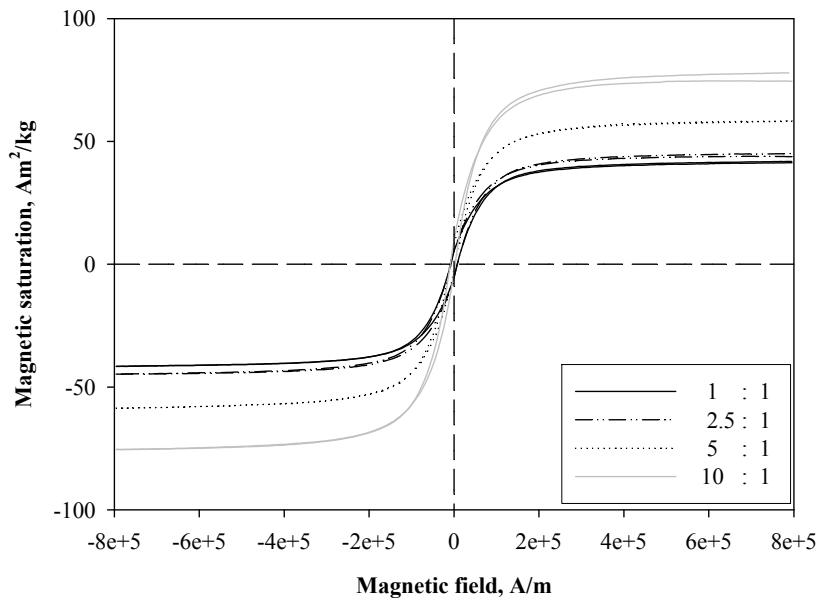


Figure 5.7: Magnetization curves of micro magnetic adsorbents for different Fe_3O_4 : MnO_2 ratios.

It is observed that for each material the magnetization increases by increasing the magnitude of the magnetic field applied until a maximum is reached, the so-called saturation magnetization (M_s).

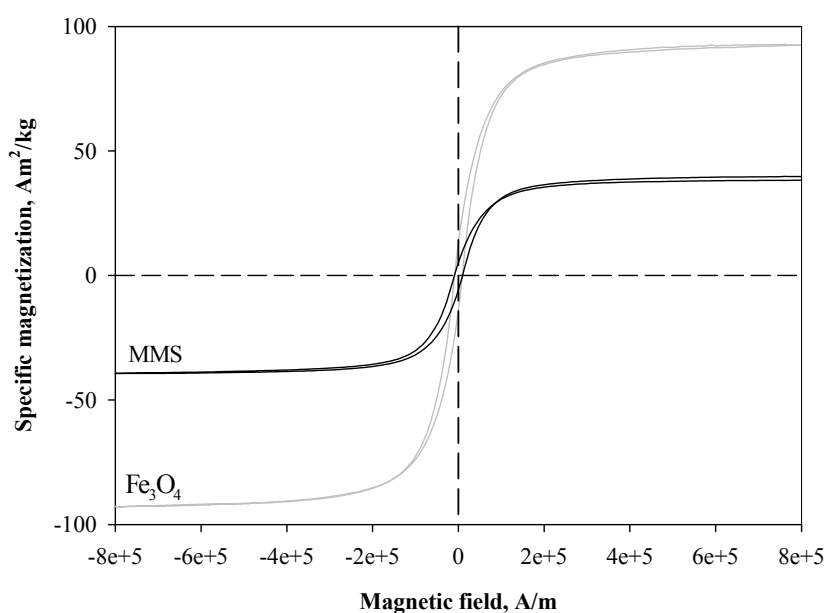
An increase in the amount of magnetite leads to an increase in the saturation magnetization values. This was expected because magnetite has a high magnetic saturation, of about $92.6 \text{ Am}^2/\text{kg}$, and it is the main component of the microsorbent with magnetic characteristics. In Table 5.4 the values obtained for the magnetic saturation (M_s) and remanent magnetization (M_r) are summarized.

Table 5.4 : Saturation magnetization of Fe₃O₄: MnO₂ materials.

Fe ₃ O ₄ : MnO ₂	M _s , Am ² /kg	M _r , Am ² /kg
10 : 1	74.5	9.92
5 : 1	58.3	7.78
2.5 : 1	44.9	5.60
1 : 1	41.3	5.39

Related to the remanent magnetization, it can be observed that the values lie between 5.39 and 9.92 Am²/kg. The values show that all Fe₃O₄: MnO₂ ratios possess ferromagnetic characteristics. The ferromagnetic characteristics observed for the Fe₃O₄: MnO₂ materials can be attributed to the magnetite used in the synthesis, which is highly ferromagnetic with a corresponding remanent magnetization value, M_r, of 13.5 Am²/kg.

According to the results obtained for the amount of MnO₂ as Mn²⁺, magnetic saturation and specific surface area, the material corresponding to the 1:1 ratio was considered as the potentially best adsorbent material. Therefore it was selected for further characterization and subsequent application in adsorption experiments. This material will be appointed later as MMS. Finally, the magnetization curve of MMS was compared to that of Fe₃O₄ (see Figure 5.8).

Figure 5.8: Magnetization curves of Fe₃O₄ and MMS.

As expected, Figure 5.8 shows that the magnetic saturation of MMS ($41.3 \text{ Am}^2/\text{kg}$) is smaller than that of pure magnetite. However, it possesses a sufficiently high level of magnetic saturation to allow the particles to be removed from a solution by using an external magnetic field. Other authors have reported values of magnetic saturation for materials used as adsorbents between 8 and $33.5 \text{ Am}^2/\text{kg}$ (Oliveira, Rios et al. 2003; Oliveira, Petkowicz et al. 2004; Shu and Wang 2009).

5.1.7 Magnetic solid-liquid separation

The magnetic solid-liquid separation of MMS was examined. For this purpose solid-liquid separation experiments under the influence of a magnetic field and in its absence were carried out. By means of relative turbidity values, T/T_0 , the effectiveness of the magnetic characteristics on the solid-liquid separation was probed. Figure 5.9 and Figure 5.10 show the relative turbidity, T/T_0 , for suspensions of MMS at different pH values.

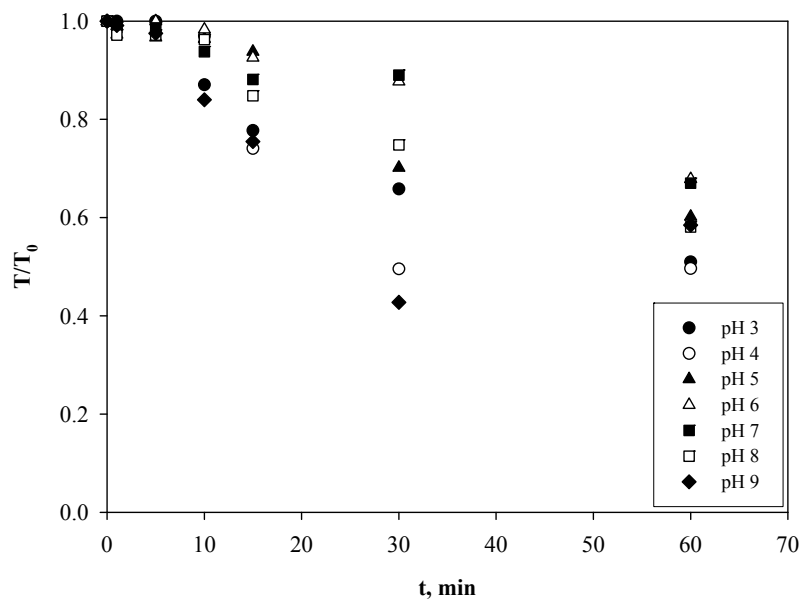


Figure 5.9: Relative turbidity of MMS suspension at various settling times and pH ranging from 3 to 9. No external magnetic field applied.

The results showed that in the absence of an external magnetic field the solid liquid-separation is insufficient. At 60 min a significant fraction of the solids remain suspended into the solution. It becomes clear that the adsorbent itself can not be separated adequately from the solution by sedimentation alone.

Figure 5.10 shows the results of the solid-liquid separation represented as relative turbidity under the influence of an external magnetic field.

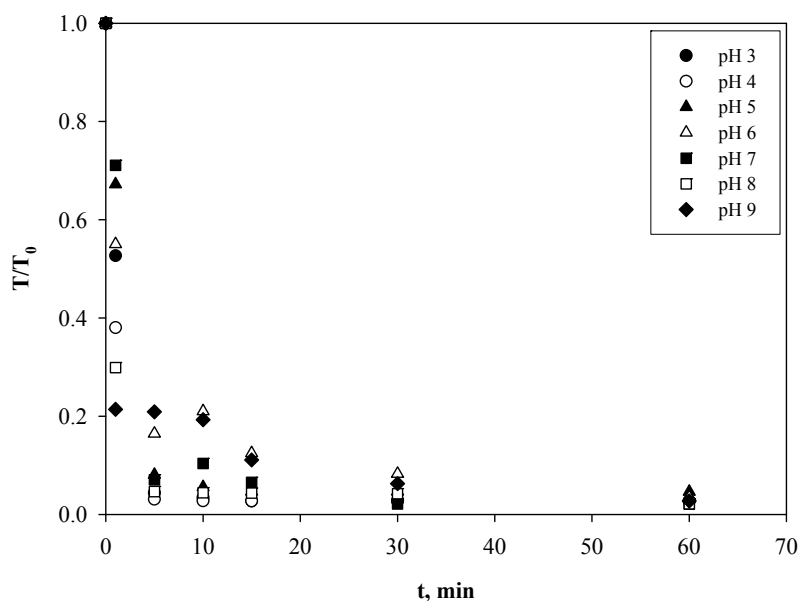


Figure 5.10: Relative turbidity of MMS suspension under a magnetic field at various settling times and pH ranging from 3 to 9.

It can be seen that in the presence of a magnetic field the settling of the suspension at each pH value is much more effective than without its influence. The values of T/T_0 decrease dramatically once the external magnetic field is applied. After 10 min the values of T/T_0 are in almost all cases under 0.1 (see Figure 5.10). It is noted that the T/T_0 were smaller at pH values 3 and 4 than at pH 6 and 7, nevertheless for all pH values the T/T_0 are under 0.1.

By comparing the results of Figure 5.9 and Figure 5.10 it can be concluded that the magnetic properties of the micro-sorbent MMS allow an effective solid-liquid separation. In order to establish whether the ionic strength of the media does have a further influence on the solid-liquid separation, experiments in presence of NaNO_3 were carried out. The experiments were similar to those presented in Figure 5.9 and Figure 5.10.

Results for the relative turbidity obtained by using a 0.001 mol/L NaNO₃ and 0.01 mol/L NaNO₃ solutions as media are shown in Figure 5.11 and Figure 5.12 respectively.

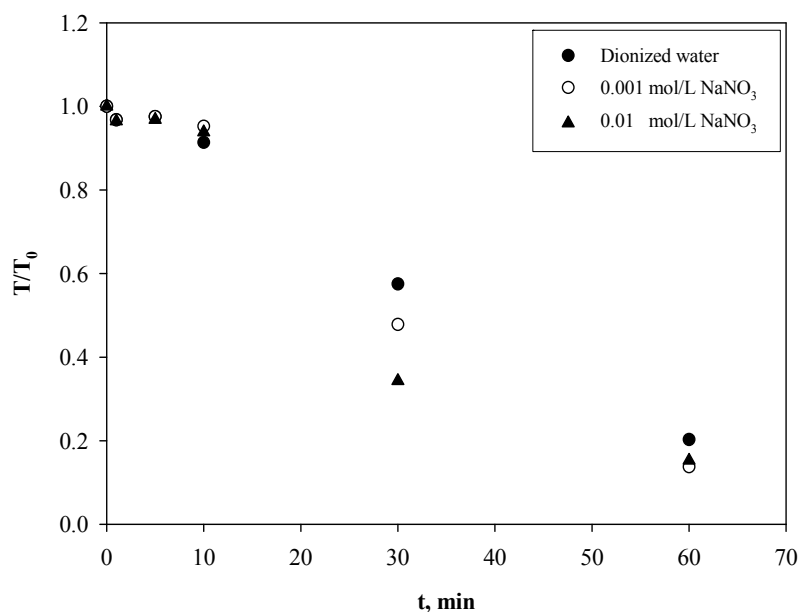


Figure 5.11: Relative turbidity of MMS suspension at various settling times in water as well as in 0.001 and 0.01 mol/L NaNO₃ solutions. No influence of an external magnetic field.

Figure 5.11 shows that not significant contribution to the solid-liquid separation can be attributed to the presence of the NaNO₃ in the solution. The behavior observed is very similar between the three solutions. Nevertheless, the values measured for 0.01 mol/L NaNO₃ solution were slightly smaller than those obtained in the presence of either deionized water or 0.001 mol/L NaNO₃ as solution media. The results can be compared with those previously presented, where at different pH values the particles in absence of an external magnetic field were not able to settle down in an adequate period of time.

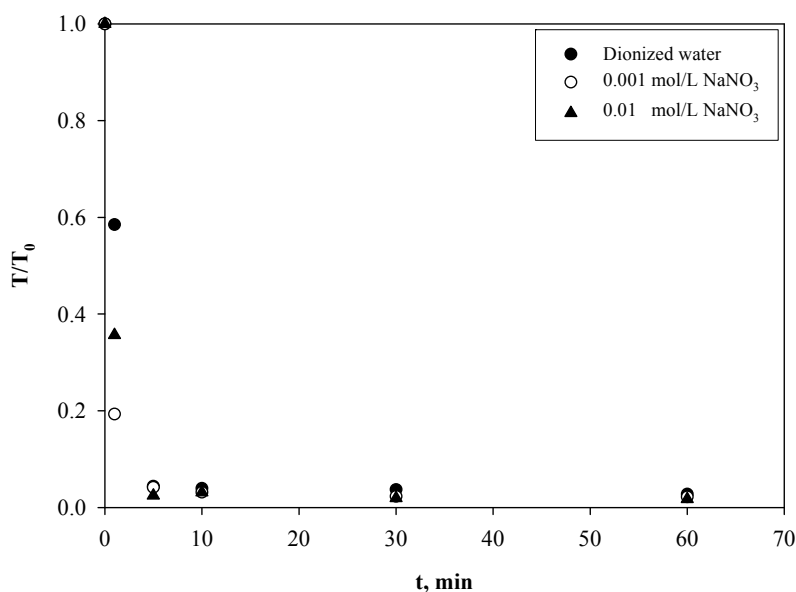


Figure 5.12: Relative turbidity of supernatants of MMS suspension at various settling times under a magnetic field for water and 0.001 and 0.01 mol/L NaNO_3 solutions.

The results for the solid-liquid separation presented in Figure 5.12 show again the significant influence of the magnetic properties of the micro-sorbent in the solid-liquid separation. The values of T/T_0 immediately decrease in the presence of an external magnetic field. After time interval of about 5 min the relative turbidity is smaller than 0.05.

With these results it is possible to consider a large scale application for using the magnetic micro-sorbent which can be removed from solution by magnetic flocculation system to reach about 90% of separation coupled with a high gradient magnetic separator (HGMS) to finally obtain more than 99% of solid separation.

5.1.8 Zeta potential

In order to determine the variation of the surface charge of the magnetic microsorbent as a function of pH, zeta potential measurements at different pH values were carried out. Given the characteristics of the microsorbent regarding to its chemical stability, the zeta potential was measured in a pH range between 3 and 9. For the measurements a microelectrophoresis technique was conducted. By means of this technique the electrophoretic mobility of the particles is obtained. As explained in section 4.6, the measurements of electrophoretic mobility are related to the zeta potential values (ζ).

The experimental curve corresponding to the micro electrophoresis measurements obtained for MMS is illustrated in Figure 5.13.

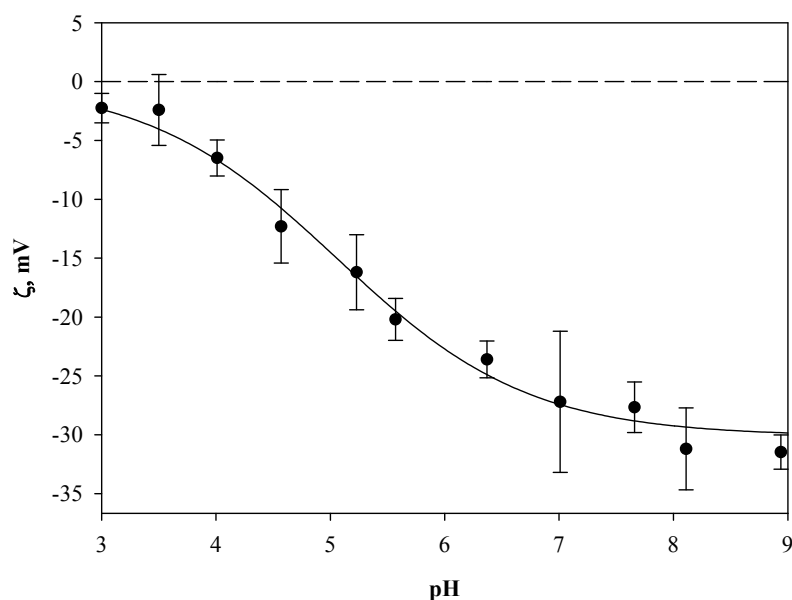


Figure 5.13: Zeta potential versus pH for the material MMS measured by means of the microelectrophoresis technique (MET). 0.01 mol/L NaNO_3 . $T = 25^\circ\text{C}$.

In Figure 5.13 it can be noted that by increasing the pH a sharp decrease of the zeta potential is observed with final values between ≈ -25 and ≈ -30 mV. At pH values greater than 7, however, a further increase in pH does not result in a further significant decrease in mV.

It was not possible by means of this technique to establish a pH value as a pH_{PZC} , but is clearly seen that above pH 3 the surface of MMS bears a negative charge. This characteristic

is a very suitable condition for sorption especially of cations, which will be attracted to the negative charged surface.

The zeta potential of pure MnO_2 was also measured by means of microelectrophoresis. The results are shown in Figure 5.14.

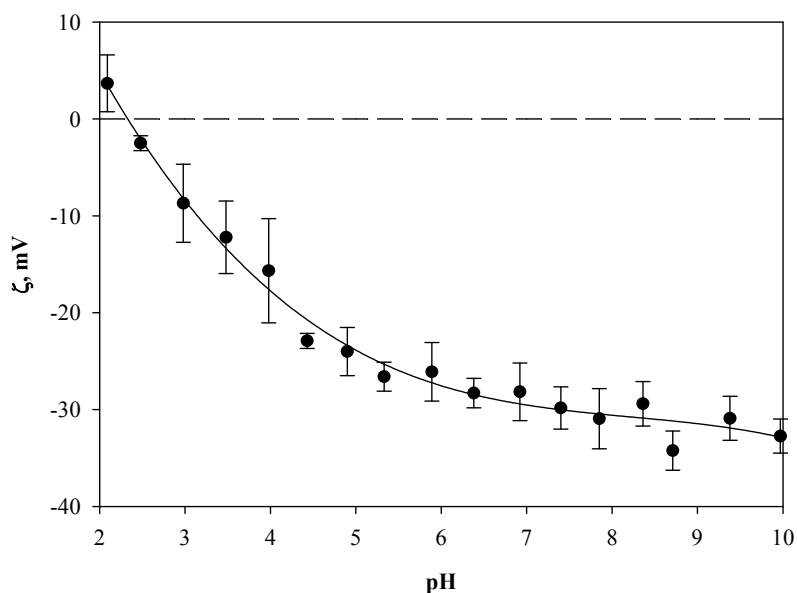


Figure 5.14: Zeta potential versus pH for pure MnO_2 measured by means of the microelectrophoresis technique (MET). 0.01 mol/L NaNO_3 . $T = 25^\circ\text{C}$.

These results show that MMS has a surface behavior very close to that of MnO_2 which has an estimated value for $\text{pH}_{(\text{PZC})}$ slightly higher than pH 2 (see Figure 5.14). Thus, the procedure by which MMS is synthesized can be regarded as successful to the extent that the surface characteristics of MnO_2 determine the ones of MMS.

In order to confirm that the $\text{pH}_{(\text{PZC})}$ of MMS is placed in the near of pH 3 a immersion technique (IT) was carried out. The experimental curve corresponding to the IT technique is presented in Figure 5.15.

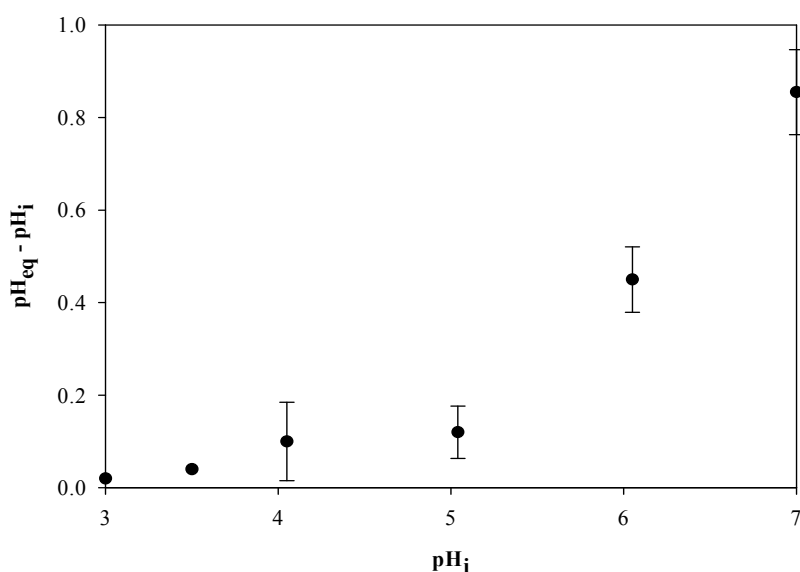


Figure 5.15: Experimental curve corresponding to the immersion technique (IT) for the determination of the $\text{pH}_{(\text{PZC})}$ of MMS. 0.01 mol/L NaNO_3 , $T = 25^\circ\text{C}$.

As can be minimum value of (ΔpH) was obtained in the range of pH 3. The $\text{pH}_{(\text{PZC})}$ is identified as the initial pH with the minimum (ΔpH) which would corresponds to pH 3.

By means of both micro electrophoresis and immersion techniques it can be estimated that the $\text{pH}_{(\text{PZC})}$ value for MMS lies close to pH 3, thus at pH over this value leads to the surface possessing negative charges, so as to facilitate the adsorption capacity of cationic species and at pH values in the neighborhood of the estimated $\text{pH}_{(\text{PZC})}$ the adsorption of anionic species could be favoured.

5.2 Equilibrium studies

As explained in section 4.7.1 the influence of different parameters such as pH, complexing ligands, and competitive ions on the sorption equilibrium of the species Cd(II), Ni(II), Pb(II), and Mo(VI) onto MMS was investigated. The evaluation of the data of the sorption experiments was carried out by means of the Langmuir and Freundlich isotherms. The descriptions of both relationships are in chapter 3.

5.2.1 Effect of pH

To assess the effect of pH on the sorption of Cd(II), Ni(II), Pb(II), and Mo(VI) onto MMS, equilibrium sorption experiments with varying pH values were carried out. The results are shown in the next figures. Figure 5.16 shows sorption isotherms of cadmium ions onto MMS from solutions containing 0.01 mol/L NaNO₃ as electrolyte for initial pH values ranging between 4 and 7.

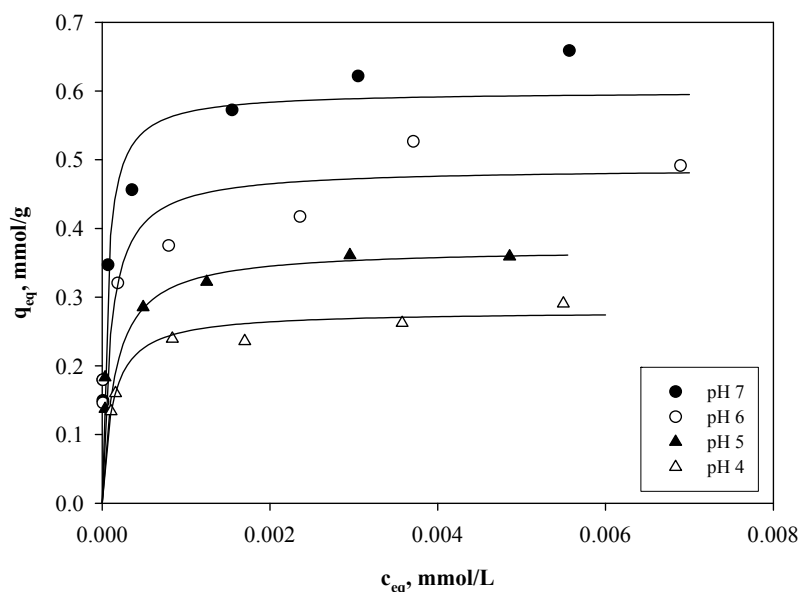


Figure 5.16: Sorption isotherms of Cd²⁺ ions at different initial pH values. $c_{\text{NaNO}_3} = 0.01$ mol/L, $m_s = 5$ mg, $T = 25^\circ\text{C}$. Evaluation by means of the Langmuir relationship.

The results shown in Figure 5.16 demonstrate an increment of maximal capacity values with increasing pH, with a maximal value at pH 7. At low pH values, the small amount of Cd²⁺ adsorbed is probably due to the competitive adsorption of H⁺ with metal ions for the exchange

sites of the adsorbent. As the pH increases, the negative charge density on the MMS surface increases (see Figure 5.13) due to the deprotonation of its surface and thus the metal ion adsorption increases. The Langmuir relationship has been applied for the evaluation of the experimental equilibrium data (solid lines). The equilibrium parameters q_{\max} and K_L deduced from the experimental data are summarized in Table 5.5. The same series of data were also analyzed using the Freundlich relationship and the adsorption isotherms are shown in Figure 5.17.

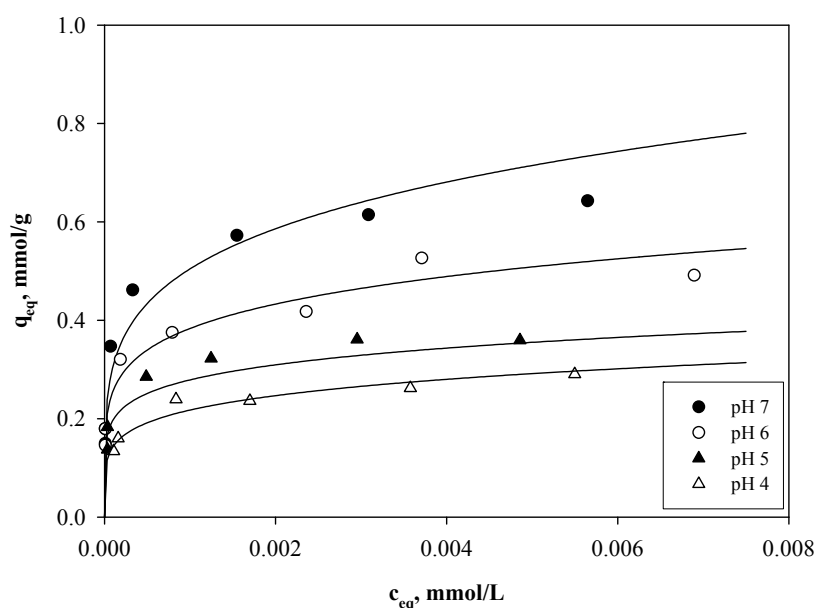


Figure 5.17: Sorption isotherms of Cd^{2+} ions at different initial pH values. $c_{\text{NaNO}_3} = 0.01$ mol/L, $m_s = 5$ mg, $T = 25^\circ\text{C}$. Evaluation by means of the Freundlich relationship.

The results, similar to the previous plot, show an increasing of the sorption equilibrium capacities of Cd^{2+} onto MMS by increasing the pH of the solution. The plotted lines, which correspond to the Freundlich isotherm evaluation, can adequately describe the experimental data. The Freundlich isotherm constants along with the correlation coefficients are also listed in Table 5.5. In Figure 5.18 sorption isotherms of nickel ions onto MMS from solutions containing 0.01 mol/L NaNO_3 as electrolyte and for initial pH values ranging between 4 and 7 are shown.

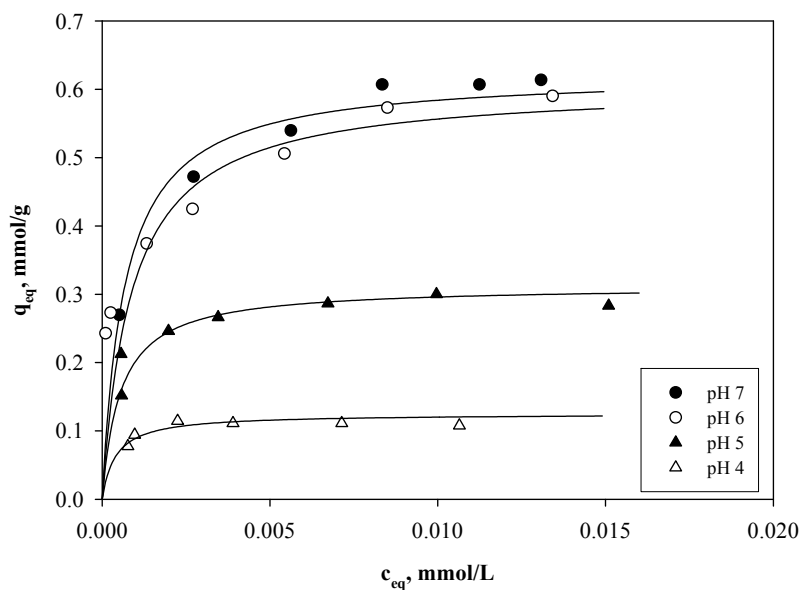


Figure 5.18: Sorption isotherms of Ni^{2+} ions at different pH values. $c_{\text{NaNO}_3} = 0.01 \text{ mol/L}$, $m_s = 5 \text{ mg}$, $T = 25^\circ\text{C}$. Evaluation by means of the Langmuir relationship.

The results demonstrate the increase of capacity with increasing pH value, reaching a maximum capacity at pH 7. As well as for cadmium ion solutions, at low pH values, the small amount of Ni^{2+} adsorbed can be attributed to the competitive adsorption of H^+ with metal ions for the exchange sites of the adsorbent. At higher pH values, the negative charge density on the MMS surface increases due to the deprotonation of its surface and thus the metal ion adsorption increases. The equilibrium parameters q_{max} and K_L deduced from the experiments data by means of the application of the Langmuir relationship are also summarized in Table 5.5.

As well as for Cd^{2+} and Ni^{2+} , the results for the effect of pH on the adsorption of Pb^{2+} onto MMS were plotted as sorption isotherms. Figure 5.19 shows isotherms of the sorption of lead ions onto MMS from solutions containing 0.01 mol/L NaNO_3 as electrolyte and for initial pH values ranging between 4 and 6.

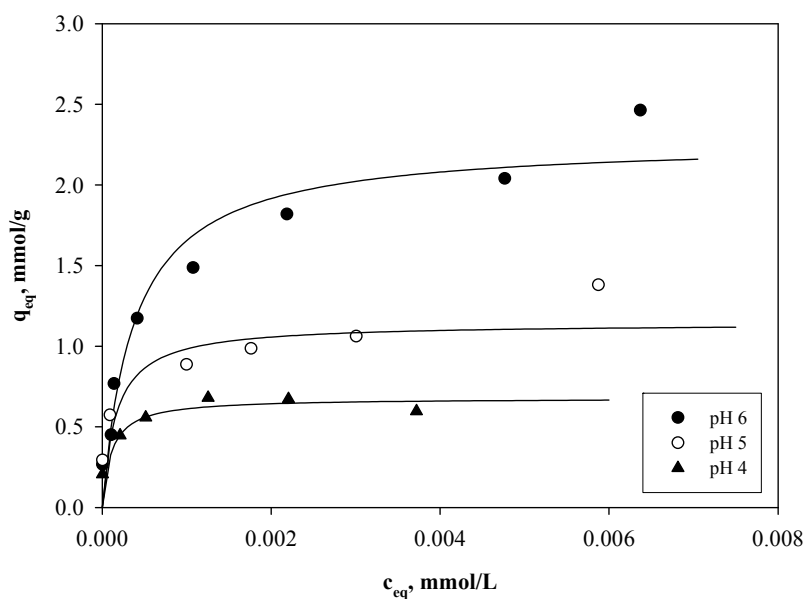


Figure 5.19: Sorption isotherms of Pb^{2+} ions at different pH values. $c_{NaNO_3} = 0.01$ mol/L, $m_s = 1.25$ mg, $T = 25^\circ C$. Evaluation by means of the Langmuir relationship.

Again the results show that by increasing the pH value an increase of the equilibrium capacity, q_{eq} , is observed; a maximum value is obtained at pH 6. By comparing these results with those presented in Figure 5.16 and Figure 5.18 it can be observed that the equilibrium sorption capacities obtained for Pb^{2+} are higher than those obtained for Cd^{2+} and Ni^{2+} .

The experimental data were also evaluated by means of the application of the Langmuir and Freundlich relationships. The equilibrium parameters q_{max} and K_L deduced from the experiments data by means of the application of the Langmuir relationship and K_F and n from the Freundlich relationship are summarized in Table 5.5. In Table 5.5 the equilibrium parameters of the sorption of Cd^{2+} , Ni^{2+} , or Pb^{2+} onto MMS deduced by means of Langmuir and Freundlich relationships at different pH values are shown.

Table 5.5 : Equilibrium parameters for sorption of Cd^{2+} , Ni^{2+} , and Pb^{2+} onto MMS at different pH values deduced by means of Langmuir and Freundlich relationships. T = 25°C.

Ion	pH	Langmuir parameters			Freundlich parameters		
		q_{max} , mmol/g	K_L , $\times 10^3$ L/mmol	R^2	K_F	n	R^2
Cd^{2+}	7	0.60	19	0.94	2.3	0.22	0.97
	6	0.49	10	0.88	1.3	0.18	0.91
	5	0.37	6.6	0.97	0.79	0.15	0.98
	4	0.28	8.5	0.99	0.77	0.18	0.97
Ni^{2+}	7	0.62	1.5	0.99	2.0	0.26	0.98
	6	0.60	1.1	0.93	1.5	0.20	0.99
	5	0.31	1.8	0.98	0.52	0.12	0.99
	4	0.13	2.5	0.85	0.25	0.15	0.82
Pb^{2+}	6	2.2	2.7	0.93	12	0.32	0.98
	5	1.0	6.2	0.94	3.8	0.22	0.99
	4	0.72	9.3	0.88	2.1	0.19	0.98

With respect to the results obtained by means of the evaluation with the Langmuir relationship the following observations for each species can be appointed:

In the case of Cd^{2+} , it can be observed that at pH 7 the value of q_{max} of 0.60 mmol/g obtained for the adsorption of Cd^{2+} onto MMS is much greater than the other values obtained at more acidic solution pH. The value obtained at pH 7, was about 2.1 times greater than at pH 4. In the same manner the parameter K_L also deduced from experimental data has a greatest value at the same pH. In the case of Ni^{2+} the value of q_{max} obtained at pH 7 was found to be about 5 times greater than that at pH 4. In case of K_L values no clear trend was observed. As for the other cations, in the case of Pb^{2+} , the value of q_{max} obtained at pH 6 was 3 times greater than that at pH 4.

The comparison of the data summarized in the mentioned table shows that the values for the maximum sorption equilibrium capacity, q_{max} , obtained for the adsorption of lead ions onto MMS were much greater than those obtained for cadmium and nickel at the same pH value. The adsorption capacity increased in the order $\text{Cd}^{2+} < \text{Ni}^{2+} < \text{Pb}^{2+}$.

Taking into account that the ratio m/V used in the adsorption experiments were different, 5×10^{-3} mg/ L for Cd^{2+} and Ni^{2+} , and 1.25×10^{-3} mg/L for Pb^{2+} , it becomes clear that Pb^{2+} is adsorbed more strongly onto MMS than Cd^{2+} and Ni^{2+} .

The results obtained by the application of the Freundlich isotherm, showed that it is also valid for the description of the adsorption of Cd^{2+} , Ni^{2+} , and Pb^{2+} onto MMS. The values of the resulting Freundlich constants K_F increased with increasing pH value; on the other hand the values of n were found to be between 0 and 1 indicating a favorable adsorption of the mentioned metal ions onto MMS.

Adsorption of the molybdenum oxyanion onto MMS was studied at varying pH values and the results are shown in Figure 5.20.

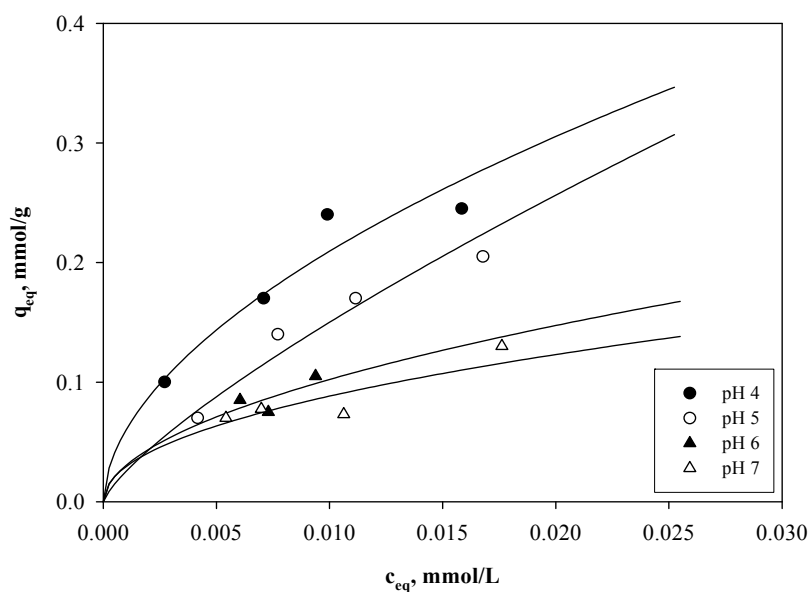


Figure 5.20: Sorption isotherms of molybdate species at various pH values. $m_s = 40$ mg. Evaluation by means of the Freundlich relationship. $T = 25^\circ\text{C}$.

The adsorption of molybdate decreases by increasing the pH showing a value of up to 0.25 mmol/g at pH 4. As commented previously the $\text{pH}_{(\text{PZC})}$ of MMS lies in an acidic pH range, close to pH 3. Thus the average surface charge of MMS is negative at pH values above 3. As is seen in Figure 5.13, the transition from a negative charged surface to a surface with positive charge is gradual, and therefore, due to the heterogeneity of the surface of the micro-sorbent, at pH 4 positively charged surface groups are still available for the sorption of negatively charged species. This behaviour has been observed also by other authors where the extent of molybdenum adsorption by Mn oxyhydroxides decreases with an increase in pH (Barling and Anbar 2004).

The evaluation of the experimental data was carried out by means of both Langmuir and Freundlich relationships. The respective equilibrium parameters are summarized in Table 5.6.

Table 5.6 : Equilibrium parameters for sorption of molybdate species onto MMS deduced by means of Langmuir and Freundlich relationships.

pH	Langmuir parameters			Freundlich parameters		
	q_{\max} , mmol/g	K_L , L/mmol	R^2	K_F	n	R^2
4	0.38	133	0.99	2.6	0.54	0.97
5	0.25	115	0.66	5.3	0.77	0.97
6	0.11	520	0.46	1.3	0.53	0.68
7	0.11	288	0.58	0.80	0.48	0.86

The results of Table 5.6 show that at the pH where a maximum adsorption of molybdenum onto MMS is exhibited, both relationships result in good correlation coefficients, $R^2 > 0.97$. In contrast, at pH values 6 and 7 low correlation coefficients were found indicating that the sorption mechanism differs from the simple assumptions of the Langmuir and Freundlich isotherms.

In the following a summarizing discussion of the role of pH on the adsorption of the four species, Cd^{2+} , Ni^{2+} , Pb^{2+} and MoO_4^{2-} is given:

As mentioned, metal oxides in aqueous solutions show surface charges which are dependent on the pH of the solution. The magnetic microsorber used in the sorption studies contains an important amount of manganese dioxide, and its surface characteristics govern the sorption abilities of MMS. The $pH_{(PZC)}$ of MMS has been found to be close to 3 ± 0.5 . This means that the surface of MMS is expected to be positively charged at $pH < 3$ and negatively charged at $pH > 3$. In Figure 5.21 a scheme of the acquisition of charge onto the manganese dioxide surface is shown.

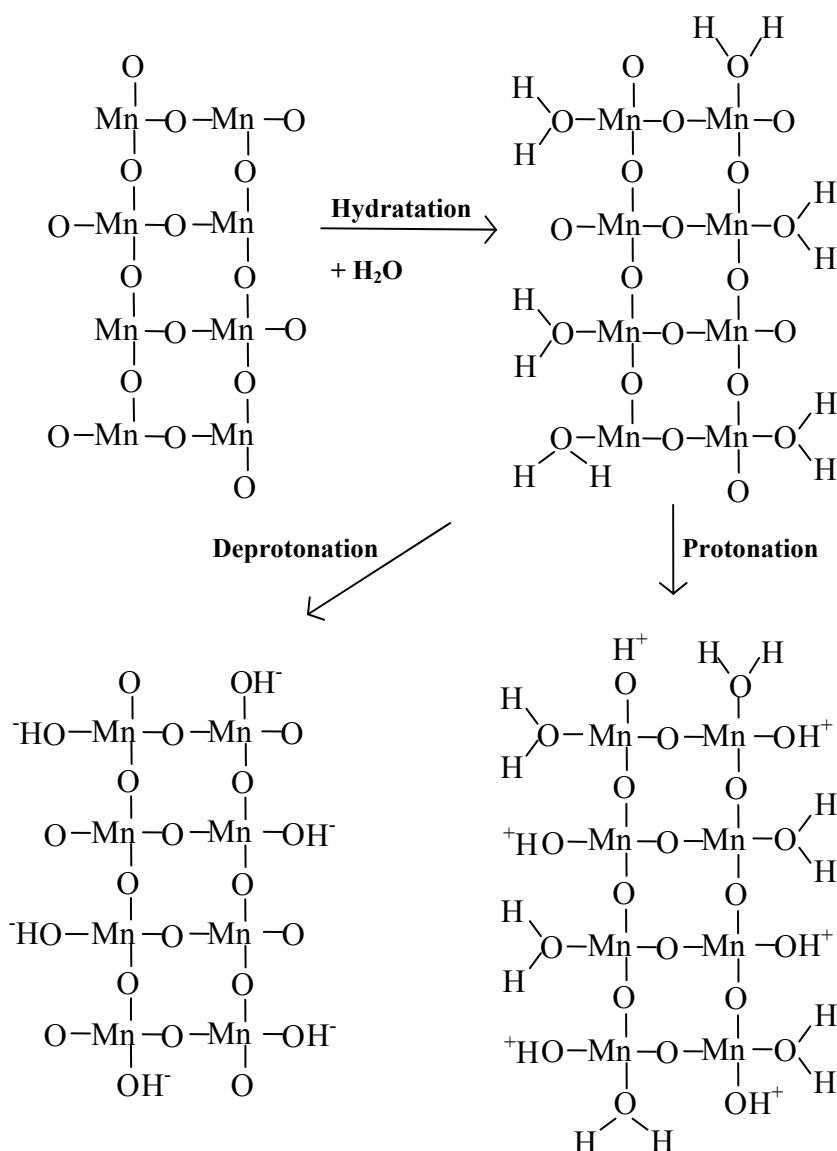


Figure 5.21: Schematic figure of the charge acquisition onto manganese dioxide surface.

The scheme shows that after hydration the surface of manganese dioxide can be charged either positively, by means of protonation, or negatively, by means of deprotonation. Thus, at pH values where protonation dominates, electrostatic repulsions between the cations and the adsorbent become significant and hence the adsorption is diminished.

This is observed in section 5.2.1 where the effect of pH was studied. In the pH range investigated, Cd²⁺, Ni²⁺, and Pb²⁺ are the predominant species present in solution (see Figure 2.3, Figure 2.4, and Figure 2.5). Thus, it seems clear that at pH values which favour the deprotonation, the electrostatic repulsions between the cations and the adsorbent surface

decrease and therefore the adsorption increases; as seen in Figure 5.16, Figure 5.17, and Figure 5.18, respectively.

An increase of adsorption capacities of positive charged species was observed by increasing the pH value. At pH 7 the highest values for the equilibrium sorption capacities for Cd^{2+} and Ni^{2+} were obtained, while for Pb^{2+} the highest values were found at pH 6. In the case of MoO_4^{2-} the opposite behavior was observed; a decrease in pH leads to an increase in sorption, and at pH 4 the highest values for the equilibrium sorption capacities were obtained. Among the species adsorbed Pb^{2+} has shown the highest sorption capacities while MoO_4^{2-} showed the lowest ones. The sorption capacity is influenced by many variables; some of them are related to the hydrated radius and hydration energy among others. The hydrated radius of Cd^{2+} , Ni^{2+} , and Pb^{2+} are, 4.26, 4.04, and 4.01 Å, respectively (Essington 2004). By comparison of the hydration radius the following capacity order is generated: $\text{Pb}^{2+} > \text{Ni}^{2+} > \text{Cd}^{2+}$. Smaller ions with the same valency, such as Cd^{2+} compared with Pb^{2+} , have higher charge densities and attract more water molecules, resulting in a larger hydration radius. Metals with higher hydration radius exert weaker Coulombic forces of attraction. Therefore, Cd^{2+} is expected to be more mobile compared with Pb^{2+} because of its larger hydration radius (Kaoser, Barrington et al. 2005).

In case of the adsorption of MoO_4^{2-} the criteria of the hydration radius can be applied also. The radius of the hydrated ion MoO_4^{2-} is 4.50 Å, which is greater than any of the metal ions included in this investigation. On this basis the order capacity, including MoO_4^{2-} should be: $\text{Pb}^{2+} > \text{Ni}^{2+} > \text{Cd}^{2+} > \text{MoO}_4^{2-}$.

Another variable which than can be considered for explaining the sorption capacity is the hydration energy. Thus, the metal having the highest hydration free energy should have the highest tendency to stay in a soluble form and therefore be adsorbed only weakly. The hydration energy for Cd^{2+} , Ni^{2+} , and Pb^{2+} are -430.5, -494.2, and -357.8 kcal/g-ion, respectively. According to these values the affinity sequence of adsorption should be $\text{Pb}^{2+} > \text{Cd}^{2+} > \text{Ni}^{2+}$. Summarizing, a similar adsorption trend is noted by the data evaluation by means of both Langmuir and Freundlich models. It can be observed that the order of adsorption is $\text{Pb}^{2+} > \text{Ni}^{2+} \geq \text{Cd}^{2+}$ which is consistent with the theoretical estimations discussed above.

5.2.2 Effect of competitive ions

The effect of the presence of competitive ions on the sorption of the metals ions, Cd^{2+} , Ni^{2+} , and Pb^{2+} was studied. Calcium, as the major cation present in natural waters, was selected for the study. The results are presented in Figure 5.22, Figure 5.23 and Figure 5.24. Figure 5.22 shows isotherms of the sorption of cadmium ions onto MMS from solutions containing different amounts of calcium.

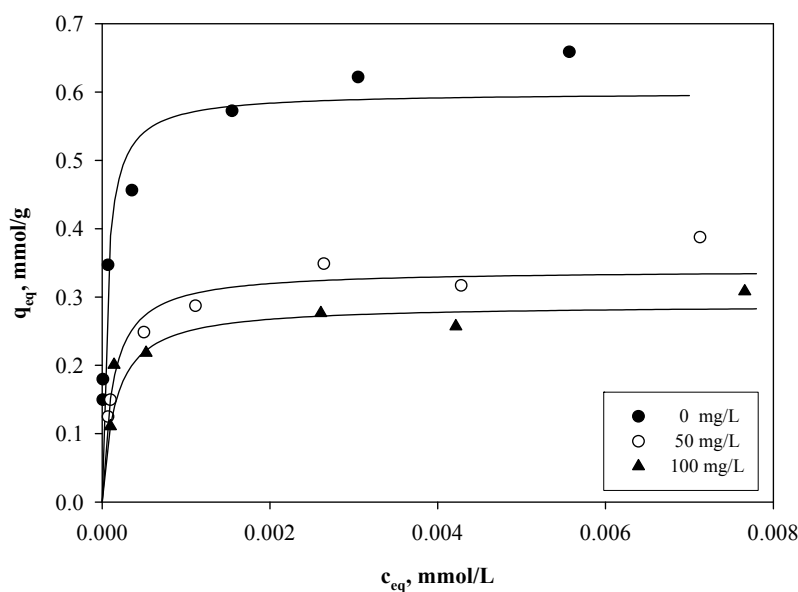


Figure 5.22: Sorption isotherms of Cd^{2+} ions at different concentrations of Ca^{2+} . $\text{pH} = 7$, $m_s = 5$ mg, $T = 25^\circ\text{C}$. Evaluation by means of the Langmuir relationship.

The presence of calcium, as Ca^{2+} ions, in a solution which contains Cd^{2+} affects its sorption. As becomes obvious, there is a competitive sorption of calcium ions. However, substantial influences occur only at concentrations much higher than that of the heavy metals. As a consequence, the figure demonstrates the preferred sorption of the heavy metal species. Figure 5.23 shows sorption isotherms of nickel ions onto MMS from solutions containing different amounts calcium.

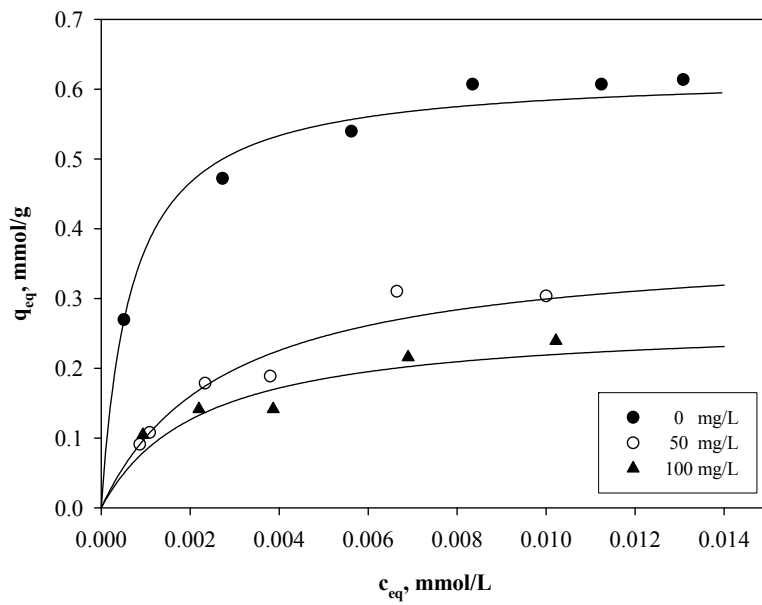
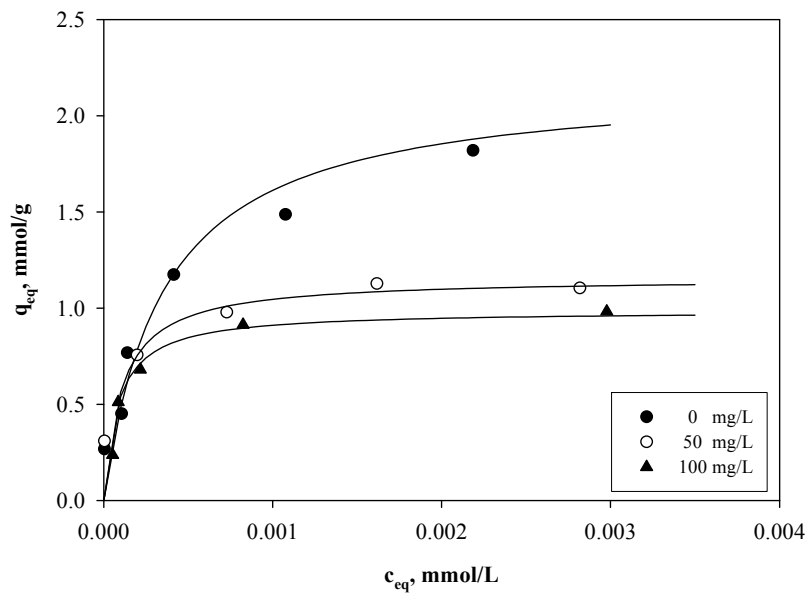


Figure 5.23: Sorption isotherms of Ni^{2+} ions at different concentrations of Ca^{2+} . $pH = 7$, $m_s = 5$ mg, $T = 25^\circ C$. Evaluation by means of the Langmuir relationship.



M

Figure 5.24: Isotherms of the sorption of Pb^{2+} ions at different concentrations of Ca^{2+} . $pH = 6$, $m_s = 1.25$ mg/L, $T = 25^\circ C$. Evaluation by means of the Langmuir relationship.

As in the case of cadmium, there is a competitive sorption of calcium ion. Values of q_{\max} decrease as the concentration of calcium increased (see Table 5.7).

Figure 5.24 shows sorption isotherms of lead ions onto MMS from solutions containing different amounts of calcium. Despite its high affinity towards MMS, the effect of competitive sorption of calcium ions is also observed in the case of lead ions (see Figure 5.24). Table 5.7 summarizes the equilibrium parameters of the adsorption of Cd^{2+} , Ni^{2+} , and Pb^{2+} onto MMS in presence of different concentrations of Ca^{2+} deduced by means of Langmuir and Freundlich relationships.

Table 5.7 : Equilibrium parameters for the sorption of Cd^{2+} , Ni^{2+} , and Pb^{2+} onto MMS at different concentrations of Ca^{2+} deduced by means of Langmuir and Freundlich relationships. $T = 25^\circ\text{C}$.

Ion	Ca^{2+} mg/L	Langmuir parameters			Freundlich parameters		
		q_{max} , mmol/g	K_L , $\times 10^3$ L/mmol	R^2	K_F	n	R^2
Cd^{2+}	0	0.60	19	0.94	2.3	0.22	0.98
	50	0.34	8.1	0.99	1.5	0.25	0.98
	100	0.29	6.4	0.99	0.48	0.10	0.95
Ni^{2+}	0	0.62	1.5	0.99	2.0	0.26	0.98
	50	0.38	0.36	0.98	3.6	0.51	0.98
	100	0.27	0.45	0.85	2.1	0.47	0.97
Pb^{2+}	0	2.2	2.8	0.91	12	0.32	0.99
	50	1.2	9.5	0.98	5.1	0.24	0.98
	100	0.99	12	0.99	19	0.45	0.90

In Table 5.7 the equilibrium parameter, q_{\max} , deduced from the Langmuir relationship reflects the competition; decreasing values with increasing amount of calcium in the solution are observed (see Table 5.7). In the case of cadmium adsorption, for a concentration of 50 mg/L Ca^{2+} , the q_{\max} is reduced 1.8 times, and for a concentration of 100 mg/L Ca^{2+} a 2.1 times reduction is observed. For nickel similar results are obtained, for the presence of Ca^{2+} in a concentration of 50 mg/L the adsorption of Ni^{2+} onto MMS decreased about 1.6 times, while a concentration of 100 mg/L Ca^{2+} results in a 2.3 times reduction. A significant decrease for lead sorption capacity onto MMS is also observed. It may be noted that although an increase in calcium concentration from 50 to 100 mg/L leads to a greater decrease in sorption capacity, this decrease is not linear and its effect is less significant. By comparison with the q_{\max} obtained for the adsorption of Pb^{2+} in the absence of Ca^{2+} , it is seen that this value is diminished 1.9 and 2.2 times for Ca^{2+} concentrations of 50 and 100 mg/L respectively (see Table 5.7). Nevertheless, it must be appointed that the competition was measured in a system where the concentration at which calcium is present in the solution is 20 or more times greater than that of metals and the metal ions Cd^{2+} , Ni^{2+} and, Pb^{2+} .

5.2.3 Effect of complexing ions

The influence of complexing ions on the adsorption of Cd^{2+} , Ni^{2+} , and Pb^{2+} onto MMS was investigated for the case of the formation of chloride complexes. Figure 5.25 shows the effect of the presence of Cl^- ions on the adsorption of Cd^{2+} onto MMS.

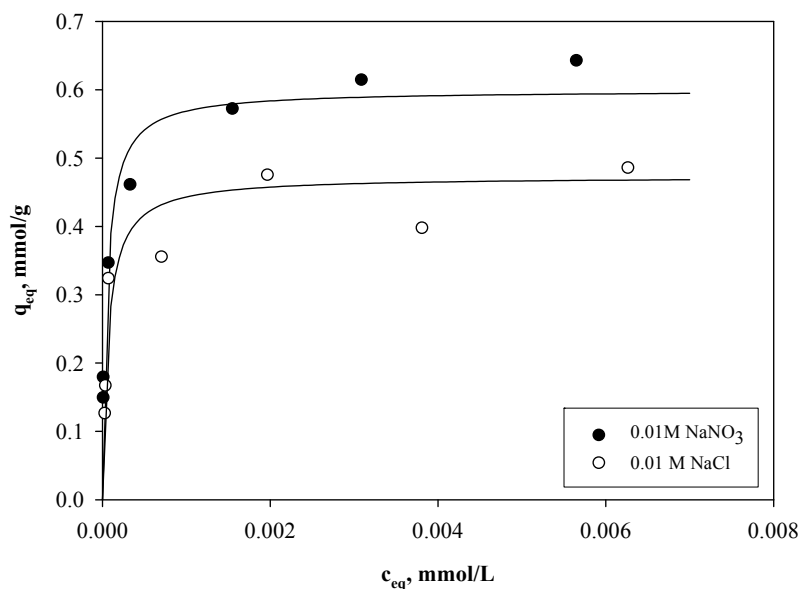


Figure 5.25: Isotherms of the sorption of Cd^{2+} ions with different electrolyte solutions. pH 7, $m_s = 5$ mg, $T = 25^\circ\text{C}$. Evaluation by means of the Langmuir relationship.

As is shown in Figure 5.25 the adsorption of Cd^{2+} from solution containing chloride diminished compared to the adsorption of Cd^{2+} from solution containing nitrate. This can be explained by the presence of complexing ions, such as Cl^- , which affects the speciation of the cadmium ions in solution. Thus, formation of other species such as CdCl^+ , the uncharged species CdCl_2 and the negatively charged complexes of cadmium with Cl^- ligands such as CdCl_3^- is expected. This change in the cadmium speciation, leading to a decrease in the presence of the species Cd^{2+} is the reason of the decrease in the adsorption capacity. The corresponding results obtained for the adsorption of Ni^{2+} onto MMS in presence of chloride ions are shown in Figure 5.26.

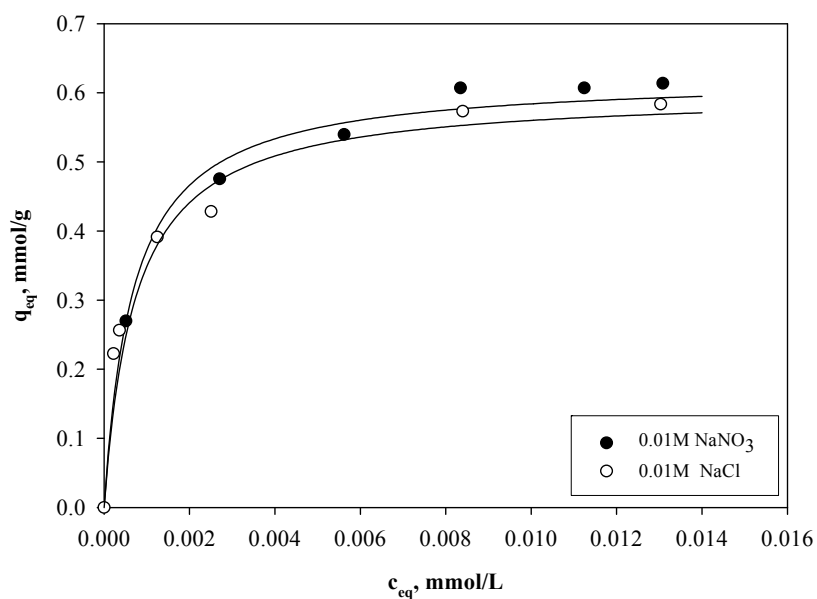


Figure 5.26: Sorption isotherms of Ni^{2+} ions with different electrolyte solutions. $\text{pH} = 7$, $m_s = 5$ mg, $T = 25^\circ\text{C}$. Evaluation by means of the Langmuir relationship.

As shown in Figure 5.26 the presence of Cl^- decreases slightly the amount of nickel adsorbed at $\text{pH} 7$. At this pH the predominant nickel species is still Ni^{2+} , $> 97\%$, followed by NiCl^+ , which is present in an amount not greater than 3% . As Ni^{2+} is preferentially adsorbed onto MMS compared to NiCl^+ thus a significant influence of chloride ions on the removal of nickel is not expected. The equilibrium parameters obtained by means of the application of the Langmuir relationship are summarized in Table 5.8.

In the same manner the results obtained for the adsorption of Pb^{2+} onto MMS in presence of chloride ions are shown in Figure 5.27.

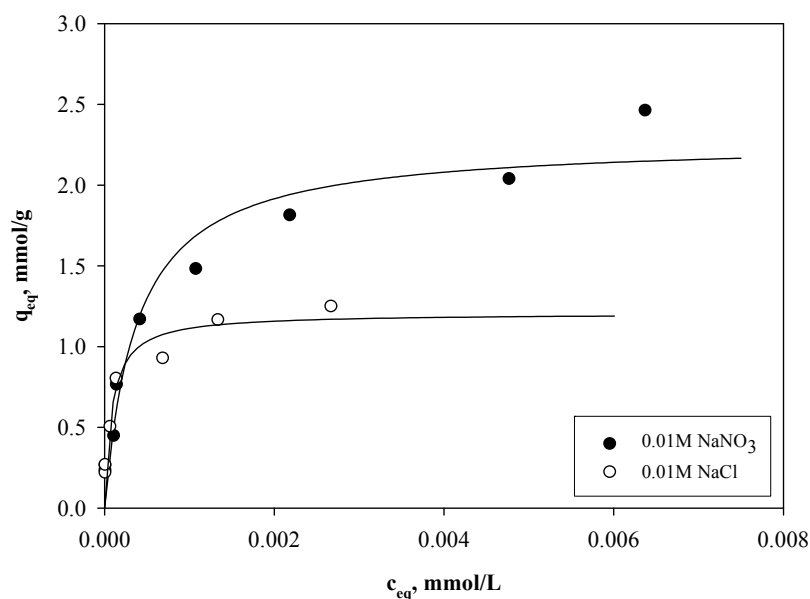


Figure 5.27: Sorption isotherms of Pb^{2+} ions with different electrolyte solutions. pH = 6, $m_s = 1.25$ mg, $T = 25^\circ C$. Evaluation by means of the Langmuir relationship.

The presence of chloride ions significantly affects the sorption of lead onto MMS. The presence of chloride ions promote the formation of chloride species of lead such as $PbCl^+$ and therefore the concentration of Pb^{2+} as divalent ion decreases. For a NaCl concentration of 0.01 mol/L, the fraction of the specie $PbCl^+$ increases from 0 to a value $>25\%$ and therefore the fraction of the specie Pb^{2+} decreases to about 75%. This effect is observed also in the q_{max} values; q_{max} was 1.88 times smaller than that in absence of Cl^- ions (see Table 5.8). Table 5.8 shows the equilibrium parameters of the adsorption of Cd^{2+} , Ni^{2+} , and Pb^{2+} onto MMS in presence of different electrolytes deduced by means of Langmuir and Freundlich relationships.

Table 5.8 : Equilibrium parameters for sorption of Cd^{2+} , Ni^{2+} , and Pb^{2+} onto MMS at different electrolyte solutions deduced by means of Langmuir and Freundlich relationships. $T = 25^\circ\text{C}$.

Ion	Electrolyte	Langmuir parameters			Freundlich parameters		
		q_{\max} , mmol/g	K_L , $\times 10^3 \text{ L/mmol}$	R^2	K_F	n	R^2
Cd^{2+}	NaNO_3	0.60	19	0.94	2.3	0.22	0.98
	NaCl	0.47	15	0.95	1.7	0.23	0.96
Ni^{2+}	NaNO_3	0.62	1.5	0.99	2.0	0.26	0.98
	NaCl	0.60	1.4	0.91	1.8	0.24	0.98
Pb^{2+}	NaNO_3	2.3	2.7	0.93	12	0.32	0.98
	NaCl	1.2	12	0.96	6.5	0.27	0.99

In Table 5.8 the values of the equilibrium parameters of q_{\max} and K_L obtained by means of the Langmuir relationship are summarized. The major effects are seen for the adsorption of Cd^{2+} and Pb^{2+} . In the case of Cd^{2+} the q_{\max} value obtained for the sorption isotherm in presence of NaNO_3 is 20% higher than the value obtained for the isotherm in presence of NaCl , while in the case of Pb^{2+} the value of q_{\max} decreases about 50%. In the case of Ni^{2+} the value of q_{\max} in presence of the Cl^- decreases only 1.04 times compared to the value obtained in its absence.

The presence of chloride ions affect negatively the sorption onto MMS of the metal ions studied. Due to the influence of chloride ions on the metal ion speciation, the effect on the sorption will depend on the metal ion concerned, thus a significantly effect in the cases Cd^{2+} and Pb^{2+} is observed while in the case of Ni^{2+} a minor effect occur. Despite the influence of chloride ions, the most adsorbed ion is still Pb^{2+} , and the order of sorption capacity is found to be $\text{Pb}^{2+} > \text{Ni}^{2+} > \text{Cd}^{2+}$.

5.3 Kinetic studies

Sorption kinetics of Cd(II), Ni(II), Pb(II) and Mo(VI) onto MMS including the effects of initial sorbate concentration and amount of adsorbent were studied. The evaluation of the experimental data was carried out by means of the application of four kinetic models, film diffusion, pseudo-first-order, pseudo-second-order, and the Elovich model. The experimental conditions for the kinetic studies and the mathematical description of the mentioned models are explained in detail in sections 4.8 and 3.2 respectively.

5.3.1 Cadmium sorption kinetics

For describing the effects of the initial concentration and the mass of adsorbent used on the sorption kinetics of cadmium onto MMS the relative concentration of cadmium as a function of contacting time was plotted. The results are presented in Figure 5.28 and Figure 5.29 respectively.

Figure 5.28 shows the relative concentration versus time for the sorption of Cd^{2+} onto MMS at different initial concentrations and constant amount of sorbent.

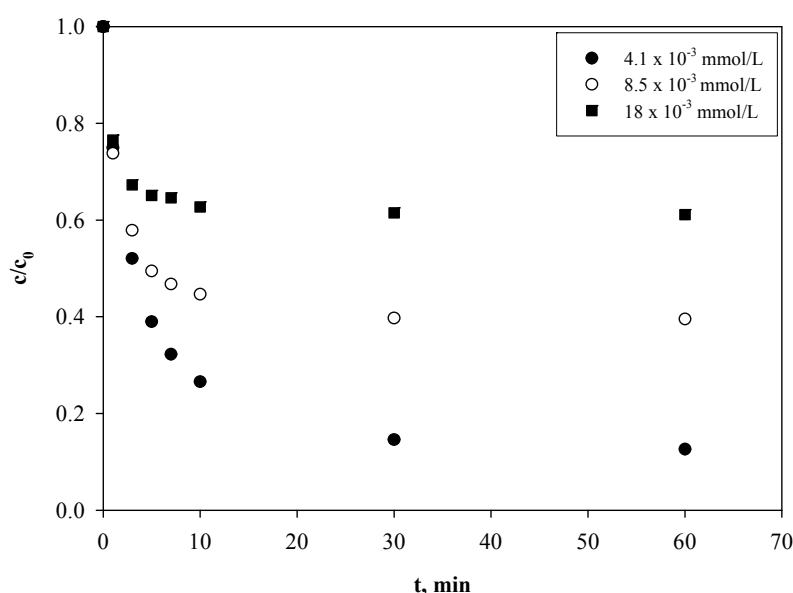


Figure 5.28: Plot of the relative concentration versus time for the sorption of Cd^{2+} onto MMS at different initial concentrations. pH = 7, $m_s = 10$ mg, T = 25°C.

According to Figure 5.28, the removal of Cd^{2+} by MMS is characterized by high sorption kinetics resulting in an almost complete equilibration within the first 10 min of contact between the solution and MMS. In the same manner the effect of the mass of adsorbent on the adsorption of cadmium onto MMS is shown in Figure 5.29. Figure 5.29 shows the relative concentration for sorption of Cd^{2+} obtained at various sorbent amounts.

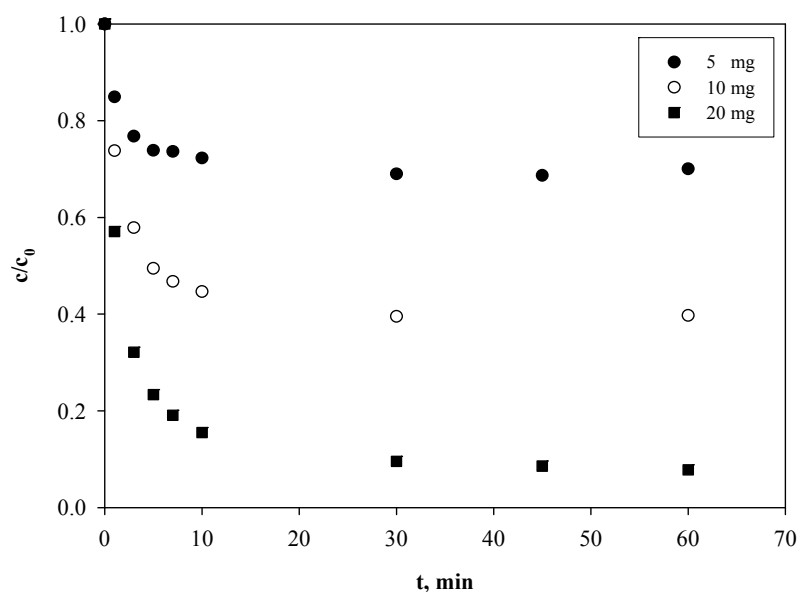


Figure 5.29: Plot of the relative concentration versus time for the adsorption of Cd^{2+} onto MMS at various sorbent dosage. $\text{pH} = 7$, $c_{\text{Cd}} = 8.5 \times 10^{-3}$ mmol/L, $T = 25^\circ\text{C}$.

As is seen, the sorption of Cd^{2+} by MMS is rather fast within the first 10 min of contact between the solution and MMS, followed by a further uptake until state of equilibrium is reached after approximately 30 min.

5.3.2 Nickel sorption kinetics

The effects of the initial concentration and the mass of adsorbent on the sorption kinetics of nickel onto MMS are shown in Figure 5.30 and Figure 5.31 respectively. Figure 5.30 shows the relative concentration versus time for the adsorption of Ni^{2+} onto MMS at different initial concentrations.

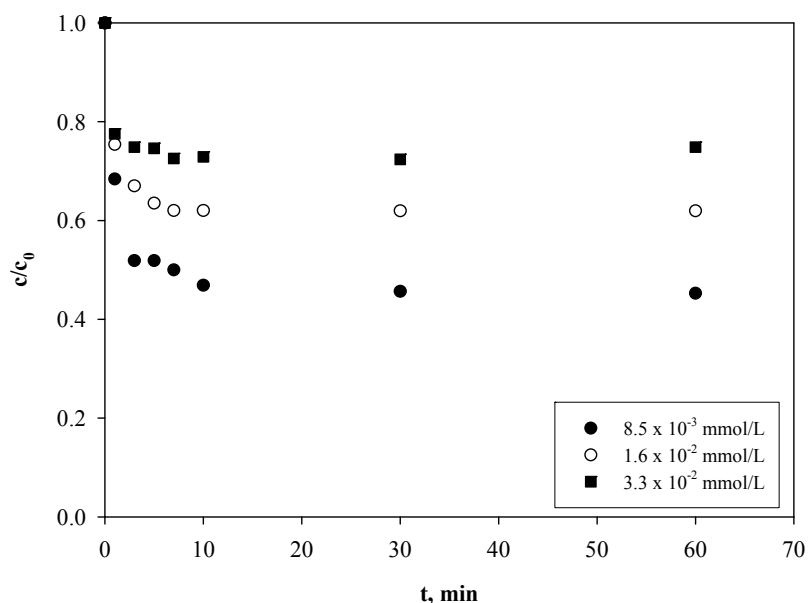


Figure 5.30: Plot of the relative concentration versus time for the adsorption of Ni^{2+} onto MMS at different initial concentrations. pH = 7, $m_s = 10$ mg, T = 25°C.

The sorption of Ni^{2+} onto MMS is characterized by a rapid increase of the adsorbed amount occurring within the first 10 min of contact between the solution and MMS, followed by a slow further increase until state of equilibrium is reached. It should be appointed that for Ni^{2+} the equilibrium was reached within the 30 min of contact, further contact time did not increase the amount of Ni^{2+} adsorbed onto MMS. In Figure 5.31 the relative concentration versus time for the adsorption of Ni^{2+} onto MMS at different sorbent dosage is shown.

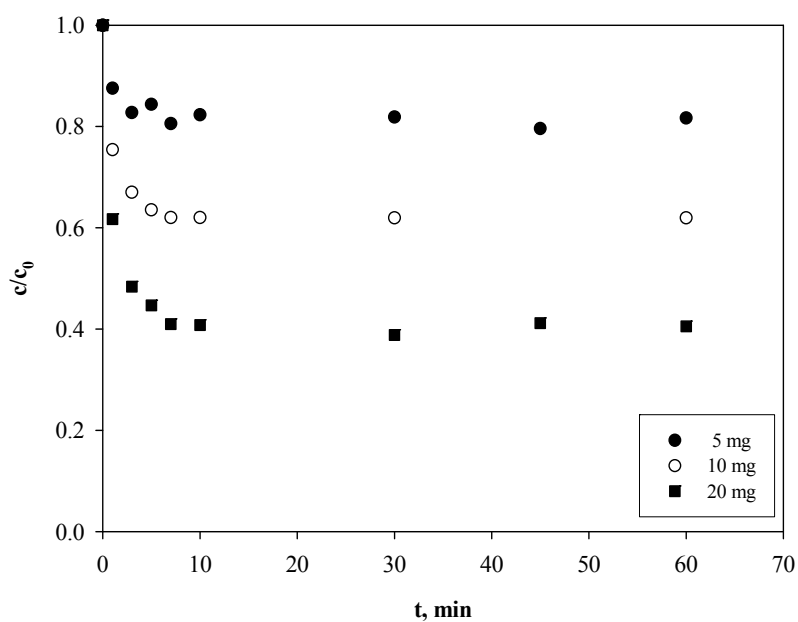


Figure 5.31: Plot of the relative concentration versus time for the adsorption of Ni^{2+} onto MMS at different amounts of adsorbent. $\text{pH} = 7$, $c_{\text{Ni}} = 1.6 \times 10^{-2}$ mmol/L, $T = 25^\circ\text{C}$.

In Figure 5.31 it can be seen that most of the sorption takes place within the first 10 min of the experiment. After 10 min, the rate of adsorption was negligible and the concentration of nickel in the solution reached almost a constant value.

5.3.3 Lead sorption kinetics

In accordance with the experiments with Cd^{2+} and Ni^{2+} , sorption kinetics of lead in dependence of the initial concentration and the mass of adsorbent are shown in Figure 5.32 and Figure 5.33 respectively. Figure 5.32 shows the kinetic adsorption of Pb^{2+} onto MMS at different initial concentrations.

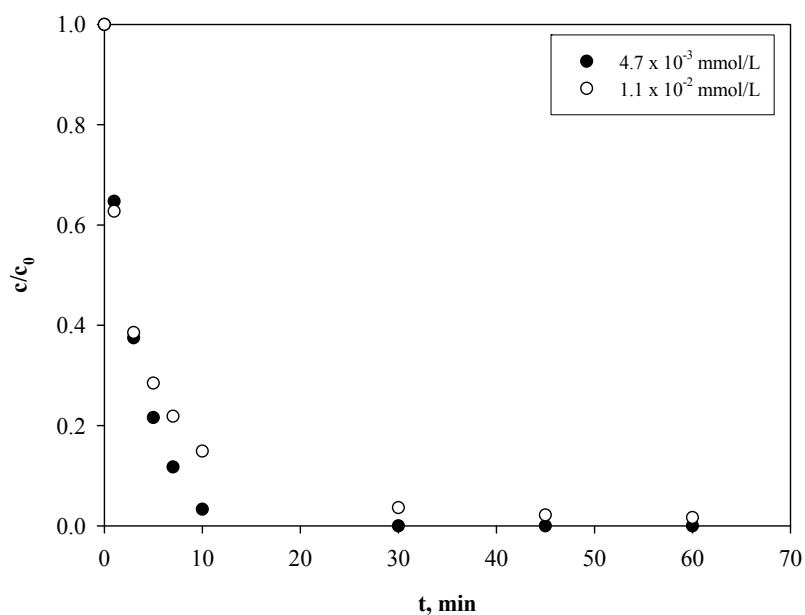


Figure 5.32: Plot of the relative concentration versus time for the adsorption of Pb^{2+} onto MMS at different initial concentrations. $\text{pH} = 6$, $m_s = 10 \text{ mg}$, $T = 25^\circ\text{C}$.

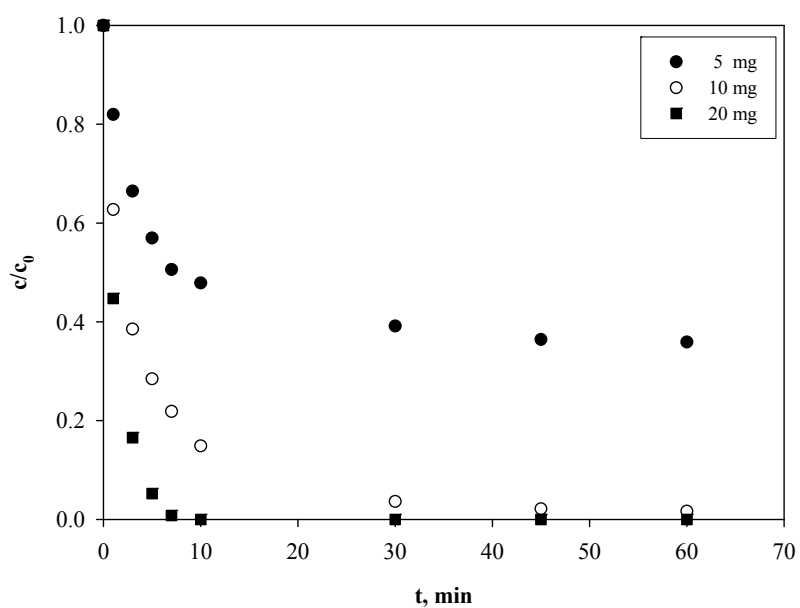


Figure 5.33: Plot of the relative concentration versus time for the adsorption of Pb^{2+} onto MMS at different amounts of adsorbent. $\text{pH} = 6$, $c_{\text{Pb}} = 10 \times 10^{-3} \text{ mmol/L}$, $T = 25^\circ\text{C}$.

As seen in Figure 5.32 and Figure 5.33 the kinetic, as for the previous metal ions, Cd^{2+} and Ni^{2+} is characterized by a strong increase of Pb^{2+} adsorption during the first 10 min; followed by a slow increase until a state of equilibrium is reached.

5.3.4 Molybdenum sorption kinetics

Sorption kinetics of oxyanion species of molybdenum onto MMS was also studied. The results are shown in Figure 5.34. Figure 5.34 shows the relative concentration for the adsorption of MnO_4^{2-} onto MMS for different initial concentrations.

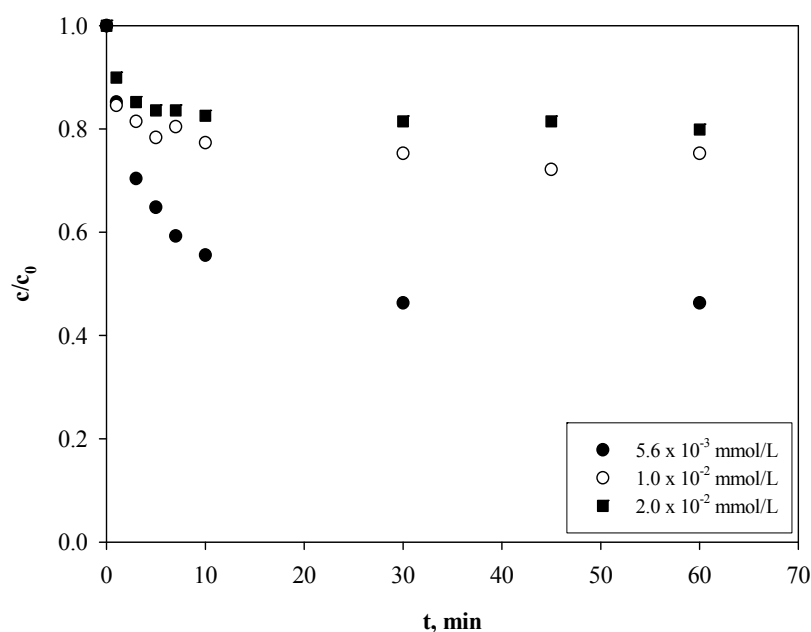


Figure 5.34: Plot of the relative concentration versus time for the adsorption of MoO_4^{2-} at different initial concentrations. $\text{pH} = 4$, $m_s = 20 \text{ mg}$, $T = 25^\circ\text{C}$.

The sorption kinetics shown in Figure 5.34, similar to the experiments with metal cations, initially are very fast; about 90% of the final uptake are reached within the first 10 min. With further increase of time the adsorption increases slowly to attain the equilibrium in about 30 min. In the next figure, Figure 5.35 the relative concentration for the adsorption of MnO_4^{2-} onto MMS at different amount of micro-sorbent.

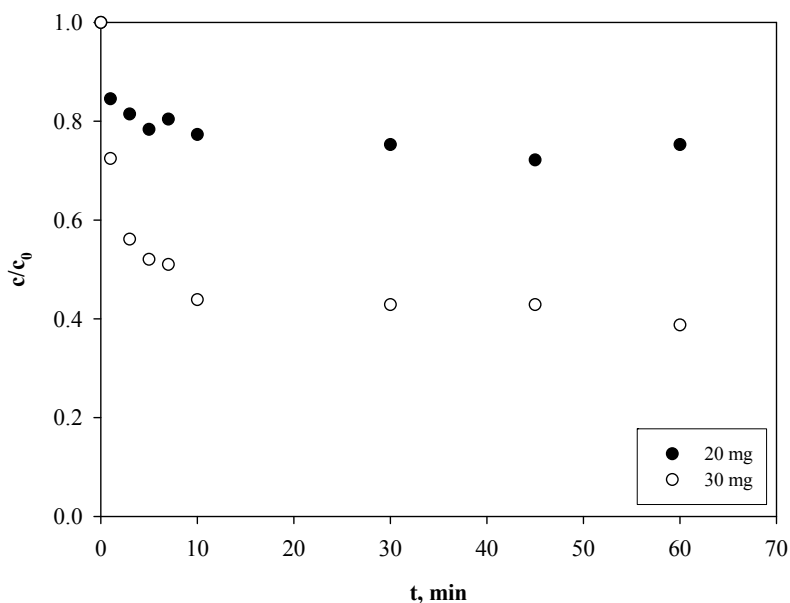


Figure 5.35: Plot of the relative concentration versus time for the adsorption of MoO_4^{2-} at different amounts of MMS. $\text{pH} = 4$, $c_{\text{M}_0} = 1.0 \times 10^{-2}$ mmol/L, $T = 25^\circ\text{C}$.

5.3.5 Numerical evaluation of the sorption kinetics

For the separated uptake of the cations Cd^{2+} , Ni^{2+} , and Pb^{2+} as well as for the oxyanion MoO_4^{2-} onto MMS four kinetics models were applied to analyse the adsorption data, including the Film diffusion, Lagergren (or pseudo-first-order), pseudo-second-order and Elovich models. The sorption developments presented in sections 5.3.1, 5.3.2, 5.3.3, and 5.3.4 were used for the respective evaluations.

The mathematical description of each model was introduced in section 3.2. Nevertheless, a more detailed description of the data analysis by these models is included in the next section.

It must be appointed that results obtained by means of Elovich equation were not included because of the unsatisfying correlation with the experimental data.

5.3.5.1 Film diffusion model

The application of the film diffusion model comprises the determination of the mass transfer coefficient. The mass transfer coefficient in the liquid phase (β_L), was determined by conducting experiments in a batch reactor system.

As explained in section 3.2.1.2 the mass transfer coefficient for a batch system can be calculated by determining the variation of the concentration of the metal ion as a function of time related to the mass of adsorbent (m), volume of solution (V_L), and the specific particle area (a_s) as constants. The determination of β_L by means of the evaluation of data, resulting from the experiments in a stirred system can be conducted as follows:

Considering that at $t = 0$ the surface concentration (c_i^*) is approximately zero, from Eq. 3.17 the following relation is obtained:

$$\beta_{L,i} = -\frac{V_L}{ma_s} \frac{1}{c_i} \frac{dc_i}{dt} \quad \text{Eq. 5.1}$$

By taking the logarithm the above equation becomes:

$$\ln \frac{c_i}{c_{i,0}} = -\beta_{L,i} \frac{ma_s}{V_L} t \quad \text{Eq. 5.2}$$

Thus, if the values of m , a_s , and V_L are known the mass transfer coefficient can be determined by means of the calculation of the initial slope of the plot of the logarithm of $c(t)/c_0$ over time for $t \rightarrow 0$.

The evaluation of the data of Figure 5.28 (effect of initial concentration), and Figure 5.29 (effect of mass of adsorbent), was carried out by means of Eq. 5.2. The mass transfer coefficient values obtained are summarized in Table 5.9.

Table 5.9 : Mass transfer coefficients experimentally obtained by means of the Film diffusion model for sorption of Cd^{2+} , Ni^{2+} , Pb^{2+} , and MoO_4^{2-} onto MMS at different initial concentrations and sorbent dosage. $T = 25^\circ\text{C}$.

Ion	Film diffusion					
	m, mg	$c_0, \times 10^{-3}$ mmol/L	$\beta_L, \times 10^{-4}$ m ² /s	$c_0, \times 10^{-3}$ mmol/L	m, mg	$\beta_L, \times 10^{-4}$ m ² /s
Cd^{2+}	10	4.1	8.7	8.9	5	9.9
		8.9	9.2		10	9.2
		18	8.1		20	8.5
Ni^{2+}	10	8.5	11	17	5	8.1
		17	8.5		10	8.5
		33	7.7		20	7.3
Pb^{2+}	10	4.7	13	9.7	5	12
		9.7	14		10	14
		-	-		20	12
MoO_4^{2-}	20	5.6	2.4	10	-	-
		10	2.5		20	2.5
		20	1.6		30	3.2

For both experiments within the experimental error similar values for the mass transfer coefficients for the adsorption of cadmium onto MMS are observed. This independence of the calculated mass transfer coefficient from the initial concentration and the mass of adsorbent used is a strong proof of the validity of the film diffusion model. The mass transfer coefficients obtained for Cd^{2+} are quite similar to those obtained for Ni^{2+} (except the value for β at an initial concentration of 8.5×10^{-2} mmol/L).

From the values obtained, Pb^{2+} has resulted to be the faster specie while MoO_4^{2-} was found to be the slowest one.

For the theoretic estimation of the mass transfer coefficient, the Sherwood-Reynolds-Schmidt numbers are used. The correlations which describe these numbers are introduced in section 3.2.1.2. First, for the determination of the Reynolds number in a batch reactor system it is considered that $v_{\text{rel}} = v_t$. It must be appointed that for deducing v_t a determined value of d_p is used. Due to the characteristics of the adsorbent material, small particle size, wide particle size distribution and formation of agglomerates, it seems difficult to have a representative particle size diameter for the system to be modeled. Nevertheless, by means of the particle size measurements it was observed that 50% of particles were ranged under $2.85 \mu\text{m}$ (see section 5.1.3), which can be considered as a representative d_p , and therefore it can be taken for further calculations. Thus, by applying Eq. 3.24 a value of 2.14×10^{-4} m/s for the Reynolds number is obtained. The value clearly shows that the liquid flow around the particles is in a laminar regime.

For the determination of the Schmidt number Eq. 3.26 is used. The Sc number depends on the kinematic viscosity of the solution media and the diffusion coefficient of a species. Diffusion coefficient values for cations including Cd^{2+} , Ni^{2+} , and Pb^{2+} and for the oxyanion MoO_4^{2-} obtained by means of the Eq. 3.27 are shown in Table 5.10.

Table 5.10 : Diffusion coefficients of cations in water at 25°C.

Ion	$D_L, \times 10^{-9} \text{ m}^2/\text{s}$
Cd^{2+}	0.72
Ni^{2+}	0.68
Pb^{2+}	0.93
MoO_4^{2-}	0.54*

*Because no mobility value of MoO_4^{2-} could be found this value was calculated by Eq. 4.28 using the radius of the hydrated ion.

Considering that the kinematic viscosity of water at 25°C of $0.89 \times 10^{-6} \text{ m}^2/\text{s}$ and the molecular diffusion coefficients of the metal ions investigated, the following Sc numbers are obtained:

Table 5.11 : Schmidt numbers for the metal ions Cd^{2+} , Ni^{2+} , Pb^{2+} , and MoO_4^{2-} at 25°C.

Metal species	Sc
Cd^{2+}	1236
Ni^{2+}	1309
Pb^{2+}	957
MoO_4^{2-}	1648

The determination of the Sherwood number, which involves the Reynolds and the Schmidt numbers is obtained by applying Eq. 3.21 for a $\text{Re} < 1$. For the conditions applied, that means a laminar regime where the contribution of the Reynolds number is negligible, the Sherwood number for the system is determined to be $\text{Sh} \approx 2$. Thus, the theoretic mass transfer coefficients, $\beta_{L,\text{theo}}$, can be calculated with Eq. 5.1., and the values obtained are shown in Table 5.12.

$$\beta_{L,\text{theo}} = \frac{\text{Sh} D_L}{d_p} \quad \text{Eq. 5.3}$$

Table 5.12 : Theoretic mass transfer coefficients for the metal ions Cd^{2+} , Ni^{2+} , Pb^{2+} , and MoO_4^{2-} .

Metal species	$\beta_{L,\text{theo}} \times 10^{-4} \text{ m/s}$
Cd^{2+}	5.1
Ni^{2+}	4.8
Pb^{2+}	6.5
MoO_4^{2-}	3.8

The calculated values of the mass transfer coefficients show Pb^{2+} is the fastest ion followed by Ni^{2+} and Cd^{2+} and finally MoO_4^{2-} .

By comparison of the values of Table 5.9 and Table 5.12 it is observed that the experimentally obtained mass transfer coefficients are somewhat larger than those theoretically calculated. However, the deviation is rather small and the theoretical calculations show the correct order between the faster and slower ions.

As mentioned in section 3.2.1.2.1 a major difficulty for applying the film diffusion model to the system investigated, lies in the strong dependency on the particle size of the adsorbent.

As explained before for the calculations a particle diameter of 2.85 μm was used. Nevertheless, the particle size measurements of Figure 5.5 show that the particle size distribution of MMS ranges between 0.5 and 18 μm . Thus, the values of mass transfer coefficient experimentally obtained reflect the contribution of the small particles in the adsorption process.

5.3.5.2 Lagergren model (pseudo-first-order model)

In this section the rate constants of sorption and the initial sorption rate as a function of the initial concentration of the metal ions and MMS were determined using the Lagergren model. The mathematical representation of the model is given in Eq. 3.31 and Eq. 3.35, respectively. For the pseudo-first-order model, the adsorption rate constant, k_1 , was calculated from the slope of the linear plot of $\ln (q_e - q_t)$ versus time. As explained in section 3.2.2.1, for the application of the pseudo-first-order model, the values of the equilibrium sorption capacity q_e , has to be known. Therefore, the first evaluation of the data of the plots c/c_0 as a function of time was the determination of the values of $q_{i,eq}$, which is obtained by the application of Eq. 3.2. Then, the pseudo-first-order model can be applied and the calculated kinetic parameter k_1 for the sorption of Cd^{2+} , Ni^{2+} , Pb^{2+} , and MoO_4^{2-} at different initial concentrations and amount of adsorbent are shown in Table 5.13.

Table 5.13 : Kinetic parameters obtained by means of the Lagergren model for sorption of Cd^{2+} , Ni^{2+} , Pb^{2+} , and MoO_4^{2-} onto MMS at different initial concentrations and amounts of sorbent. T = 25°C.

Ion	Lagergren model							
	m, mg	c_0 , x 10 ⁻³ mmol/L	k_1 , 1/min	R ²	c_0 , x 10 ⁻³ mmol/L	m, mg	k_1 , 1/min	R ²
Cd^{2+}	10	4.1	0.11	0.97	8.9	5	0.13	0.97
		8.5	0.17	0.98		10	0.17	0.98
		18	0.11	0.89		20	0.10	0.90
Ni^{2+}	10	8.5	0.12	0.86	17	5	0.20	0.60
		1.6	0.60	0.89		10	0.60	0.89
		33	0.32	0.62		20	0.55	0.94
Pb^{2+}	10	4.7	0.33	0.98	9.7	5	0.093	0.97
		10	0.10	0.98		10	0.10	0.98
		-	-	-		20	0.66	0.97
MoO_4^{2-}	20	5.6	0.16	0.98	10	-	-	-
		10	0.15	0.95		20	0.15	0.75
		20	0.21	0.71		30	0.34	0.89

5.3.5.3 Pseudo-second-order

In the case of the pseudo-second-order model, kinetic data were plotted in a form t/q_t versus t . From the slope the rate constants of sorption and the initial sorption rate, h , can be determined. The mathematical representation of the model is given in Eq. 3.35. As well as for the previous model, the kinetic parameter k_2 for the sorption of Cd^{2+} , Ni^{2+} , Pb^{2+} , and MoO_4^{2-} at different initial concentrations and amount of adsorbent are shown in Table 5.14. Values for the initial sorption rate were also calculated and the results are presented in Table 5.15.

It is seen that the adsorption capacities, q_e , were high at lower doses and reduced at higher doses. This behaviour is consistent with results obtained for the adsorption e.g. of Pb^{2+} onto an adsorbent which contains manganese dioxide, such as manganese dioxide coated zeolite (Zou 2006).

The factor which explains this characteristic is that adsorption sites remain unsaturated during the adsorption reactions whereas the number of sites available for adsorption increases by increasing the adsorbent dose.

Table 5.14 : Kinetic parameters obtained by means of the pseudo-second-order model for sorption of Cd^{2+} , Ni^{2+} , Pb^{2+} , and MoO_4^{2-} onto MMS at different initial concentrations and amounts of sorbent. T = 25°C.

Ion	Pseudo-second-order model							
	$c_0, \times 10^{-3}$ mmol/L	q_e , mmol/g	k_2 , g/(min mmol)	R^2	m, mg	q_e , mmol/g	k_2 , g/(min mmol)	R^2
Cd^{2+}	4.1	0.37	1.1	0.99	5	0.54	1.5	0.99
	8.5	0.52	1.6	0.99	10	0.52	1.6	0.99
	18	0.68	2.3	0.99	20	0.48	2.2	0.99
Ni^{2+}	8.5	0.46	3.0	0.99	5	0.59	3.6	0.99
	1.6	0.65	2.4	0.99	10	0.65	2.4	0.99
	33	0.92	3.4	0.99	20	0.52	2.9	0.99
Pb^{2+}	4.7	0.45	1.5	0.99	5	1.3	0.28	0.99
	10	1.1	0.46	0.99	10	1.1	0.46	0.99
	-	-	-	-	20	0.49	2.2	0.99
MoO_4^{2-}	5.6	0.16	0.37	0.99	20	0.13	0.82	0.99
	10	0.13	0.82	0.99	30	0.21	0.69	0.99
	20	0.19	0.71	0.99	-	-	-	-

By means of the pseudo-second-order kinetic model, a value for the initial sorption rate, called h , can be obtained. As described in Eq. 3.36 from the intercept of a plot of t/q as function of time the term $1/h$ is obtained, and therefore the value of h can be deduced (see Table 5.15).

Table 5.15 : Kinetic parameters obtained by means of the pseudo-second-order model for sorption of Cd^{2+} , Ni^{2+} , Pb^{2+} , and MoO_4^{2-} onto MMS at various initial concentrations and amount of adsorbent.

Ion	Pseudo-second-order model			
	$c_0, \times 10^{-3}$ mmol/L	h , mmol/(min g)	m , mg	h , mmol/(min g)
Cd^{2+}	4.1	0.15	5	0.43
	8.5	0.44	10	0.44
	18	1.1	20	0.39
Ni^{2+}	8.5	0.63	5	1.2
	1.6	1.0	10	1.1
	33	2.9	20	0.78
Pb^{2+}	4.7	0.34	5	0.46
	10	0.58	10	0.58
	-	-	20	0.52
MoO_4^{2-}	5.6	0.0093	20	0.014
	10	0.014	30	0.029
	20	0.027	-	-

Values for the initial sorption rates, h , for the four species investigated, were found to increase with an increase in the initial concentration. In the case of Pb^{2+} similar results have been found by using manganese dioxide coated zeolite as adsorbent for removal of Pb^{2+} (Zou 2006). Nevertheless, the values obtained by increasing the mass of adsorbent show an erratic trend. As it is seen in Table 5.13 and Table 5.14 the correlation coefficients (R^2), for the pseudo-first-order approach were considerably lower than those for the pseudo-second-order approach. This shows that the sorption of Cd(II), Ni(II), Pb(II), and Mo(VI) onto MMS is more accurately described by the pseudo-second-order kinetic model.

5.3.6 Sorption kinetic modelling

For modelling the sorption kinetics of Cd(II), Ni(II), Pb(II), and Mo(VI) onto MMS a set of equation are needed. The first to be mentioned is the Langmuir relationship (see Eq. 3.7); by means its application the equilibrium parameters q_{\max} and K_L for the adsorption of the mentioned metal ions in a batch system were determined. The Langmuir parameters q_{\max} and K_L used for modelling are shown in Table 5.16 (extracted from Table 5.5 and Table 5.6).

Table 5.16 : Langmuir parameteres for Cd(II), Ni(II), Pb(II), and Mo(VI) used for sorption kinetic modelling.

Ion	Langmuir parameters			
	pH	q_{\max} , mmol/g	K_L , $\times 10^3$ L/mmol	R^2
Cd^{2+}	7	0.60	19	0.94
Ni^{2+}	7	0.62	1.5	0.99
Pb^{2+}	6	2.2	2.7	0.93
MoO_4^{2-}	4	0.14	1.3	0.99

With the above parameters, the concentration of the metal ion at the surface of the adsorbent can be calculated. By rearranging Eq. 3.7 the following relation is obtained:

$$c_i^* = \frac{1}{K_L} \frac{\bar{q}_i}{q_{\max} - \bar{q}_i} \quad \text{Eq. 5.4}$$

The kinetics of the sorption process is given by (see also Eq. 3.17):

$$-\frac{d\bar{q}_i}{dt} = a_s \beta_{L,i} (c_i - c_i^*) \quad \text{Eq. 5.5}$$

This corresponds to the film diffusion through a stagnant liquid film at the surface of the MMS. The mass transfer coefficients which have been experimentally obtained for each cation and their values, in the order of $10^{-4} \text{ m}^2/\text{s}$, are shown in Table 5.12.

The value of a_s , which corresponds to the specific external interfacial area, is calculated according to Eq. 5.6 for a sphere particle:

$$a_s = \frac{6}{d_p \rho_p} \quad \text{Eq. 5.6}$$

The value of a_s for the magnetic microsorbent was $553 \text{ m}^2/\text{kg}$.

Finally, by using the mass balance of the system, described in Eq. 3.18 the concentration, c_i , can be determined as follows:

$$c_i = \frac{V_L c_{i,0} - m \bar{q}_i}{V_L} \quad \text{Eq. 5.7}$$

By combining the above set of equations, the sorption kinetic of metal ions onto MMS in a batch reactor can be modelled.

5.4 Consecutive cycles of adsorption – desorption

The reusability of the MMS was tested in five consecutive cycles of Pb(II) adsorption and desorption. Pb(II) was selected for the test due to the high affinity observed between this metal ion and the magnetic microsorbent. The experimental conditions for both processes are described in section 4.9. Figure 5.36 shows experimental results for the adsorption of Pb²⁺ onto MMS in a series of five consecutive cycles.

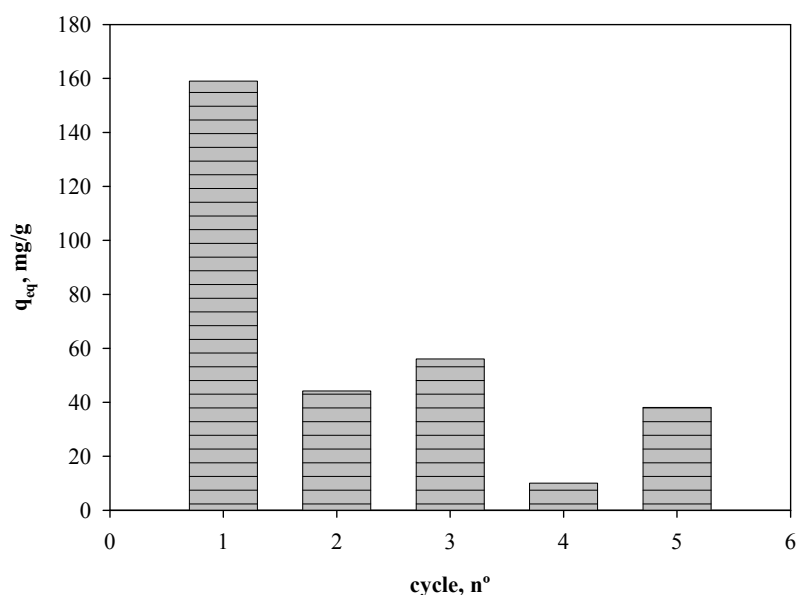


Figure 5.36: Sorption of Pb onto MMS for five consecutive cycles. $c_{pb} = 3.6 \times 10^{-3}$ mmol/L, pH = 6, $V_{L,s} = 1$ L, $m = 3.4$ mg, $T = 25^\circ\text{C}$.

From Figure 5.36 it can be noted that the sorption efficiency decreases significantly after the first cycle. This can be due to the fact that a fraction of the MMS surface remains occupied with sorbed ions during the desorption process. Thus, in the next sorption cycle the possibility of an ion to be adsorbed is diminished. In Figure 5.37 the experimental data obtained for the desorption of Pb²⁺ from MMS for five consecutive cycles are shown.

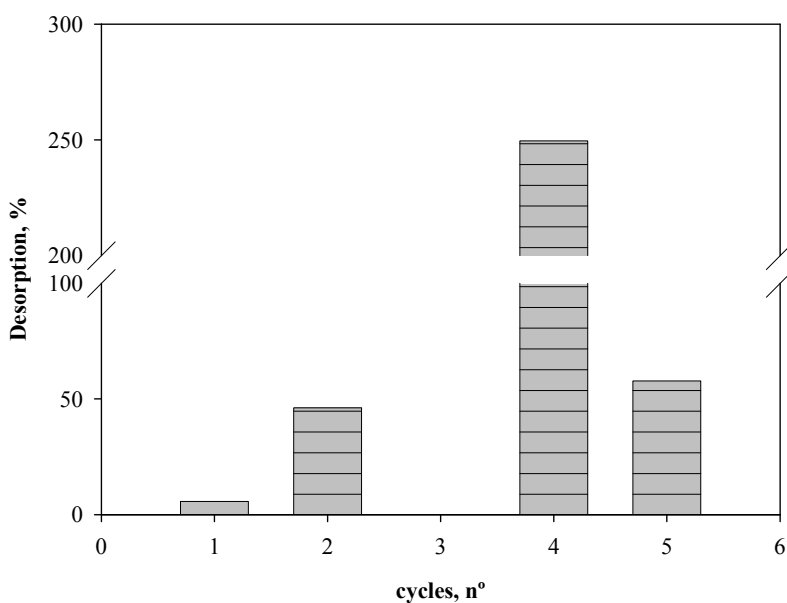


Figure 5.37: Desorption of Pb^{2+} from MMS for five consecutive cycles. $V_L = 0.01$ L, $\text{pH} = 3.5$, $T = 25^\circ\text{C}$.

The plotted data show values for the amount of Pb^{2+} released from the surface of the MMS to the desorption solution (solution $\text{pH} 3.5$). The values are related to the amount adsorbed in each cycle. The values showed are in a good connection with those presented in Figure 5.36, where a small desorption efficiency leads to an also small sorption amount within the next cycle.

In front of the results, two points must be commented. The first is related to the desorption solution volume. With the objective to produce a final solution with a concentrated amount of metal ions, the desorption process was carried out with a solution volume 100 times smaller than that during the sorption steps.

The second comment is related to the reusability of the microsorber. As explained in section 2.3 the adsorption process can be separated in two groups, specific and non-specific sorption. The type of adsorption depends on the extent of affinity of the adsorbent for the species to be adsorbed, in this case for metal ions. If a metal ion is bound by electrostatic forces simply to balance the negative charge on the surface of an adsorbent, then we are in presence of a non-specific process, and the ions adsorbed are equivalent to those exchangeable. The metal ions adsorbed through this way can be replaced for other cations. On the other hand, in a specific

adsorption the ions are bound much more tightly to the adsorbent surface and therefore, they are much less easily removed.

The metal ions examined are able to form hydroxyl complexes, which are specifically adsorbed to a greatest extent. Therefore, the pK values of the reaction of Eq. 5.8 can determine the adsorption behavior of the metals:



with $M = Cd^{2+}$, Ni^{2+} , and Pb^{2+} .

The specific adsorption increases with decreasing the pH values. The increasing specific adsorption follows the order: $Cd^{2+} < Ni^{2+} < Pb^{2+}$ with values of pK of 10.1, 9.9, and 7.6, respectively. The not easy desorption of Pb^{2+} from the surface of MMS can be taken as an evidence that Pb^{2+} is specifically adsorbed onto the surface of the magnetic micro-sorbent. This strong adsorption involves the formation of an inner-sphere surface complex of Pb^{2+} , which is consistent with other investigations (Morin, Ostergren et al. 1999). Nevertheless, the amounts desorbed allow the reusability of the micro-sorbent in an adequate extent to be considered for being used in a large scale.

6 Conclusions

The overall objective of this PhD thesis was to develop a magnetic microsorbent (MMS) for the removal of metal ions from aqueous solutions which exhibits features that significantly improve the solid-liquid separation needed after the sorption process. In the present investigation important conclusions are generated with regard to the synthesis of the magnetic microsorbent as well as with regard to the factors affecting its performance in the sorption process.

Synthesis of MMS:

Manganese dioxide was successfully deposited onto magnetite used as core material by means of a coating process. ESEM analysis combined with EDAX technique showed the presence of Mn and Fe, together forming agglomerates which confirm that the coating process effectively occurred.

By means of magnetization curves it was demonstrated that the microsorbent shows good magnetic characteristics, and therefore an effective solid-liquid separation is possible. This could be shown by the fact that by applying a magnetic field the settling rate was much faster than without. Zeta potential measurements showed that the microsorbent should be suitable for removing metal cations, showing values of the zeta potential of ~ -30 mV at pH 7 and a $pH_{(PZC)}$ close to pH 3.

It can be concluded that a main objective of this investigation, which comprised the synthesis of a microsorbent with magnetic properties to be recovered easily from aqueous solution systems was achieved.

Equilibrium investigations:

The analysis of the sorption equilibrium of the metal ions Cd, Ni, and Pb as well as of Mo was carried out by means of the Langmuir and Freundlich relationships. A similar adsorption trend is noted by the data evaluation of both models. On the basis of the correlation coefficients it can be stated that both models properly describe the sorption of the mentioned species onto MMS.

The removal of Cd^{2+} , Ni^{2+} , and Pb^{2+} as well as MoO_4^{2-} from aqueous solutions by MMS was found to be highly dependent on the solution pH, because it affects the surface charge, degree of ionization and speciation of the metal ions.

It was found that Pb^{2+} is the most preferred metal ion to be adsorbed, followed by Ni^{2+} and Cd^{2+} with very similar behaviours; MoO_4^{2-} was less preferred. By means of the Langmuir evaluation values for the maximum equilibrium sorption capacities, q_{max} , were found to be 2.2 mmol/g for Pb^{2+} at pH 6, for Ni^{2+} and Cd^{2+} at pH 7 the values of q_{max} were 0.62 mmol/g and 0.60 mmol/g respectively, and for MoO_4^{2-} at pH 4 q_{max} was 0.38 mmol/g.

The order of adsorption is $\text{Pb}^{2+} > \text{Ni}^{2+} \geq \text{Cd}^{2+} \gg \text{MoO}_4^{2-}$ which is consistent with results presented by other authors that have stated that lead shows particularly strong affinity for hydrous oxides of manganese and iron. Thus, the results obtained for the effect of pH showed that MMS has amphoteric properties and could eventually, by controlling the pH of the system, be used as an adsorbent to remove cations as well as anions.

The presence of competing cations can also affect the sorption of metal ions. Divalent cations such as Ca^{2+} can compete effectively for sorption sites, nevertheless, at the concentrations of Ca^{2+} studied, the adsorption of the metal ions, Cd^{2+} , Ni^{2+} , and Pb^{2+} was still very significant, although the concentration of Ca^{2+} was 20 times higher than the concentration of the metal ions in the same solution.

The presence of chloride ions affected the sorption of the metal ions onto MMS. Complexes of divalent metals are less strongly adsorbed than the uncomplexed ions. Sorption equilibrium capacities showed a major influence of chloride onto the sorption of Pb^{2+} followed by Cd^{2+} and Ni^{2+} . The values of q_{max} decreased 1.88, 1.27, and 1.04 times compared to those in absence of chloride ions respectively. This is consistent with the speciation change due to the presence of the anions where PbCl^+ and CdCl^+ showed greater formation percentage than NiCl^+ .

Kinetic investigations:

The main characteristic of the sorption kinetics exhibited by the microsorber was the fast adsorption process of metal ions, where the equilibrium is reached in a time not longer than 60 min; moreover it was observed that within the first 10 min 90 -95% of the finally adsorbed amount is already bound.

The sorption development was evaluated by means of film diffusion model as well as by means simplified approaches, like the Lagergren pseudo-first-order model and the pseudo-second-order model.

The sorption kinetics were adequately described by means of the film diffusion model. Nevertheless, the assumed average particle size of the microsorbents showed a strong influence on the result. The theoretic values obtained for the mass transfer coefficient were found to be slightly smaller than the experimental ones, something which clearly related to the particle size assumption used in the calculations.

In case of the simplified approaches, the pseudo-second-order model delivers a better description of the sorption behavior of the metal ions Cd^{2+} , Ni^{2+} , and Pb^{2+} as well as the oxyanion MoO_4^{2-} onto MMS than the Lagergren model.

Recommendations for future research:

The results of this PhD thesis have demonstrated that metal ions as well as oxyanions can be effectively removed from aqueous solutions by sorption process using manganese dioxide with magnetic properties. This investigation was carried out in a batch operation system. However, in order to be implemented in industrial applications, a continuously operated scale-up system needs to be designed and investigated to determine how effective the performance of the microsorbent is in an industrial scale.

Considering a large scale application, an almost complete separation of the magnetic microsorbents could be achieved using a combined separation system consisting of a magnetic flocculation device, a settling tank and a high gradient magnetic separation (HGMS) device. The following magnetic separation process is proposed (see Figure 6.1).

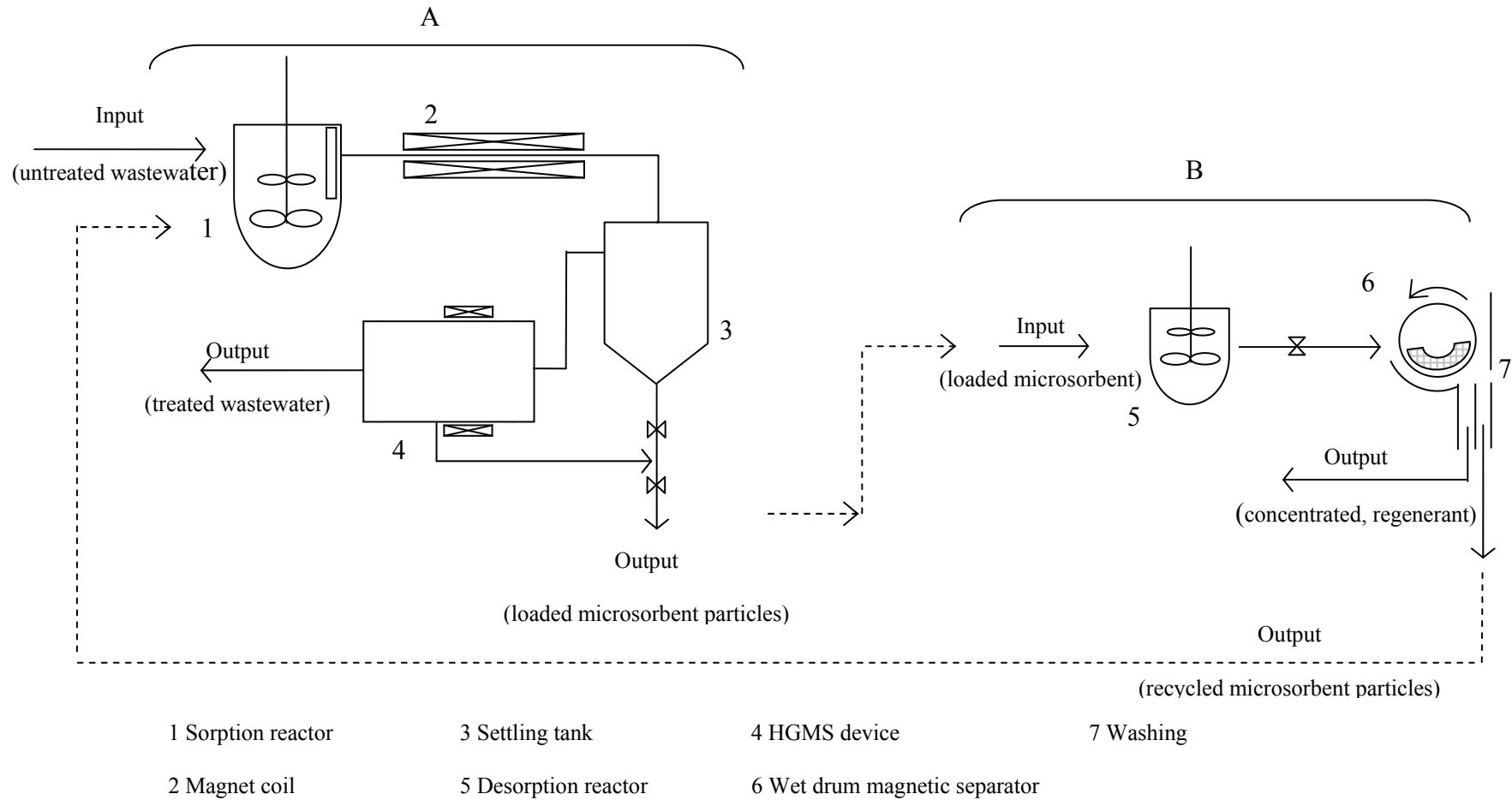


Figure 6.1: Illustration of a heavy metal treatment process using magnetic microsorbents and different solid-liquid separations applying magnet technology. A: Sorption process, B: Desorption and washing processes.

Although the microsorber could be separated by the HGMS system alone (4), this would require frequent washing steps of the magnetic filter and would result in a rather dilute recycling suspension of the particles. In order to reduce the load of the HGMS device a settling tank could be installed (3). Previous to this step the particles would pass through a weak magnetic field generated by a magnet coil (2), which induces particle aggregation.

With the experimental data shown in Figure 5.10 and Figure 5.12 can be estimated that about 10 minutes will be required for the sedimentation of a great percentage of the microparticles. Then the aqueous solution would be introduced into the HGMS unit where a final magnetic separation is performed.

For a reuse of the microsorbers, an additional desorption process must be considered (B). The loaded microsorbers will be contacted in a reactor (5) with a solution which allows the metal ion release from the adsorbent. The volume of this desorption solution must be much smaller than the initial wastewater solution in order to obtain a concentrated final metal ion solution. The separation of the microsorbers from the concentrated metal ion solution can be carried out by means of a wet drum magnetic separator (6). Thus, the recovered adsorbent can be washed (7) and subsequently being reused for another adsorption cycle.

7 Bibliography

- Aksu, Z., Ü. Açıkel, et al. (2002). "Equilibrium modelling of individual and simultaneous biosorption of chromium(VI) and nickel(II) onto dried activated sludge." Water Research **36**(12): 3063-3073.
- Al-Degs, Y., M. A. Khraisheh, et al. (2001). "Sorption of lead ions on diatomite and manganese oxides modified diatomite." Water Research **35**(15): 3724-3728.
- Al-Degs, Y. S., M. F. Tutunju, et al. (2000). "The Feasibility of Using Diatomite and Mn-Diatomite for Remediation of Pb^{2+} , Cu^{2+} , and Cd^{2+} from Water." Separation Science and Technology **35**(14): 2299 - 2310.
- Al-Sewailem, M. S., E. M. Khaled, et al. (1999). "Retention of copper by desert sands coated with ferric hydroxides." Geoderma **89**(3-4): 249-258.
- Anders Johnson, R. L., Council of Europe, Ad Hoc Group of Experts on Non-Agricultural Pesticides (1996). Risk Assessment of Antifoulants: Report, Council of Europe.
- Apak, R. (2006). Adsorption of heavy metal ions on soil surfaces and similar substances: theoretical aspects. Encyclopedia of surface and colloid science. P. Somasundaran, Taylor & Francis Group. **1**.
- Bajpai, S. and M. Chaudhuri (1999). "Removal of Arsenic from Ground Water by Manganese Dioxide-Coated Sand." Journal of Environmental Engineering **125**(8): 782-787.
- Balistreri, L. S. and T. T. Chao (1990). "Adsorption of selenium by amorphous iron oxyhydroxide and manganese dioxide." Geochimica et Cosmochimica Acta **54**(3): 739-751.
- Balistreri, L. S. and J. W. Murray (1982). "The surface chemistry of δ - MnO_2 in major ion sea water." Geochimica et Cosmochimica Acta **46**(6): 1041-1052.
- Barling, J. and A. D. Anbar (2004). "Molybdenum isotope fractionation during adsorption by manganese oxides." Earth and Planetary Science Letters **217**(3-4): 315-329.
- Begum, A. S. (2005). Diffusion. Elements of Mass Transfer (Part I), PHI Learning Pvt. Ltd.
- Bourikas, K., J. Vakros, et al. (2003). "Potentiometric Mass Titrations: Experimental and Theoretical Establishment of a New Technique for Determining the Point of Zero Charge (PZC) of Metal (Hydr)Oxides." The Journal of Physical Chemistry B **107**(35): 9441-9451.
- Brandao, M. and F. Galembeck (1990). "Copper, lead and zinc adsorption on MnO_2 impregnated cellulose acetate." Colloids Surf. **48**: 351-362.

- Burns, R. G. and V. M. Burns (1978). Mineralogy. Marine Manganese Deposits. G. P. Glasby, Elsevier Scientific Publishing Company.
- Chester, R. (1965). "Adsorption of zinc and cobalt on illite in seawater." Nature **206**: 884-886.
- Christensen, E. R. and J. T. Delwiche (1982). "Removal of heavy metals from electroplating rinsewaters by precipitation, flocculation and ultrafiltration." Water Research **16**(5): 729-737.
- Crerar, D. A. and H. L. Barnes (1974). "Deposition of deep-sea manganese nodules." Geochimica et Cosmochimica Acta **38**(2): 279-300.
- Das, N. and R. K. Jana (2006). "Adsorption of some bivalent heavy metal ions from aqueous solutions by manganese nodule leached residues." Journal of Colloid and Interface Science **293**(2): 253-262.
- Davis, J. A. and J. O. Leckie (2002). "Effect of adsorbed complexing ligands on trace metal uptake by hydrous oxides." Environmental Science & Technology **12**(12): 1309-1315.
- Davranche (2000). "Heavy metals desorption from Synthesized and Natural iron and manganese oxyhydroxides: effect of reductive conditions." Journal of colloid and interface sciences **227**: 531-539.
- Dong, D., L. Liu, et al. (2007). "Comparison of lead, cadmium, copper and cobalt adsorption onto metal oxides and organic materials in natural surface coatings." Microchemical Journal **85**(2): 270-275.
- Driehaus, W. (1994). Arsenentfernung mit Mangandioxid und Eisenhydroxid in der Trinkwasseraufbereitung. Berlin, Technischen Universität Berlin: 117.
- Dzombak, D. A. and F. Morel (1990). Surface complexation modeling: hydrous ferric oxide, Wiley-Interscience
- Economopoulos, A. P. (1996). "A rapid approach to rational water pollution control strategies." Environmental Monitoring and Assessment **43**(1): 49-64.
- Essington, M. E. (2004). Soil and water chemistry: an integrative approach, CRC Press.
- Étienne Guyon, J.-P. H., Luc Petit (2001). Physical hydrodynamics, Oxford University Press.
- Fan, H.-J. and P. R. Anderson (2005). "Copper and cadmium removal by Mn oxide-coated granular activated carbon." Separation and Purification Technology **45**(1): 61-67.
- Faust, S. D. and O. M. Aly (1998). Chemistry of water treatment, CRC Press.
- Furrer, W. S. a. G. (1987). The dissolution of oxides and aluminum silicates. Aquatic surface chemistry: chemical processes at the particle-water interface. W. Stumm, Wiley-IEEE **87** 205-206.

- Glasby, G. P. and P. Lawrence (1974). "Manganese deposits in the South Pacific Ocean." NZOI Chart. Misc. Ser. **33**.
- Goldberg, E. D. (1954). "Marine geochemistry I. Chemical scavengers of the sea." J. Geol. **62**: 249-265.
- Han, R., W. Zou, et al. (2006). "Copper(II) and lead(II) removal from aqueous solution in fixed-bed columns by manganese oxide coated zeolite." Journal of Hazardous Materials **137**(2): 934-942.
- Han, R., W. Zou, et al. (2006). "Removal of copper(II) and lead(II) from aqueous solution by manganese oxide coated sand: I. Characterization and kinetic study." Journal of Hazardous Materials **137**(1): 384-395.
- Healy, T. W., A. P. Herring, et al. (1966). "The effect of crystal structure on the surface properties of a series of manganese dioxides." Journal of Colloid and Interface Science **21**(4): 435-444.
- Hoins, U., L. Charlet, et al. (1993). "Ligand Effect on the Adsorption of Heavy-Metals - the Sulfate Cadmium Goethite Case." Water Air and Soil Pollution **68**(1-2): 241-255.
- Jenkins, D. (2004). Química del Agua Mexico, LIMUSA, Noriega Editores.
- Jenne, E. A. (1968). Controls on Mn, Fe, Co, Ni, Cu, and Zn Concentrations in Soils and Water: the Significant Role of Hydrous Mn and Fe Oxides. Trace Inorganics in Water. R. F. Gould, American Chemical Society Publications: 337-387.
- Kanungo, S. B. and K. M. Parida (1984). "Interfacial behavior of some synthetic MnO₂ samples during their adsorption of Cu²⁺ and Ba²⁺ from aqueous solution at 300°K." Journal of Colloid and Interface Science **98**(1): 252-260.
- Kanungo, S. B., S. S. Tripathy, et al. (2004). "Adsorption of Co²⁺, Ni²⁺, Cu²⁺, and Zn²⁺ onto amorphous hydrous manganese dioxide from simple (1-1) electrolyte solutions." Journal of Colloid and Interface Science **269**(1): 11-21.
- Kanungo, S. B., S. S. Tripathy, et al. (2004). "Adsorption of Co, Ni, Cu, and Zn on hydrous manganese dioxide from complex electrolyte solutions resembling sea water in major ion content." Journal of Colloid and Interface Science **269**(1): 1-10.
- Kaoser, S., S. Barrington, et al. (2005). "Copper Adsorption with Pb and Cd in Sand-Bentonite Liners under Various pHs. Part II. Effect on Adsorption Sites." Journal of Environmental Science and Health, Part A: Toxic/Hazardous Substances and Environmental Engineering **39**(9): 2241 - 2255.

- Kinniburgh, D. G. and M. L. Jackson (1981). Cation Adsorption by Hydrous Metal Oxides and Clay. Adsorption of Inorganics at Solid-Liquid Interfaces. M. A. Anderson and A. J. Rubin. Michigan, Ann Arbor Science: 91-160.
- Kiss, T. a. s. and A. Odani (2007). "Demonstration of the Importance of Metal Ion Speciation in Bioactive Systems." Bulletin of the Chemical Society of Japan **80**(9): 1691-1702.
- Kosmulski, M. (2001). Chemical Properties of Material Surfaces, CRC Press.
- Kurbatov, M. H., G. B. Wood, et al. (1951). "Isothermal adsorption of cobalt from dilute solutions." The Journal of Physical Chemistry **55**(7): 1170-1182.
- Lagergren, S. (1898). "Zur theorie der sogenannten adsorption gelöster stoffe. Kungliga Svenska Vetenskapsakademiens." Handlingar **24**(4): 40.
- Leyva-Ramos, R., J. R. Rangel-Mendez, et al. (1997). "Adsorption of cadmium(ii) from aqueous solution onto activated carbon." Water Science and Technology Selected Proceedings of the 1st International Specialized Conference on Adsorption in the Water Environment and Treatment Processes **35**(7): 205-211.
- Louis W. Chang, T. S. (1996). Toxicology of metals, CRC Press.
- Margolis, S. V. and R. G. Burns (1976). "Pacific Deep-Sea Manganese Nodules: Their Distribution, Composition, and Origin." Annual Review of Earth and Planetary Sciences **4**: 229-263.
- Marmier, N. (2002). Metal ion adsorption on silica, alumina, and related surfaces. Encyclopedia of surface and colloids science. A. T. Hubbard. **3**.
- Mc Kenzie, R. M. (1971). "The Synthesis of Birnessite, Cryptomelane, and Some Other Oxides and Hydroxides of Manganese." Mineralogical Magazine **38**(296): 493-502.
- Mc Kenzie, R. M. (1989). Manganese oxides and hydroxides. Minerals in Soil Environments. J. B. a. W. Dixon, S. B. Madison, Wisconsin, USA, Soil Science Society of America: 439-465.
- McBride, M. B. (1994). Chemisorption and Precipitation of Inorganic Ions. Environmental Chemistry of Soils. New York, Oxford University Press: 121-168.
- Menard, H. W. and C. J. Shipek (1958). "Surface Concentrations of Manganese Nodules." **182**(4643): 1156-1158.
- Mergen, M. R. D., B. Jefferson, et al. (2008). "Magnetic ion-exchange resin treatment: Impact of water type and resin use." Water Research **42**(8-9): 1977-1988.
- Mitchell, P. C. H. (1990). Molybdenum and molybdenum compounds. Ullmann's Encyclopedia of Industrial Chemistry. **A16**: 675-682.

- Morgan, J. J. and W. Stumm (1964). "Colloid-chemical properties of manganese dioxide." Journal of Colloid Science **19**(4): 347-359.
- Morin, G., J. D. Ostergren, et al. (1999). "XAFS determination of the chemical form of lead in smelter-contaminated soils and mine tailings; importance of adsorption processes." American Mineralogist **84**(3): 420-434.
- Murray, D. J., T. W. Healy, et al. (1968). "The adsorption of aqueous metal on colloidal hydrous manganese oxide." Adv. Chem. Ser. **79**(74-81).
- Murray, J. W. (1974). "The surface chemistry of hydrous manganese dioxide." J. Colloid Interface Sci. **46**: 357-371.
- Murray, J. W. (1975). "The interaction of cobalt with hydrous manganese dioxide." Geochimica et Cosmochimica Acta **39**: 635-647.
- Murray, J. W. (1975). "The interaction of metal ions at the manganese dioxide-solution interface." Geochimica et Cosmochimica Acta **39**(505-519).
- Nernst, W. (1904). "Theorie der Reaktionsgeschwindigkeit in heterogenen Systemen." Zeitschrift für Physikalische Chemie **47**(1): 52.
- Nguyen, N.-T. (2008). Micromixers: fundamentals, design and fabrication.
- Nies, D. H. (1999). "Microbial heavy-metal resistance." Applied microbiology and biotechnology **51**(6): 730-750.
- OECD, O. f. E. C.-o. a. D. (1994). Risk Reduction Monograph No. 5: Cadmium OECD Environment Directorate. Paris, France.
- Office, U. N. O. E. T. (1979). Manganese Nodules: Dimensions and Perspectives, D. Reidel Publishing Company.
- Oliveira, L., D. Petkowicz, et al. (2004). "Magnetic zeolites: a new adsorbent for removal of metallic contaminants from water." Water Research **38**(17): 3699-3704.
- Oliveira, L., R. Rios, et al. (2002). "Activated carbon/iron oxide magnetic composites for the adsorption of contaminants in water." Carbon **40**(12): 2177-2183.
- Oliveira, L., R. Rios, et al. (2003). "Clay-iron oxide magnetic composites for the adsorption of contaminants in water." Applied Clay Science **22**(4): 169-177.
- Peng, X., Z. Luan, et al. (2005). "Carbon nanotubes-iron oxides magnetic composites as adsorbent for removal of Pb(II) and Cu(II) from water." Carbon **43**(4): 880-883.
- Peric, J., M. Trgo, et al. (2004). "Removal of zinc, copper and lead by natural zeolite--a comparison of adsorption isotherms." Water Research **38**(7): 1893-1899.
- Perk, M. v. d. (2006). Soil and water contamination: from molecular to catchment scale, Taylor & Francis.

- Posselt, H. S., F. J. Anderson, et al. (1968). "Cation sorption on colloidal hydrous manganese dioxide." Environmental Science & Technology **2**(12): 1087-1093.
- Post, J. E. (1999). "Manganese oxide minerals: Crystal structures and economic and environmental significance." Proceedings of the National Academy of Sciences of the United States of America. **96**(7): 3447-3454.
- Puls, R. W. and H. L. Bohn (1988). "Sorption of Cadmium, Nickel, and Zinc by Kaolinite and Montmorillonite Suspensions." Soil Sci Soc Am J **52**(5): 1289-1292.
- Rahaman, M. N. (2006). Ceramic processing, CRC Press.
- Reddy, K., L. Munn, et al. (1997). Chemistry and mineralogy of molybdenum in soils. Molybdenum in Agriculture. U. Gupta, Cambridge University Press.
- Riley, J. P. and P. Sinhaseni (1958). "The determination of copper in sea water, silicate rocks and biological materials." Analyst **58**: 299-304.
- Safarik, I., K. Nymburská, et al. (1997). "Adsorption of Water-Soluble Organic Dyes on Magnetic Charcoal." Journal of Chemical Technology & Biotechnology **69**(1): 1-4.
- Scheffer, F. and P. Schachtschabel (1989). Lehrbuch der Bodenkunde.
- Schindler, P. W. and W. Stumm (1987). The surface chemistry of oxides, hydroxides, and oxide minerals. Aquatic surface chemistry. Chemical processes at the particle-water interface. W. Stumm, John Wiley & Sons, Inc.
- Shu, Z. and S. Wang (2009). "Synthesis and Characterization of Magnetic Nanosized Fe₃O₄/MnO₂ Composite Particles." Journal of Nanomaterials **2009**: 5.
- Small, H. (1989). Ion chromatography, Springer.
- Speight, J. G. (2003). Perry's standard tables and formulas for chemical engineers, McGraw-Hill
- Stenström, S. (1987). "Extraction of cadmium from phosphoric acid solutions with amines. Part III. A thermodynamic extraction model." Hydrometallurgy **18**(1): 1-20.
- Stiefel, E. (2002). The Biochemistry of Molybdenum and Tungsten. Metal ions in biological systems, Molybdenum and Tungsten: Their roles in Biological Processes. H. Sigel and A. Sigel, CRC Press. **39**.
- Stumm, W. and J. J. Morgan (1966). Aquatic Chemistry. Chemical Equilibria and Rates in Natural Waters. New York, Wiley.
- Stumm, W. and J. J. Morgan (1996). Aquatic Chemistry: Chemical Equilibria and Rates in Natural Waters, Wiley-Interscience publications.

- Towler, P. H., J. D. Smith, et al. (1996). "Magnetic recovery of radium, lead and polonium from seawater samples after preconcentration on a magnetic adsorbent of manganese dioxide coated magnetite." Analytica Chimica Acta **328**: 53-59.
- Tripathy (2006). "Adsorption of Cd on hydrous manganese dioxide from aqueous solutions." Desalination **194**: 11-21.
- Tripathy, S. S. and S. B. Kanungo (2005). "Adsorption of Co^{2+} , Ni^{2+} , Cu^{2+} and Zn^{2+} from 0.5 M NaCl and major ion sea water on a mixture of $\delta\text{-MnO}_2$ and amorphous FeOOH ." Journal of Colloid and Interface Science **284**(1): 30-38.
- Tripathy, S. S., S. B. Kanungo, et al. (2001). "The electrical double layer at hydrous manganese dioxide/Electrolyte interface." Journal of colloid and interface sciences **241**(1): 112-119.
- Tripathy, S. S., K. Sarangi, et al. (2002). "Extraction of Cadmium (II) by supported liquid membrane using TOPS-99 as mobile carrier." Separation Science and Technology **37**(12): 2897 - 2911.
- Ure, A. and C. Davidson (2002). Chemical Speciation in the Environment, Wiley-Blackwell.
- Vadivelan, V. and K. V. Kumar (2005). "Equilibrium, kinetics, mechanism, and process design for the sorption of methylene blue onto rice husk " Journal of Colloid and Interface Science **286**(1).
- Victor A. Atiemo Obeng, W. R. P., Piero Armenante (2004). Solid-liquid mixing. Handbook of industrial mixing: science and practice. V. A. A.-O. Edward L. Paul, Suzanne M. Kresta, Wiley-IEEE: 543-582.
- Volesky, B. (2001). "Detoxification of metal-bearing effluents: biosorption for the next century." Hydrometallurgy **59**(2-3): 203-216.
- Wang, S.-G., W.-X. Gong, et al. (2007). "Removal of lead(II) from aqueous solution by adsorption onto manganese oxide-coated carbon nanotubes." Separation and Purification Technology **58**(1): 17-23.
- Watson, S., D. Beydoun, et al. (2002). "Synthesis of a novel magnetic photocatalyst by direct deposition of nanosized TiO_2 crystals onto a magnetic core " Journal of Photochemistry and Photobiology A: Chemistry **148**(1-3): 11.
- WHO (2007). Health risks of heavy metals from long-range transboundary air pollution
- Wood, J. M. (1975). "Biological cycles for elements in the environment." Naturwissenschaften **62**(8): 357-364.

- Wu, H.-X., T.-J. Wang, et al. (2007). "Effects of SO₄²⁻ on the Heterogeneous Precipitation Coating of Hydrous Alumina on TiO₂ Particles in an Aqueous Process." Industrial & Engineering Chemistry Research **46**(11): 3590-3594.
- Wu, R., J. Qu, et al. (2005). "Magnetic powder MnO-Fe₂O₃ composite: a novel material for the removal of azo-dye from water." Water Research **39**(4): 630-638.
- Yao, W. and F. J. Millero (1996). "Adsorption of Phosphate on Manganese Dioxide in Seawater." Environmental Science & Technology **30**(2): 536-541.
- Zasoski, R. J. and R. G. Burau (1988). "Sorption and Sorptive Interaction of Cadmium and Zinc on Hydrous Manganese Oxide." Soil Sci Soc Am J **52**(1): 81-87.
- Zhang, L., J. Ma, et al. (2008). "The microtopography of manganese dioxide formed in situ and its adsorptive properties for organic micropollutants." Solid State Sciences **10**(2): 148-153.
- Zhang, R., S. Vigneswaran, et al. (2006). "Magnetic ion exchange (MIEX®) resin as a pre-treatment to a submerged membrane system in the treatment of biologically treated wastewater." Desalination International Congress on Membranes and Membrane Processes **192**(1-3): 296-302.
- Zou (2006). "Kinetic study of adsorption of Cu(II) and Pb(II) from aqueous solutions using manganese oxide coated zeolite in batch mode." Colloids and Surfaces A: Physicoquimical and Engineering Aspects **279**(1-3): 238-246.

8 Appendix

8.1 List of symbols

Latin symbols

A	m ²	Area
a	m ² /g	Specific surface area
a _s	m ² /g	External interfacial area
c	mmol/L or mg/L	Concentration
c _{i,0}	mmol/L or mg/L	Initial concentration of “i”
c _{i,eq}	mmol/L or mg/L	Equilibrium concentration of “i”
D _L	m ² /s	Molecular diffusion coefficient
d	m	Diameter
d _p	m	Particle diameter
h	mmol/(min g)	Initial sorption rate
K	mol/L	Equilibrium constant
K _L	L/mmol	Langmuir constant
K _{sp}	mol/L	Solubility constant
k ₁	1/min	Pseudo-first-order adsorption rate constant
k ₂	g/(min mmol)	Pseudo-second-order adsorption rate constant
m _s	g or mg	Mass of adsorbent
\dot{N}	mol/s	Molar flow rate
n	-	Freundlich-Exponent
q	mmol/g or mg/g	Loading
q _{i,0}	mmol/g or mg/g	Initial loading of “i”
q _{i,eq}	mmol/g or mg/g	Equilibrium loading of “i”
q _t	mmol/g or mg/g	Loading at any time
\bar{q}	mmol/g	Loading average
r	m or Å	Radius
T	°C	Temperature
T	K	Absolute temperature
T	NTU	Turbidity

T_0	NTU	Turbidity at time zero
t	s	Time
V	L	Volume
v	m/s	Velocity
v_{rel}	m/s	Relative velocity
v_t	m/s	Settling velocity

Greek symbols

β	m/s	Mass transfer coefficient
η	Pa·s	Dynamic viscosity
δ	m	Thickness of boundary layer
μ	m ² /sV	Ion mobility
ν	m ² /s	Kinematic viscosity
ρ	g/L	Density
ζ	mV	Zeta potential

List of constants

F	96484 C/mol	Faraday's constant
R	8.314 J/Kmol	Universal gas constant
k_B	1.380 J/K	Boltzmann constant

8.2 Analytical methods, Chemicals and Apparatus

8.2.1 Analytical methods

Parameter	Equipment	Method	Detection limit
Cd(II)	AAS	DIN EN ISO 17294-2	1 µg/L
Ni(II)	AAS	ION PAC AS 11	2.0 mg/L
Pb(II)	AAS	ION PAC AS 11	1.7 mg/L
Mo(VI)	AAS	ION PAC AS 11	2.2 mg/L
pH	Combination electrode	-	-

8.2.2 Used chemicals

Cadmium standard solution, Cd(NO₃)₂ in HNO₃ 0.5 % 1000 mg/L Cd, Merck

Calcium nitrate (Ca(NO₃)₂ x 4H₂O), Merck

Chlorhydric acid (HCl) Merck

Lead standard solution, Pb(NO₃)₂ in HNO₃ 0.5 % 1000 mg/L Pb, Merck

Manganese chloride (MnCl₂ x 4H₂O), Merck

Molybdenum standard solution in HNO₃ 2 – 5% 1000µg/mL, Chem-Lab NV

Sodium hydroxide (NaOH) Merck

Sodium nitrate (NaNO₃), Merck

Nitric acid(HNO₃) suprapure, Merck

Potassium permanganate (KMnO₄), Merck

8.2.3 Apparatus

Ultra pure water	Millipore Milli-Q Plus
Flasks shaker	VKS 75 Edmund Bühler GmbH
Mechanical stirrer	IKA Labortechnik
Atomic Absorption Spectrometer (AAS)	VARIAN Spectra AA-220-FS

8.3 Others

Table 8.1 : Physicochemical characteristics of magnetite (Bayoxide E 8710), Bayer.

Specification	min.	max.
Total iron oxide content, determined as Fe ₂ O ₃	98%	
Specific surface area, m ² /g	3	6
Coercivity IHc, Oe	90	105
Remanence, emu/g	13	16.8
Saturation magnetization, emu/g	84.8	91.7
Density, g/mL	app. 4.6	
Predominant particle size, μm	app. 0.5	-

8.4 Curriculum vitae

Name	Carla Andrea Calderón Rosas
Date of Birth	October 12 th , 1977
Place of Birth	Antofagasta – Chile
Nationality	Chilean
Marital status	Married, one child
E-Mail	calderon_carla@yahoo.com

Academic Records

2005 - 2010	PhD Student, Karlsruhe University, Germany. PhD Thesis: Synthesis and application of manganese dioxide coated magnetite for removal of metal ions from aqueous solutions.
2002	Faculty of Sciences, University of Chile, Santiago, Chile. Degree: Environmental Chemist
2000 - 2001	Faculty of Chemical and Pharmaceutical Sciences, University of Chile, Santiago, Chile Thesis: Design of a wastewater decontamination process for mining wastewaters including the Study of the removal and recovery of metal ions by means of the extraction process in liquid membranes reactors.
1995 - 2000	Faculty of Sciences, University of Chile, Santiago, Chile. Environmental Chemistry
1994	Academic Aptitude Test. National Examination for applying to the Chilean universities.
1991 - 1994	Secondary Education. Sagrados Corazones School, La Serena, Chile.

Professional Experience

2005 - 2009	Karlsruhe Institute for Technology (former Forschungszentrum Karlsruhe), Germany. Researcher at Institute of Functional Interfaces.
2003 - 2005	Hanna Instruments Equipments, Chile. Handling of laboratory equipments and field water analysis Preparation of technical seminaries and assistance to clients on water treatment issues
2002 - 2003	FONDEF Project, University of Chile, Chile. Development of a primary treatment to remove heavy metals and other pollutants from mining wastewaters.
2000 - 2001	Faculty of Chemical and Pharmaceutical Sciences, University of Chile, Santiago, Chile. Thesis.
1997 - 2000	Faculty of Sciences and Chemical and Pharmaceutical Sciences, University of Chile, Santiago, Chile. Laboratory assistant for the lectures of Water Chemistry, Instrumental Analysis and Unitary Operations.

Courses

2000	Metallurgical-Mining Chemistry, Faculty of Chemical and Pharmaceutical Sciences, University of Chile, Santiago, Chile. Pollution and Wastewater treatment, Faculty of Chemical and Pharmaceutical Sciences, University of Chile, Santiago, Chile.
------	--

Scholarships

2005 - 2007	PhD scholarship, DFG Research Training Group 366, Interfacial phenomena in aquatic systems and aqueous phases, Germany.
2009	PhD scholarship, Beca Gestión Propia 2008, CONICYT, Chile

Conferences and Publications

- 2010 Calderon Rosas C.A., Franzreb M., Valenzuela F., Höll W.H., Magnetic manganese dioxide as amphoteric adsorbent for removal of harmful inorganic contaminants from water. *Reactive and Functional Polymers*. Article in Press, published online.
- 2008 IEX 2008 Recent advances in ion exchange theory and practice Cambridge United Kingdom. Calderon C, Höll W.H., Synthesis and application of manganese dioxide coated magnetite for selective removal of trace contaminants from water. p. 253-258
Wasser 2008 - Jahrestagung der Wasserchemischen Gesellschaft Trier, Germany
Poster: Calderon C., Höll W.H., Application of manganese dioxide coated magnetite for removal of trace contaminants from water. p. 304-308.
- 2006 International Workshop on Frontiers and Interfaces of Ion Exchange, Antalya, Turkey. ,
Poster: Calderon. C., Holzinger S., Höll W. H. (2006): "Synthesis, development and application of magnetic manganese dioxide for selective removal of trace contaminants from water". p. 57.

Languages

Spanish	Native Language
English	Intermediate - Advanced
German	Intermediate